Oxford Research Encyclopedia of Climate Science
https://doi.org/10.1093/acrefore/9780190228620.013.879
Published online: 18 September 2024

CO_2 in Earth's Ice Age Cycles

Mathis P. Hain[1,*] and Daniel M. Sigman[2]

[1] University of California Santa Cruz, 1156 High St, 65064, CA, U.S.A.
[2] Princeton University, Washington Rd, 08540, NJ, U.S.A.
[*] Correspondence to: mhain@ucsc.edu

Summary Earth's history is marked by episodes of large-scale continental glaciation. Most recently, beginning 3 million years ago, northern hemispheric glaciation expanded and developed cyclic variations known as the *ice age cycles*. With the 19th-century discovery of these cycles in ice extent and climate, changes in atmospheric carbon dioxide (CO_2) concentration were proposed as a possible cause. Since the 1980s, scientists have produced detailed reconstructions revealing that, during ice ages, atmospheric CO_2 was as much as a third lower than its preindustrial concentration—enough to explain almost half of the approximately 5 °C ice age cooling by weakening the Earth's natural greenhouse effect. The consensus is that the ice age climate cycles result from cyclic changes in Earth's orbit, which redistribute sunlight between regions and seasons but do not in themselves significantly heat or cool the globe on an annual- average basis. If so, the regional and seasonal effects of orbital change must cause changes in aspects of the Earth system that then induce changes in global annual-average climate. Changes in the reflection of sunlight by the ice sheets are widely believed to have played such a role. Atmospheric CO_2 appears to be a second key Earth system property, and one that caused the ice age cycles to be global rather than simply regional phenomena. The ocean was likely the dominant driver of atmospheric CO_2 change between warm "interglacial" and cold "glacial" periods, through multiple aspects of its behavior. First, ice age cooling and other changes allowed bulk global seawater to absorb additional CO_2 from the atmosphere. Second, during ice ages, the ocean's "biological carbon pump" was stronger: Ocean plankton and their sinking debris more effectively removed CO_2 from surface waters and the atmosphere, sequestering it in the ocean interior. Polar ocean changes were key to this stronger biological pump, involving some combination of changes in biological productivity, ocean circulation, and air–sea gas exchange. Third, the net effect of these ocean changes was to enhance deep ocean CO_2 storage and thus to dissolve calcium carbonate sediment off the seafloor, changing the ocean's acid/base chemistry so that it absorbed additional CO_2 from the atmosphere. The specific polar ocean changes that drove the strengthening of the biological carbon pump and the ensuing seafloor calcium carbonate response are a topic of ongoing debate.

Keywords: ice age, carbon cycle, carbon dioxide, climate, ocean chemistry, Southern Ocean, biological productivity, biological pump, alkalinity
Subjects: Climate Systems and Climate Dynamics, Past Climates, Climate Systems and Climate Dynamics: Theoretical Foundations, Climate Systems and Climate Dynamics: Biogeochemistry

Theory

From Ice Age Theory to Observations

The discovery of widespread geologic evidence for large-scale advances of continental glaciation led 19th-century Earth scientists to advance the "Eiszeit" (Ice Age) theory (e.g., Agassiz, 1840; Charpentier, 1841; Schimper, 1837; cf. Evans, 1887; Krüger, 2013): that Earth's climate had experienced multiple ice ages (e.g., Geikie, 1874, 1896; Penck & Brückner, 1901). Key early evidence came in the form of glacial deposits and landforms as well as plant and animal fossils and remains that hinted at past changes in regional climate and vegetation cover on land (Köppen & Wegener, 1924; Summerhayes, 2019). Methods for temperature reconstruction from microfossils in deep sea sediments (Anand et al., 2003; Emiliani, 1955, 1966) then yielded a continuous record of climatic change, with alternation between long and cold glacial stages, abrupt glacial terminations, and ensuing short and warm interglacial stages (Figure 1). The climate amelioration from the Last Glacial Maximum (LGM) to the current Holocene interglacial period may have spurred the Neolithic Revolution, with diverse human cultures transitioning to agriculture and settlement (Bar-Yosef, 2011; Betti et al., 2020; Gupta, 2004).

The water reservoir on Earth's surface is partitioned among ocean, ice sheets, and groundwater in the proportions of approximately 96%:2%:2%, respectively. During the LGM, some 20,000 years ago, as well as during other peak glacial intervals, the expansion of continental glaciation corresponded to the removal of approximately 3% of Earth's seawater volume, yielding an LGM partitioning of water of approximately 93%:5%:2% (cf. Adkins et al., 2002). The reconstructed global mean sea-level during glacial maxima was about 120–130 m lower than in the Holocene

(Figure 1), causing dramatic coastal landform changes, such as the draining of the North Sea, the Bering Strait, and the Bosporus (Batchelor et al., 2019; Clark et al., 2009; Farmer et al., 2023; Hopkins, 1959; Peltier, 2004). The Laurentide ice sheet of North America and the Fennoscandian ice sheet of Europe held most of the additional ice (Clark & Mix, 2002), but mountain glaciers also formed and expanded in diverse regions around the globe (Ehlers et al., 2011), and the Antarctic ice sheet may also have changed mass (Blackburn et al., 2020; Piccione et al., 2022; Raymo et al., 2006).

With the occurrence of ice age (or glacial) cycles broadly accepted, the search began for their cause, and many hypotheses have been proposed (De Marchi, 1895; Donn & Ewing, 1966; Ewing & Donn, 1956; Fairbridge, 1987; Weart, 2008). The following two sections address only the orbital theory and CO_2 theory for ice ages: The evidence suggests that subtle changes in Earth's orbit around the Sun and resulting changes in the global greenhouse effect are required elements in explaining the timing, magnitude, and spatial footprint of ice ages as glaciologic and climatic phenomena. Albedo, Earth's reflectivity, is also central to the orbital theory and interacts strongly with the CO_2 theory; however, it is not addressed in detail here.

Orbital Theory for Ice Ages

One of the earliest hypotheses to explain ice ages involves the changing solar insolation that Earth receives because of cyclic changes in Earth's rotation and orbit, which affect the orientation of Earth's spin axis relative to the direction of sunlight and the distance from the Sun (Adhémar, 1842; Croll, 1875). Early attempts to formulate an *orbital theory* for ice ages were found to contradict geologic evidence (Hann, 1908). In a major breakthrough, Milutin Milankovitch

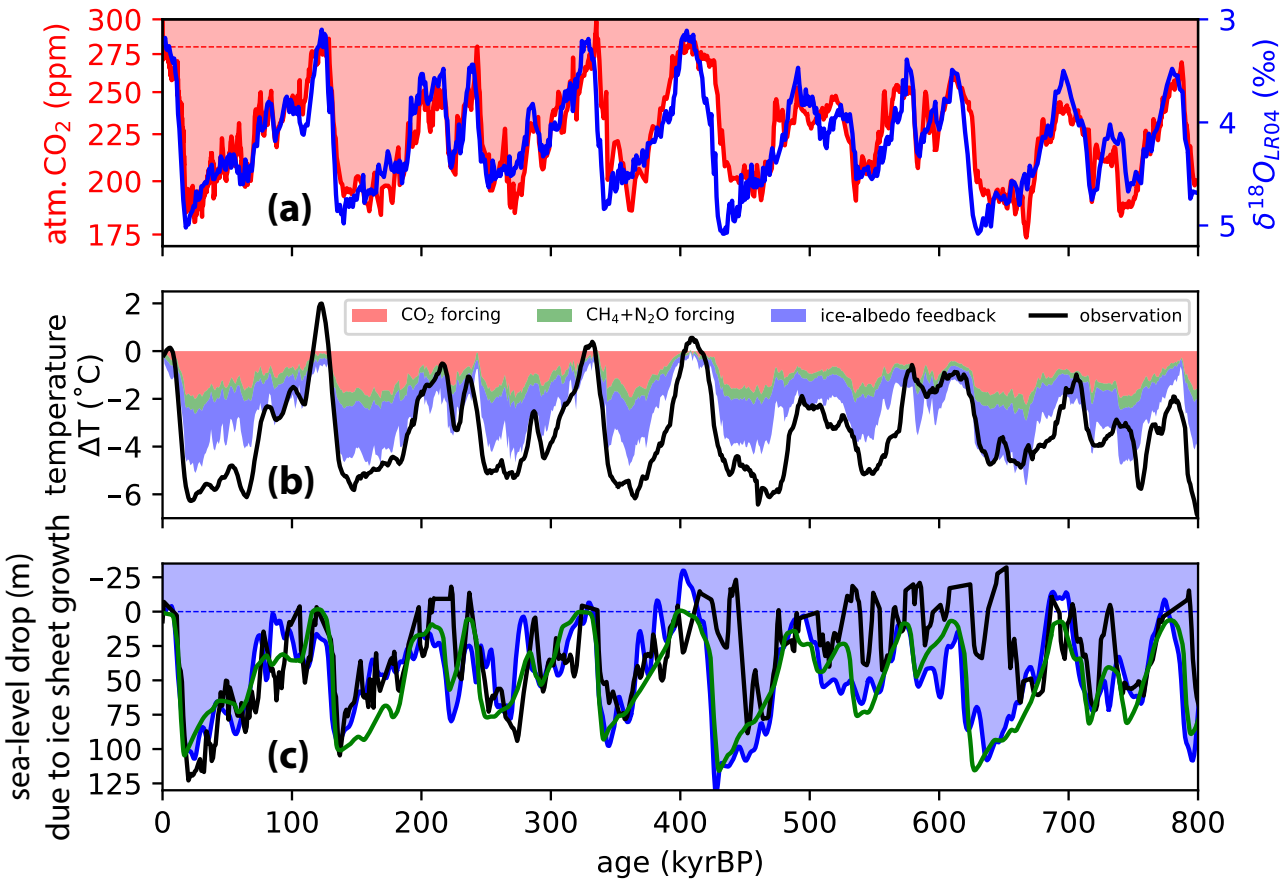

Figure 1. 800 kyr of coupled CO_2 and climate. Records of atmospheric CO_2 reconstructions (red in panel a; compiled by Bereiter et al., 2015) correlate tightly with the oxygen isotopic composition ($\delta^{18}O$) of deep-sea benthic foraminifera (blue in panel a; Lisiecki & Raymo, 2005), which serves as a proxy measure for combined waxing and waning of continental ice sheets and cooling and warming of the deep ocean; the ice ages are downward excursions (i.e., to higher $\delta^{18}O$). These ice age cycles do not follow orbital forcing in a simple way, but there is strong statistical evidence that their timing (especially of glacial termination and deglaciation; Figure 9) is controlled by orbital changes in the distribution of insolation with latitude and season (Hays et al., 1976; Huybers; 2011; Huybers & Wunsch, 2005; Imbrie et al., 1984). Combining estimates of Earth's equilibrium climate sensitivity (Hegerl et al., 2007; Sherwood et al., 2020) with the radiative effect of reconstructed change in CO_2 and the minor greenhouse gases methane and nitrous oxide (Bereiter et al., 2015; Etminan et al., 2016; Loulergue et al., 2008; Schilt et al., 2010) and a 3-Wm^{-2} surface albedo effect of maximum ice extent (Köhler et al., 2010) suggests that most of reconstructed global surface cooling (black in panel b: Snyder, 2016) may have been driven by CO_2 change as amplified by the ice albedo feedback (Equation 1), broadly consistent with reconstructed sea-level changes resulting from ice sheet advances (c; blue: Elderfield et al., 2012; green: de Boer et al., 2013, black: Rohling et al., 2014). Similar results can be obtained with numerical climate models (e.g., Ritz et al., 2011). The question of why CO_2 changed as reconstructed is the topic of this article. In panel b, the expected temperature effects are calculated with Equation 1 of the main text where ice sheet albedo is treated as feedback to greenhouse gas forcing, using 500-year binned greenhouse gas data.

calculated and graphed an accurate orbital solution for Earth insolation that reflected the approximately 23,000-year (23-kyr) cycle of precession of the equinox, the approximately 41-kyr cycle of rotation axis obliquity, and the approximately 100-kyr cycle of eccentricity of the orbit (Berger, 1988; Köppen & Wegener, 1924; Lourens et al., 2010; Loutre, 2003; Milankovitch, 1920, 1941; Szarka et al., 2021). Eccentricity and precession primarily shift sunlight between the seasons, while obliquity also shifts sunlight between latitude zones. The cycles in these orbital parameters, however, do not significantly alter the total sunlight that Earth receives in a year. Milankovitch, Köppen, and Wegner postulated that relatively cold summers in the Arctic would favor ice sheet growth, and they matched the summer insolation minima at 65 °N with the various ice advances that were known at the time (Milankovitch, 1930). Because there was no reliable method to independently date the age of glacial deposits from distinct periods of ice advance, the Milankovitch theory of northern summer insolation as a key driver for ice ages could not be immediately tested in a rigorous way.

Orbital solutions have since been improved and extended back in deep geologic time (e.g., Berger, 1977, 1978; Laskar, 1988; Laskar et al., 2004, 2011; Vernekar, 1972). More critically for understanding the ice ages of the last 3 million years, the development of dating techniques has led to repeated validation of the orbital theory for these ice ages. Uranium-thorium dating of marine carbonates (Broecker & Thurber, 1965; Thurber et al., 1965) revealed sea-level high stands in synchrony with warm northern hemisphere summers (Mesolella et al., 1969). Dating of the Brunhes–Matuyama reversal of Earth's magnetic field at approximately 440 kyr before present provided the first independent age control for sediment cores recovered from the deep sea (Shackleton & Opdyke, 1973), revealing the temporal fingerprint of orbital change in ocean temperature, global ice volume, and sea-level (Elderfield et al., 2012; Hays et al., 1976; Huybers, 2011; Huybers & Wunsch, 2005; Imbrie et al., 1984, 1992; Kukla et al., 1981; Lisiecki & Raymo, 2005, 2007; Raymo et al., 2006; Figure 1). The direct dating of moraines and other glacial landforms has progressed from measuring the colonization of glacial boulders by slow-growing lichens that led to the discovery of distinct glacial advances (Schimper, published posthumously in 1885; Beschel, 1950) to modern dendrochronology of tree fossils, geochemical methods on volcanic ash embedded in moraines near volcanoes such as in Patagonia and Hawai'i (Porter, 2005; Singer et al., 2013), and cosmogenic exposure dating of glacial deposits (Briner, 2011; Federici et al., 2017; Gosse & Phillips, 2001; Phillips et al., 1990, 1997; Putnam et al., 2013; Schaefer et al., 2006; Smith et al., 2005; Valletta et al., 2017) that highlight the dual importance of local and global climate change for glacial systems. Ice cores drilled and recovered from the Antarctic and Greenland ice sheets have been precisely dated and synchronized with each other and with orbital change (Bender, 2002; Bender et al., 1994, 2006; Blunier & Brook, 2001; Blunier et al., 1998; Sowers & Bender, 1995; Sowers et al., 1989; Suwa & Bender, 2008) to yield records of changing polar climate and environmental conditions as well as changing atmospheric composition that strongly support orbital forcing of climate (EPICA Community Members, 2006; Kawamura et al., 2007).

Geologic, paleoceanographic, and ice core evidence has all but confirmed the Milankovitch theory. However, this has deepened the conundrum of how—mechanistically—modest redistribution of solar insolation between seasons and latitudes can explain the global distribution of the cooling during ice ages (e.g., Broecker, 1966; Huybers, 2011; Imbrie et al., 1993; Raymo & Huybers, 2008; Raymo et al., 2006). The widely shared understanding is that orbital changes pace the rhythm of the ice age cycles but that strong feedbacks internal to the Earth system are required to translate the nearly net-zero changes in global insolation into ≥5 °C global ice age coolings (cf., Arrhenius, 1896; CLIMAP Project Members, 1976; Crowley, 2000; Köppen & Wegener, 1924; Osman et al., 2021; Seltzer et al., 2021; Tierney et al., 2020). Albedo changes have long been considered a source of rectification and amplification of orbital changes that lead to the observed glacial cycles. The greenhouse effect, dominantly modulated by atmospheric CO_2, has been identified as a second potential source.

CO_2 Theory for Ice Ages

The discovery of the greenhouse effect (Fourier, 1822)—that trace gases of water vapor, CO_2 and methane allow incoming sunlight to pass through the atmosphere but partially block outgoing long-wave radiation to space (Foote, 1856; Tyndall, 1861)—prompted the idea that changes in atmospheric composition would cause climate change (cf., Held & Soden, 2000; Manabe & Broccoli, 2020). Water vapor in the atmosphere accounts for most of Earth's greenhouse effect. However, because evaporation and condensation of water are governed by temperature (Clapeyron, 1834; Clausius, 1850), it was understood by Arrhenius (1896) and Chamberlin (1899) that

> *[if] an increase of carbon dioxide raises the temperature, it increases the quantity of water vapor and this by its thermal absorption further increases the temperature and calls forth more vapor [...]. The carbon dioxide becomes therefore the determinative factor, and the question of the thermal absorption of the atmosphere may be discussed for convenience as though it were solely dependent upon the fluctuations in the content of this constituent, although this will not be strictly exhaustive. (Chamberlin, 1899, p. 552)*

Spurred by debate after an 1894 conference talk by A. G. Högbom, Svante Arrhenius translated parts of Högbom's conference paper in his proposal that atmospheric CO_2 change was the cause for past climate changes from the Eocene "hot house" to the recurring ice ages (Arrhenius, 1896; cf. Crawford, 1997). However, Arrhenius left out Högbom's description of the prevailing view that atmospheric CO_2 is set by equilibration with the much larger

ocean carbon inventory (Högbom, 1894, translated in Berner, 1995, p. 494):

> *Suppose e.g. that a sudden addition of CO_2, by an amount equal to that already existing in the atmosphere, should take place in one way or another. By this act the CO_2 in the atmosphere would not at all be doubled because the major part of the addition would be offset by increased CO_2 absorption in seawater because of the increased partial pressure. Therefore, the increase of CO_2 in the atmosphere would be insignificant. On top of that the increase of absorption of CO_2 in the minerals and increase in the biosphere would make the CO_2 increase in the atmosphere negligible. A similar tendency to maintain the equilibrium would occur if there were a decrease of the CO_2 in the atmosphere.*

In comments on the dispute as to whether atmospheric CO_2 could readily and rapidly change so as to cause climate change, Chamberlin (1899) and Callendar (1938) presciently identified mass balance considerations and the importance of seawater carbonate chemistry in governing atmospheric CO_2 (Harvey, 1945; Eriksson & Welander, 1956; Revelle & Suess, 1957), as is discussed later. Gilbert Plass (Plass, 1956b, 1956c) computerized spectral calculations to demonstrate that CO_2 absorption of infrared radiation contributes to the greenhouse effect (Plass, 1956a). This result elevated CO_2-related theories of climate and climate change, including the CO_2 theory for ice ages (Callendar, 1949). Ultimately, this line of inquiry led to the discovery of the ongoing CO_2 change caused by humans (Keeling, 1960; Pales & Keeling, 1965) and ultimately the discovery that atmospheric CO_2 could be reconstructed from ice age air trapped in ice core samples (Berner et al., 1978; Delmas et al., 1980; Neftel et al., 1982; Raynaud & Barnola, 1985; Raynaud et al., 1982; Stauffer et al., 1984).

These ice core studies indicated that, during the *Last Glacial Maximum* (LGM; the apparent peak of the last ice age approximately 20–30 kyr ago), atmospheric CO_2 was roughly 190 ppm, a 32% (~90 ppm) reduction relative to the approximately 280-ppm CO_2 level during the most recent preindustrial times of the *Holocene*, the current interglacial. Subsequent reconstructions progressively further back in time revealed a close and stable coupling between ice age climate cycles and atmospheric CO_2 over the 800-kyr reach of existing Antarctic ice cores (Barnola et al., 1987; Bereiter et al., 2015; Lüthi et al., 2008; Petit et al., 1999; Siegenthaler et al., 2005; Figure 1). This has been complemented by a progressive increase in temporal resolution of the CO_2 record (Ahn & Brook, 2008, Bereiter et al., 2012), especially for the time period since the last ice age (Marcott et al., 2014; Monnin et al., 2001), as well as reconstruction of changes in the stable isotopic composition (Schmitt et al., 2012) and radiocarbon content of atmospheric CO_2 (Reimer et al., 2020). Additionally, less direct reconstructions of atmospheric CO_2 yield evidence for ice age CO_2 cycles extending further back in geologic time (Chalk et al., 2017; Hönisch et al., 2009; Martínez-Botí, Foster, et al., 2015; Yamamoto et al., 2022).

These data collectively support the CO_2 hypothesis for ice ages (e.g., Genthon et al., 1987) by providing a mechanism by which orbital changes could be, and apparently were, rectified and amplified by the CO_2 greenhouse effect to yield global climate change—with CO_2 change broadly following orbital pacing and ice sheet change broadly following CO_2 forcing (Figure 1). That is, Earth's radiative imbalance (δF) in response to a change in greenhouse gas radiative forcing (F_{GHG}) will raise or lower global surface temperatures so as to restore radiative balance (Equation 1a), with an equilibrium climate sensitivity ($1/\lambda_{ECS}$; see List of Symbols) of roughly 3 °C warming per 4 Wm^{-2} (Sherwood et al., 2020), and perhaps some 6% greater (Hegerl et al., 2007) when including climate feedbacks that unfold over decades (i.e., −1.26 Wm^{-2} of radiative feedback per 1 °C of surface warming). The peak ice age reduction of CO_2 exerts a radiative forcing (F_{GHG}) of −2.2 Wm^{-2} (−2.9 Wm^{-2} when including other reconstructed greenhouse gases; Etminan et al., 2016; Sherwood et al., 2020), which is expected to yield 2.3 °C of cooling (ΔT_{GHG}; Equation 1b).

$$\delta F = F_{GHG} + \lambda_{ECS} * \delta T_{GHG} = 0 \quad (1a)$$

$$\Delta T_{GHG} = \frac{F_{GHG}}{-\lambda_{ECS}/(1+0.06)} = \frac{-2.9 Wm^{-2}}{1.26\frac{Wm^{-2}}{^\circ C}} = -2.3^\circ C \quad (1b)$$

Furthermore, including the albedo change due to ice sheet expansion as a 3 Wm^{-2} radiative feedback per 5 °C of reconstructed peak ice age cooling ($1/\lambda_{icesheets}$), 4.5 °C of cooling is estimated (Equation 1c; Köhler et al., 2010; Sherwood et al., 2020).

$$\Delta T_{GHG+ICE} = \frac{F_{GHG}}{\lambda_{ECS}/(1+0.06)+\lambda_{icesheets}} = \frac{-2.9 Wm^{-2}}{1.26\frac{Wm^{-2}}{^\circ C} - \frac{3 Wm^{-2}}{5^\circ C}} = -4.5^\circ C \quad (1c)$$

That is, the lowering of CO_2 during the ice ages appears to have been comparable to the increase in Earth's albedo in explaining the observed global cooling, and the total suite of observed changes appears adequate to explain the amplitude of cooling (e.g., Snyder, 2016; Tierney et al., 2020; Figure 1). What remains to be established is how—mechanistically—the redistribution of solar insolation between seasons and latitudes caused the atmospheric CO_2 changes. This question, an active area of research, is the main subject from hereon. As will become apparent, the ocean is central to all proposals, regardless of whether it is envisioned as the driver of the CO_2 change (Broecker, 1982a, 1982b; Sigman & Boyle, 2000). Thus, the treatment necessarily begins with the carbon chemistry of seawater.

Seawater Carbon Chemistry

Equilibria and Speciation

Our modern understanding of the inorganic chemistry of carbon in seawater (seawater carbonate chemistry) is

typically framed in terms of the concentration of inorganic carbon species (dissolved inorganic carbon, DIC) and alkalinity. DIC and alkalinity, in the context of laws of mass action and temperature- and salinity-dependent equilibrium constants, determine the concentrations of the different inorganic carbon species (Buch, 1929, 1933, 1951; Buch et al., 1932; Harvey, 1945, 1955). The laws of mass action and equilibrium constants are as follows:

$$CO_2 + H_2O \overset{K_0}{\Leftrightarrow} H_2CO_3 \overset{K_1}{\Leftrightarrow} H^+ + HCO_3^{2-} + H_3BO_3 \overset{K_2,K_B}{\Longleftrightarrow} 2H^+ + \alpha CO_3^{2-} + \beta B(OH)_4^- \quad (2a)$$

$$K_0(\mathrm{T,S}) = \frac{H_2CO_3}{CO_2} \quad (2b)$$

$$K_1(\mathrm{T,S}) = \frac{H^+ * HCO_3^-}{H_2CO_3} \quad (2c)$$

$$K_2(\mathrm{T,S}) = \frac{H^+ * CO_3^{2-}}{HCO_3^-} \quad (2d)$$

$$K_\mathrm{B}(\mathrm{T,S}) = \frac{H^+ * B(OH)_4^-}{H_3BO_3} \quad (2e)$$

where CO_2 refers to the carbon dioxide concentration[i] of air that would be in equilibrium with the seawater; H_2CO_3, HCO_3^-, and CO_3^{2-} are the concentrations of carbonic acid, bicarbonate ion and carbonate ion, respectively, the dissolved inorganic carbon species (Figure 2); $B(OH)_4^-$ and H_3BO_3 are the concentrations of borate ion and boric acid species of seawater boron; H^+ is the total proton concentration; K_0, K_1, K_2, and K_B are the equilibrium constants; and α and β reflect the differential action of the carbonate buffer system and the borate buffer system, respectively, as addressed in the section "Seawater Buffering." By convention, the equations refer to concentration—not activity —in units of moles per kilogram of seawater, μmol/kg. Also by convention, the equilibrium constants are on the total *p*H scale (Dickson, 1984, 1993; Dickson & Millero, 1987; Sillén, 1967; colored shading in Figure 2), which includes the small proportion of protons complexed to sulfate ion in the total concentration of protons (H^+). It should be noted that there are additional weak acids and bases in seawater (e.g., those of inorganic silicon and phosphorus), the effects of which are too weak to warrant consideration here and are, thus, neglected in Equation 2. Best practices for the seawater equilibrium constants and seawater carbonate system measurements are described by Dickson et al. (2007).

Inorganic Carbon, *p*H, and Alkalinity

The following is the CO_2 system of equations for the concentrations of CO_2, carbonic acid (H_2CO_3), its products of deprotonation, bicarbonate and carbonate ion (HCO_3^-, CO_3^{2-}); boric acid and borate (H_3BO_3 and $B(OH)_4^-$); *p*H; total DIC; and alkalinity (ALK):

$$DIC = \left(H_T^+ / K_1 + 1\right) * HCO_3^- + CO_3^{2-} \quad (3a)$$

$$ALK \cong HCO_3^- + 2 * CO_3^{2-} + B(OH)_4^- \quad (3b)$$

$$pH_T = -log_{10}(H_T^+) = -log_{10}\left(K_2 \frac{HCO_3^-}{CO_3^{2-}}\right) \approx -log_{10}\left(K_2 \frac{2*DIC-ALK}{ALK-DIC}\right) \quad (3c)$$

$$CO_2 = \frac{K_2}{K_0 * K_1} * \frac{(HCO_3^-)^2}{CO_3^{2-}} \approx \frac{K_2}{K_0 * K_1} \frac{(2*DIC-ALK)^2}{ALK-DIC} \quad (3d)$$

$$B(OH)_4^- = \frac{11.86 \mu mol/kg * S}{H_T^+ / K_B + 1} \quad (3e)$$

If any two of the parameters on the left are measured or known, the others can be calculated using the equilibrium constants (K_0, K_1, K_2, K_B) defined in Equation 2. For example, in Figure 2, ALK and DIC were chosen as the *x*- and *y*-ordinates and solved for CO_2, HCO_3^-, CO_3^{2-} and pH_T. The least intuitive aspect of the seawater carbonate system is alkalinity, which is not composed of any particular element or compound; rather, alkalinity relates to the overall charge balance of all ions in seawater. Alkalinity speaks to the basic nature of seawater, which causes CO_2 that is dissolved in seawater to largely be deprotonated to form bicarbonate or carbonate ions. Alkalinity is defined as the amount of strong acid that must be added to seawater to titrate its *p*H to the point where the total proton concentration equals the bicarbonate ion concentration. This *p*H (roughly 4.5 in seawater; Morel & Hering, 1993) is often known as the "CO_2 equivalence point," as inorganic carbon chemistry at this *p*H can be understood simply as the deprotonation equilibrium of dissolved CO_2 to yield equivalent amounts of bicarbonate ion and H^+ (Equations 2a, 2c), with no additional reactions. Given this definition, alkalinity is independent of DIC: Alkalinity does not change when CO_2 is added to or removed from seawater. Whether and how much DIC changes for a given change in ALK depends on the processes occurring. For example, when atmospheric CO_2 is dissolved into seawater, DIC increases while ALK is unaffected. In contrast, when $CaCO_3$ is precipitated from seawater, ALK and DIC decrease in a 2:1 ratio (see the sections "Biological Pump" and "Mean Ocean Alkalinity Change"). When a given concentration of CO_2 is extracted from seawater by photosynthetic growth of organic matter biomass, DIC declines by this amount, while ALK increases just slightly because of the accompanying consumption of certain nutrients (Brewer & Goldman, 1976; Figure 2; see Equation 10).

Seawater Buffering

While seawater *p*H is buffered against change by the DIC species themselves, even minor *p*H changes greatly affect the concentration of aqueous CO_2. Based on this insight (Buch et al., 1932) and the known alkalinity of the ocean, Revelle and Suess (1957) derived the sensitivity of seawater CO_2 concentration to incremental change in DIC at constant ALK:

$$\frac{\delta CO_2}{CO_2} = R \frac{\delta DIC}{DIC} \quad (4)$$

where R is known as the Revelle buffer factor and the prefix δ refers to a small change (differential) in the constituent of interest. Typical ocean values of R range from 8.5 in the low

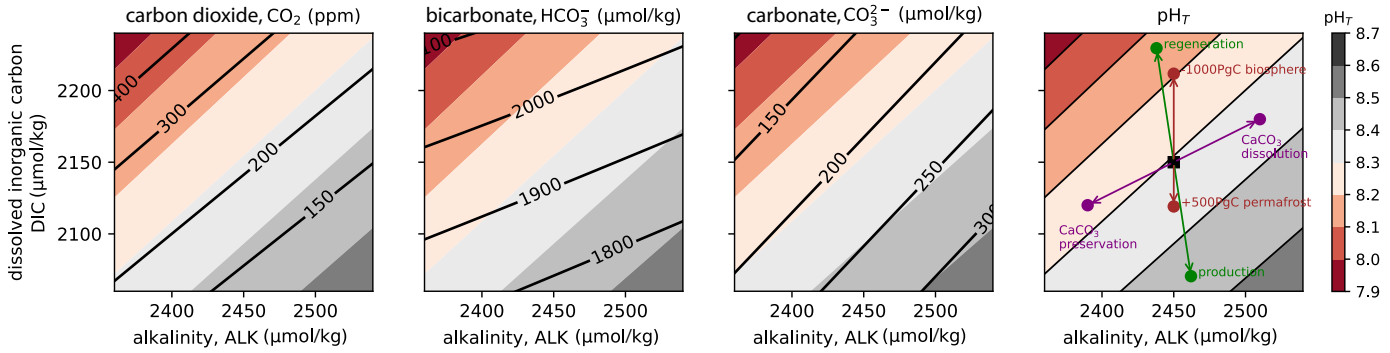

Figure 2. Inorganic carbon chemistry of seawater. Most of the dissolved inorganic carbon (DIC; vertical axis in all panels) in seawater is in the form of bicarbonate ion (HCO_3^-; center left) and carbonate ion (CO_3^{2-}; center right), and these two species are linked by mass balance laws (Equation 2): Individual carbon species must add up to the total DIC concentration, and the net charge of anions and cations in seawater must be zero. Hence, adding DIC in the form of uncharged CO_2 raises HCO_3^- and consumes CO_3^{2-} but does not change the net charge of the combined DIC species (i.e., it shifts seawater upward in the plots). In contrast, increasing alkalinity (adding base and thus raising pH (right panel); toward the right in all panels) strips protons from bicarbonate to form carbonate ion, raising the net charge of the DIC species without any change in total DIC. Dissolved CO_2 (and its extremely scarce hydrated form, carbonic acid, H_2CO_3) is only a minor contributor to DIC in seawater, and its ratio with the dominant species bicarbonate is also tied to pH. For example, if DIC and/or ALK changes cause the carbonate-to-bicarbonate ratio to increase by +25%, pH will increase by approximately 0.1 (a proton concentration decrease of 20%, i.e., $10^{-0.1}$), and the ratio CO_2-to-bicarbonate will decrease by about 25%. For any given values of seawater temperature and salinity, dissolved CO_2 determines the equilibrium CO_2 gas partial pressure, thereby determining the CO_2 concentration of the atmosphere at equilibrium (left panel). The arrows in the right panel indicate the direction of change for the production/regeneration of marine organic matter (green), preservation/dissolution of $CaCO_3$ (purple), and growth/decay of terrestrial carbon stocks (red).

latitudes to 15 in the Southern Ocean surface. This statement of finite seawater buffering was primarily motivated by the question of how easily anthropogenic carbon could raise the seawater CO_2 so as to allow a fraction of that added carbon to remain in the atmosphere in equilibrium. Regarding lower ice age CO_2 levels, for example, a 5% proportional reduction in DIC (i.e., a δDIC/DIC of −0.05) causes an approximate 50% reduction in seawater CO_2 (i.e., a $\delta CO_2/CO_2$ of −0.5)—sufficient to generate the amplitude of the reduction in atmospheric CO_2 during ice ages. This diagnosis by Revelle and Suess was subsequently extended and reformulated to yield other relevant buffer factors as fractional CO_2 sensitivities (Egleston et al., 2010; Hain et al., 2018; Sarmiento & Gruber, 2006). In this buffering system, bicarbonate/carbonate contributes approximately 65% of the buffer action, and the approximately residual 35% primarily arises from the acid/base chemistry of boric acid/borate (see the factors α and β in Equation 2a). The net effect on seawater *p*H and CO_2 primarily results from the combined buffering of both carbonate and borate, so that for every unit of CO_2 or other acid added to seawater, only 0.65 units (i.e., 65%) of carbonate ion are consumed (Equation 5a), a conversion that is referred to here as the carbonate proton fraction (CPF; Hain et al., 2015):

$$\frac{\delta_{DIC}CO_3^{2-}}{\delta DIC} \cong -\frac{\delta_{ALK}CO_3^{2-}}{\delta ALK} \cong \frac{\delta_{ALK}HCO_3^-}{\delta ALK} = CPF \approx -0.65 \quad (5a)$$

$$\frac{\delta_{DIC}HCO_3^-}{\delta DIC} = (1 - CPF) \approx 1.65 \quad (5b)$$

$$\frac{\delta_{DIC}CO_2}{CO_2} = \frac{\delta_{HCO3}CO_2}{CO_2} + \frac{\delta_{CO3}CO_2}{CO_2} \cong \left(2 * \frac{1-CPF}{HCO_3^-} - \frac{CPF}{CO_3^{2-}}\right) * \delta DIC \approx \frac{0.66\%}{\mu mol/kg} * \delta DIC \quad (5c)$$

$$\frac{\delta_{ALK}CO_2}{CO_2} \cong \left(2\frac{CPF}{HCO_3^-} + \frac{CPF}{CO_3^{2-}}\right) * \delta ALK \approx \frac{-0.56\%}{\mu mol/kg} * \delta ALK \quad (5d)$$

$$\Delta_{DIC+ALK} lnCO_2 = \Delta_{DIC} lnCO_2 + \Delta_{ALK} lnCO_2 =$$

$$\int \frac{0.66\%}{\mu mol/kg} * \delta DIC + \int \frac{-0.56\%}{\mu mol/kg} * \delta ALK \quad (5e)$$

$$CO_2 = CO_2^{initial} * e^{\left(\frac{0.66\%}{\mu mol/kg} * \delta DIC + \frac{-0.56\%}{\mu mol/kg} * \delta ALK\right)} \quad (5f)$$

where δDIC and δALK refer to differential changes in DIC or ALK and their resulting differential changes in bicarbonate, carbonate ion, or CO_2 are referred to with subscripted DIC or ALK, respectively ($\delta_{DIC/ALK}HCO_3^-$, $\delta_{DIC/ALK}CO_3^{2-}$, or $\delta_{DIC/ALK}CO_2$). An increase in bicarbonate ion due to the addition of DIC or acid (Equation 5b) is approximately balanced by a change in carbonate ion (Equation 5a), so as to obey the constraint of total DIC (see Equation 3a), yielding the full set of partial derivative "sensitivities" of the carbonate buffer species that determine seawater CO_2. Similar to Revelle's expression, the quotient rule is applied to CO_2 (Equation 3d) and then the species sensitivities (Equations 5a–5b) are substituted in, which yields fractional CO_2 change as approximate linear functions of DIC and ALK change (Equation 5c, 5d). The fractional CO_2 effects of changes in DIC and ALK are additive (Equation 5e), with compounding exponential effects on absolute CO_2 (Equation 5f; see also Hain et al., 2018; Marinov, Follows, et al., 2008; Marinov, Gnanadesikan, et al., 2008). Equations 5a–5f refer to the carbon chemistry of seawater before considering equilibrium CO_2 transfers between the global ocean and the atmosphere, which is done in the next section. To clarify the key consequence of Equation 5f, changes in DIC and ALK that individually lower CO_2 by 10% and 20%, respectively, compound to a new CO_2 that is 72% (i.e., 80% of 90%) of the original value. As will be shown, the main effects on ice age CO_2 all cause fractional changes that must be compounded (Equations 5e, 5f), as

opposed to the intuitive and common approach of summing distinct effects on atmospheric CO_2 in absolute ppm terms. In Tables 1–3, a carbonate chemistry solver is used to compute the capacity of different mechanisms to effect CO_2 change, reported in both fractional terms and in terms of absolute concentration (i.e., CO_2 mixing ratio in units of ppm). These results agree well with the approximate analytical solutions (Equations 7–10, 13, 15, 18). Thus, the approximate solutions are used in the discussion below of the chemical basis of different CO_2 effects and the different hypotheses for ice age CO_2 drawdown, while the more accurate carbonate chemistry solver is used in Tables 1–3.

Air–Sea CO_2 Exchange

In the 1950s, based on the rate with which radiocarbon (^{14}C) from aboveground nuclear testing was disappearing from the atmosphere, it became apparent that the entire CO_2 inventory of the atmosphere is exchanged with surface ocean DIC in roughly 5–10 years (Bolin, 1960; Craig, 1957; Revelle & Suess, 1957), indicating that gas exchange is adequately rapid to keep the atmosphere in approximate CO_2 equilibrium with the globally averaged surface ocean. Changes in the DIC, ALK, temperature, or salinity of ocean surface water would change its CO_2 concentration, causing a CO_2 disequilibrium between ocean and atmosphere that then drives net air–sea exchange, which repartitions the CO_2 change between ocean and atmosphere:

$$N_{atm} * \Delta_A CO_2 = -M_{oc} * \Delta DIC = -M_{oc} * \frac{DIC}{R*CO_2} * \Delta_O CO_2 \quad (6a)$$

$$\Delta_{O-A} CO_2 = \Delta_A CO_2 - \Delta_O CO_2 = \left(1 + R * \frac{N_{atm}}{M_{oc}} \frac{CO_2}{DIC}\right) * \Delta_A CO_2 \quad (6b)$$

$$\frac{\Delta_A CO_2}{\Delta_{O-A} CO_2} = \left(1 + R * \frac{N_{atm}}{M_{oc}} \frac{CO_2}{DIC}\right)^{-1} = \Phi \cong 85\% \quad (6c)$$

where $\Delta_{O-A}CO_2$ represents an initial CO_2 disequilibrium between ocean and atmosphere (with a positive value indicating a higher CO_2 in the surface ocean than in the atmosphere), $\Delta_O CO_2$ is the CO_2 change of the ocean during equilibration, $\Delta_A CO_2$ is the total CO_2 change realized in the atmosphere during equilibration, and R is the Revelle buffer factor of the seawater as identified in Equation 3. The terms N_{atm} and M_{oc} refer to the number of gas molecules in the atmosphere and the mass of the ocean, 1.773×10^{20} mol and 1.4×10^{21} kg, respectively (see Table A.1 in Sarmiento & Gruber, 2006). Based on the preceding discussion, if the preindustrial atmosphere was "magically" reduced from 280 to 190 ppm (i.e., to LGM CO_2 levels), the resulting disequilibrium ($\Delta_{O-A}CO_2$) of +90 ppm would be resolved by ocean CO_2 release that adds +76.5 ppm of CO_2 back to the atmosphere (i.e., 85%, identified as Φ), yielding a final atmospheric CO_2 decline of only −13.5 ppm, approximately 15% (1 − Φ) of the initial "magic" atmospheric CO_2 decline.

Likewise, if one unit of carbon was suddenly added to the atmosphere, the "airborne fraction" (Keeling, 1973) of that carbon after equilibration with the bulk ocean would be approximately 15% (Maier-Reimer & Hasselmann, 1987), corresponding to an effective value for R of 10. Alternatively, if the typical Southern Ocean value for R of 14 is assumed, the estimate of the airborne fraction would increase to about 20%. Since this factor simply accounts for the relative size of ocean and atmosphere carbon reservoirs (i.e., N_{atm}/M_{oc} term) and seawater buffering (R), it applies to disequilibria regardless of their cause, not just to the airborne fraction of net CO_2 emissions to the atmosphere. For example, if the chemistry of the ocean were magically changed so that the CO_2 of the surface ocean was reduced from 280 to 190 ppm, after equilibration, both the ocean and the atmosphere will have experienced 85% of the initial 90-ppm CO_2 reduction. The helpful approximation of Φ = 0.85 is used to account for the finite buffering of seawater in the assessment of different ocean-based mechanisms for driving atmospheric CO_2 change (i.e., the factor is included in Tables 1–3 and Figures 3, 6). Importantly, the buffering described here does not include the tendency of the whole ocean to change its alkalinity in response to $CaCO_3$ cycle changes, which is discussed next.

Ocean Alkalinity Budget

Alkalinity is a measure of the history of the net addition of acids and bases to seawater, framed in terms of hypothetical strong acids and bases. In seawater, 546mM HCl + 28mM H_2SO_4 is hypothetically neutralized by 469mM NaOH + 53mM $Mg(OH)_2$ + 10mM $Ca(OH)_2$ + 10mM KOH and then concentrated in the ocean by evaporation. As a result, the positive charge from cations (Na^+, Mg^{2+}, Ca^{2+}, K^+) exceeds the negative charge of hard anions (Cl^-,SO_4^{2-}, excluding soft ions such as HCO_3^-, CO_3^{2-}, $B(OH)_4^-$) by about 2.3 mM—mean ocean alkalinity—with about 35 g dissolved sea salt per kilogram (i.e., roughly per liter) of seawater (For more convenient formulations of seawater-like solutions, see, e.g., Harrison et al., 1980). That is, the weak acid carbonic acid is largely neutralized to the deprotonated forms, bicarbonate and carbonate ion, thereby accounting for almost all the ocean's 38,000 PgC carbon storage. This has raised the ongoing research question of how changes in ocean alkalinity during ice ages may have contributed to atmospheric CO_2 change (Archer & Maier-Reimer et al., 1994; Berger, 1982a, 1982b; Broecker, 1982a, 1982b; Broecker & Peng, 1989; Cartapanis et al., 2016; Hain et al., 2010; Sigman et al., 1998; Toggweiler, 1999; cf. Arrhenius, 1896; Högbom, 1894).

A change in the ocean's mean alkalinity concentration can occur due to (a) addition/removal of water from the ocean associated with ice sheet melting/growth or (b) net addition/removal of acid or base from seawater by exchange with the solid Earth. The first driver is considered to be a *closed system* change because the quantity of solute alkalinity in the seawater is constant, with the ocean alkalinity concentration change achieved simply by the reversible movement of water (solvent) between the ocean and cryosphere. In contrast, the second driver is considered to be an *open system* change because it arises from temporary imbalances between alkalinity input primarily

from weathering and alkalinity removal dominated by the burial of $CaCO_3$ on the seafloor. This same distinction between open and closed system changes can also be applied to carbon. In this case, the relevant carbon reservoir would be the combined carbon inventories of the ocean and the atmosphere, and open system processes would include net land organic carbon changes, organic carbon burial in sediments, and weathering of geologic carbon, as well as the carbon fluxes that come with $CaCO_3$ weathering and burial (Hain et al., 2024).

Earth's natural $CaCO_3$ cycle dominates the open system changes in alkalinity: The primary input of alkalinity to the ocean is by the weathering of limestone on land, with the weathering products brought to the ocean by rivers. This is balanced by a loss of ocean alkalinity through $CaCO_3$ precipitation by calcifying marine organisms in the surface ocean followed by preservation and burial on the seafloor. Importantly, most $CaCO_3$ precipitation in the ocean is followed by dissolution of this same $CaCO_3$. Thus, the factors controlling $CaCO_3$ preservation and burial as opposed to redissolution are critical to the dynamics of ocean alkalinity. A substantial fraction of newly precipitated $CaCO_3$ is preserved and buried on the shallow seafloor, with the resulting burial flux of $CaCO_3$ ultimately removing alkalinity from the ocean, transferring its chemical constituents to the solid Earth. In contrast, a larger fraction of the $CaCO_3$ is dissolved prior to burial on the deeper seafloor, with very little being preserved and buried on seafloor deeper than 4 km. In terms of chemical accounting, treating this dissolution of marine $CaCO_3$ as the prevention of alkalinity loss from the ocean, not as an additional input of alkalinity to the ocean, is favored here.

A long-term balance between weathering and burial of alkalinity is maintained by a negative feedback involving the saturation state of $CaCO_3$ in the deep ocean, as described below in section "Lysocline Constraints". In this feedback, any surplus/deficit of weathering relative to burial would raise/lower global ocean alkalinity and thus the $CaCO_3$ saturation of the deep ocean, causing burial to increase/decrease to remove the imbalance between weathering and burial. As a consequence, when considering specific hypotheses for ice age atmospheric CO_2 drawdown, the effects on atmospheric CO_2 of both "closed system" alkalinity change and the "open system" change in alkalinity that stems from $CaCO_3$ weathering and burial reaching long-term alkalinity mass balance must be taken into account.

Effects on Atmospheric CO_2

Terrestrial Carbon Storage

The reservoir of organic carbon in the terrestrial biosphere includes both living and dead biomass, such as in trees and soil, respectively, and is estimated at roughly 2,500 PgC (see Intergovernmental Panel on Climate Change, 2000). Among biomes, forests are the single greatest contributor (1,150 PgC), with about 560 PgC in boreal forests (9% of land area), 430 PgC in tropical forests (12% of land area), and 160 PgC in temperate forests (7% of the land area), alongside tropical savannas (330 PgC, 15%), temperate grasslands (300 PgC, 8%), wetlands (240 PgC, 2%; or higher Yu et al., 2021), and another 460 PgC in all other land biomes combined (47% of land area). The predominance of data and model results indicates that less carbon was stored on land during the LGM than in the early 21st century (Adams et al., 1990; Crowley, 1991, 1995; Duplessy et al., 1988; Jeltsch- Thömmes et al., 2019; Prentice et al., 1993; Shackleton, 1977).

In addition to these active biospheric carbon pools, there is calculated to be a large carbon pool associated with permafrost. The top 3 m of permafrost soils of the arctic and boreal regions are thought to contain approximately 1,000 PgC (Hugelius et al., 2014), with another 200–1,000 PgC stored at greater depth and in subsea permafrost (Schuur et al., 2015). Permafrost conditions help preserve and accumulate organic carbon over long timescales, yielding a distinct organic carbon reservoir that responds differently to climatic drivers than the combined ecosystems that make up the terrestrial biospheric carbon reservoir. In contrast to the terrestrial biosphere, the size of permafrost carbon stocks during the LGM appears to have been greater than in the Holocene (Crichton et al., 2016; Köhler et al., 2014; Winterfeld et al., 2018).

If the land carbon inventory was to decline by a small differential amount (negative δC_{Land}), that carbon would be released to the atmosphere as CO_2, and it would then equilibrate with the ocean DIC reservoir. The resulting inorganic carbon partitioning is dictated by mass balance (Equation 6a; cf. Högbom, 1894) and by 6-to-1 equilibration (i.e., 6 of 7, or 0.85; Φ) between the ocean (δDIC) and atmosphere (δCO_2; Equation 6b; Keeling, 1973; Maier-Reimer & Hasselmann, 1987; Revelle & Suess, 1957). When it comes to integrating these three differentials (Equation 7a; δCO_2, δDIC, δC_{Land}) for a substantial change in land carbon storage, Equation 6c can be used to compute the realized ocean DIC change (Equation 7b), and it can be combined with Equation 5c to compute the resulting CO_2 change (Equation 7c). For example, reducing the land carbon reservoir from 2,500 to 2,400 PgC (negative δC_{Land}) raises atmospheric CO_2 by 3.4% (Equation 7d).

$$\delta C_{Land} = (-N_{atm} * \delta CO_2 - M_{oc} * \delta DIC) * \frac{12\ gC}{mol} \quad (7a)$$

$$\delta_{DIC} CO_2 = -\Phi * \frac{\frac{mol}{12gC}}{M_{oc}} * \delta C_{Land} \quad (7b)$$

$$\frac{\delta_{Land} CO_2}{CO_2} = \Phi * \frac{\frac{mol}{12gC}}{M_{oc}} * \frac{\delta C_{Land}}{\delta_{Land} DIC} * \frac{-\delta_{DIC} CO_2}{CO_2} = \Phi * \frac{-3.9\%}{100 PgC} * \delta C_{Land} \quad (7c)$$

$$\Delta_{Land} ln CO_2 \approx \Phi * \int_{2500 PgC}^{2400 PgC} \frac{-3.9\%}{100 PgC} * \delta C_{land} = +3.4\% \quad (7d)$$

In Equation 7, δCO_2 refers to the change in CO_2 concentration in either the atmosphere or the surface ocean because the two are assumed to be in equilibrium. Based on the preceding, 6 of 7 carbon atoms absorbed by an expansion of the land carbon reservoirs ultimately come from the ocean

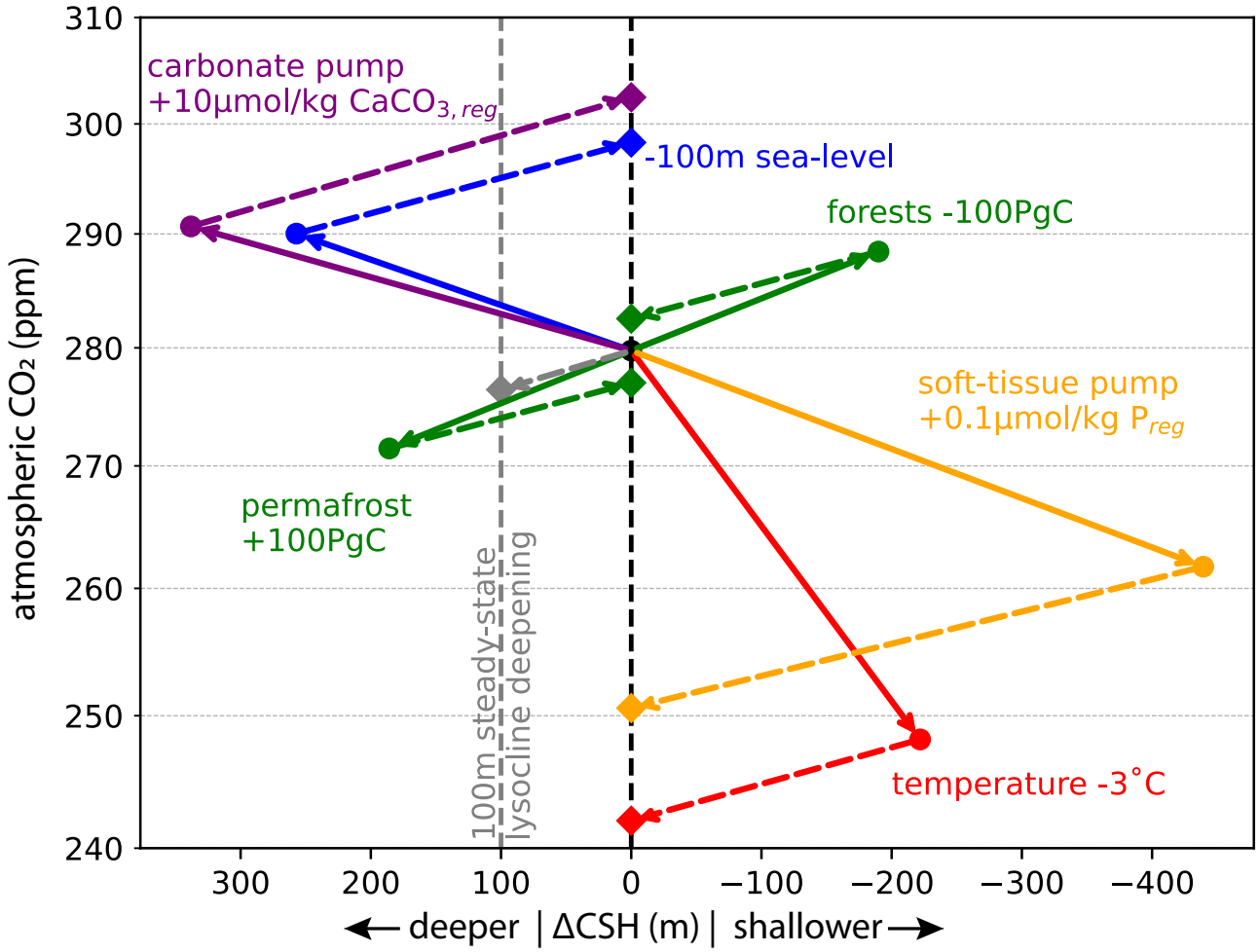

Figure 3. Sensitivities of CO_2 to carbon cycle changes. Overview of the CO_2 responses caused by changes in land carbon storage (green), ocean temperature (red), the volume of the ocean as affected by land ice (i.e., sea-level, blue), and the soft-tissue (orange) and carbonate (purple) components of the biological pump. These changes have distinct direct exponential effects on CO_2 (*y*-axis is logarithmic) as well as on $CaCO_3$ saturation in the deep ocean (i.e., linear effect on the depth of the calcite saturation horizon [CSH], on the *x*-axis), which are shown with solid arrows. Dashed arrows indicate CO_2 and CSH change caused by transient differences between $CaCO_3$ weathering and burial, as part of the carbonate compensation response that acts to restore a balanced ocean alkalinity budget. A deepening of the steady-state lysocline (and thus the CSH), for example, in response to reduced $CaCO_3$ burial on the continental shelves, is shown in grey. The indirect CO_2 effect from carbonate compensation generally magnifies the direct CO_2 effects, except for land carbon changes, which are nearly canceled by carbonate compensation. The mean ocean temperature, salinity, DIC, and ALK are taken from Table A.3 in Sarmiento and Gruber (2006), and carbonate chemistry is solved using $PyCO_2sys$ (Humphreys et al., 2022) assuming a constant Φ of 0.85 to account for equilibration with the atmosphere. For the soft-tissue and carbonate pump, regenerated DIC and ALK are assumed to be concentrated in the deeper half of the ocean ($X_{STP} = X_{CP} = 2$; Equations 16d, 16e). Detailed results are given in Table 1.

(Φ = 85%), and only 1 of 7 comes from the atmosphere (1 − Φ = 15%) when assuming an R of 10 in Equation 6c; or 4 of 5 partitioning (Φ = 80%) when assuming an R of 14, which is more approporiate for the Southern Ocean. Conversely, a sudden land carbon release of 100 PgC might instantaneously raise CO_2 by as much as 47 ppm, but 6 of 7 of those CO_2 molecules will be absorbed by the ocean, such that the equilibrium CO_2 change after a few centuries is only about +8 ppm (+3%, Table 1, Figure 3). In this latter case, 1 − Φ can be identified as the "airborne fraction" of anthropogenic fossil fuel carbon emissions, the fraction that will remain in the atmosphere after equilibration with the bulk ocean (Joos et al., 2013; Keeling, 1973; Maier-Reimer & Hasselmann, 1987), when appropriately accounting for changes in land carbon storage (Gloor et al., 2010). This general differential partitioning of added carbon between ocean and atmosphere can be framed either as the fractional sensitivity of CO_2 ($\delta_{Land}CO_2/CO_2$) to a differential change in land carbon storage (δC_{Land}) in Equation 7c, or as the integrated fractional CO_2 change ($\Delta_{Land}\ln CO_2$) resulting from a large change in land carbon (ΔC_{Land}; i.e., based on the integration bounds) in Equation 7d. In the rest of this article, this same notation is used, where the differential change in causative factor X (δX) integrates to some larger change (ΔX), where the differential fractional sensitivity of CO_2 to X ($\delta_X CO_2/CO_2$) integrates to some proportional atmospheric CO_2 change ($\Delta_X \ln CO_2$)—hence the logarithmic CO_2 axis in Figures 3 and 6. Further below, it is described how the ocean acidification from such land carbon release would drive transient $CaCO_3$ dissolution to raise ocean alkalinity such that only about 1 of 15 of the CO_2 molecules would ultimately remain in the atmosphere.

Table 1. Sensitivity of Atmospheric CO_2 to Earth System Changes

forcing	effect	value	direct CO_2	compensated CO_2	$\Delta CaCO_3$	direct ΔCSH	compensated ΔCSH	mean ocean DIC	mean ocean ALK	deep ocean O_2
			(ppm)	(ppm)	(μmol/kg)	(m)	(m)	(μmol/kg)	(μmol/kg)	(μmol/kg)
modern reference			280	280	+0	3656	3656	2249	2364	165
land C uptake		100 PgC	271 (−3%)	277 (−1%)	-5	186	0	2238	2353	165
land C release		−100 PgC	288 (+3%)	283 (+1%)	+5	−190	−0	2260	2375	165
temperature	DIC speciation (K_0, K_1, K_2)	−3.0 °C	248 (−11%)	248 (−11%)	+0	0	0	2249	2364	191
temperature	$CaCO_3$ saturation (K_{sp})	−3.0 °C	280 (0%)	273 (-2%)	+7	−222	0	2256	2377	165
temperature	combined	−3.0 °C	248 (-11%)	242 (-13%)	+7	−222	0	2256	2377	191
ice volume	DIC, ALK, & AOU concentration	−100 m	284 (+1%)	290 (+4%)	−6	192	0	2305	2418	161
ice volume	salinity & Ca concentration	−100 m	286 (+2%)	284 (+2%)	+1	-46	-0	2250	2367	163
ice volume	seafloor pressure (K_{sp})	−100 m	280 (+0%)	283 (+1%)	−3	110	0	2246	2358	165
ice volume	all combined	−100 m	290 (+4%)	298 (+7%)	-8	257	0	2303	2414	159
lysocline change	steady-state deepening	+100 m	280 (+0%)	276 (−1%)	+3	-11	100	2252	2370	165
biological pump	organic matter (P_{reg})	+0.1 μmol/kg	262 (−6%)	251 (−10%)	+12	-439	-0	2261	2389	131
biological pump	regenerated $CaCO_3$	+10 μmol/kg	291 (+4%)	302 (+8%)	−10	338	0	2239	2344	165

Note: The sensitivities of atmospheric CO_2 and ocean carbonate chemistry are based on known principles of seawater carbon chemistry, can be derived analytically, and computed without analytical approximation using established carbon chemistry solver software (PyCO2sys was used to compute this table; Humphreys et al., 2022). From a modern reference with a preformed CO_2 of 280 ppm and a calcite saturation horizon (CSH) at 3,656 m depth, the isolated sensitivities are computed for each of the main forcings on atmospheric CO_2: land carbon storage, mean ocean temperature, ice and ocean volume, as well as the effect of the biological pump to sequester respired soft-tissue carbon and re-dissolved $CaCO_3$ alkalinity. (1) The "direct effect" and (2) the "compensated (i.e., net) effect" are distinguished. The "direct CO_2 effect" is the atmospheric CO_2 change due only to the immediate forcing factor, whereas the "compensated CO_2 effect" includes the direct effect and the atmospheric CO_2change caused by resulting "open-system" changes in mean ocean alkalinity, assuming that the CSH is perfectly restored back to the reference depth by net addition or removal of dissolved $CaCO_3$ (as per dashed arrows in Figure 3). The exception is "lysocline change," in which an imposed increase in $CaCO_3$ rock weathering on land (or a reduction in $CaCO_3$ burial on the continental shelves or in the $CaCO_3$ rain rate out of the surface ocean) adds "dissolved $CaCO_3$" ($\Delta CaCO_3$) to the ocean, deepening the CSH by 100 m. "Direct" and "compensated" ΔCSH refer to the change in CSH depth due to the indicated forcing prior to and after the response of the ocean's $CaCO_3$fluxes (positive being a deepening). A positive value for $\Delta CaCO_3$ indicates the net addition of dissolved $CaCO_3$ to the ocean, due to a temporary excess in $CaCO_3$ rock weathering relative to $CaCO_3$ burial in the ocean. For the forcings involving the biological pump, two-fold deep ocean concentration factors are assumed for the storage of regenerated phosphorus and alkalinity (X_{STP} and X_{CP} in Equations 16e, 16f in Box 2), as appears appropriate for changes in the Southern Ocean. Percentages in the CO_2 columns refer to the proportional change in atmospheric CO_2 relative to the reference value of 280 ppm. The reference deep ocean conditions are based on mean ocean temperature, salinity, dissolved inorganic carbon (DIC) and alkalinity (ALK) from Table A.3 in Sarmiento and Gruber (2006). The reference preformed CO_2 (Hain et al., 2010) is based on the same mean ocean properties but adjusted for respired organic matter as measured by mean ocean apparent oxygen utilization from the same Table A.3, and further adjusted for re-dissolved $CaCO_3$ assuming a global mean ALK_{reg} of 80 μmol/kg, accounting separately for the action of the soft-tissue and carbonate components of the biological pump (see Box 1).

Temperature Effect

The solubility of CO_2 (K_0) and the first and second deprotonation constants of carbonic acid (K_1, K_2) are all significantly sensitive to temperature (Equation 2). With cooling, K_0 increases (CO_2 becomes more soluble) while K_1 and K_2 decrease (carbonic acid and bicarbonate tend to deprotonate less). As a result, effective CO_2 solubility (K_0 times K_1 in Equation 3d) is relatively insensitive to cooling, while seawater *p*H (Equation 3c) rises substantially due to decreasing K_2. Hence, the K_0, K_1, and K_2 terms compound to yield proportionally equivalent changes in dissolved CO_2 and H^+, with a differential temperature (δT) change causing a linear change in *p*H and a fractional change in CO_2 (Hain et al., 2018):

$$\frac{\delta_T CO_2}{CO_2} \cong \Phi * \left(\frac{1}{K_2}\frac{\delta_T K_2}{\delta T} - \frac{1}{K_0}\frac{\delta_T K_0}{\delta T} - \frac{1}{K_1}\frac{\delta_T K_1}{\delta T}\right) * \delta T \approx \Phi * \frac{4\%}{^\circ C} * \delta T \quad (8a)$$

Following Equation 8a, for each degree of cooling, seawater CO_2 declines by approximately 4% such that atmospheric CO_2 must be transferred into the ocean to return to air–sea equilibrium. For a global mean ocean cooling of 3 °C, such as from 4 to 1 °C into the LGM, the percentage change in atmospheric CO_2 is thus approximated as

$$\Delta_T ln CO_2 \approx \Phi * \int_{4^\circ C}^{1^\circ C} \frac{4\%}{^\circ C}\delta T = -10\% \quad (8b)$$

This approximate solution—a 10% (−27 ppm) CO_2 reduction predicted for a 3 °C cooling—is in good agreement with a more accurate calculation with a carbon chemistry solver (−11%, −32 ppm; see Table 1) and with numerical carbon cycle model integrations yielding a 21- to 30-ppm CO_2 decrease when forced with reconstructed LGM sea surface temperatures (Kohfeld & Ridgwell, 2009, and references therein). These estimates do not yet take into account the

effect of temperature on the expected response of global mean ocean alkalinity, which slightly magnifies the CO_2 decline per cooling.

Ocean Volume Effect

Ice ages involve the large-scale sequestration of water into continental ice sheets, and the repeated removal and release of that water from the ocean is the principal driver for reconstructed oscillations in sea-level, with high stands similar to the modern sea-level (Kopp et al., 2013) and glacial low stands up to 135 m below current (e.g., Bard et al., 1990; Elderfield et al., 2012; Fairbanks, 1989; Gowan et al., 2021; Grant et al., 2012; Lambeck et al., 2014; Figure 1). Any such closed system change would have predictable consequences for global mean seawater carbonate chemistry and atmospheric CO_2, as well as a host of less predictable environmental effects on carbon cycling in the coastal zone as it shifts onto and off the continental shelf. As to the direct *ocean volume effect* on CO_2, 100 m of sea-level lowering (i.e., δSL of −100 m) multiplied by the ocean's area (A_{oc}) corresponds to an approximately 2.7% reduction in ocean volume ($\delta V_{oc}/V_{oc}$). With less water in the ocean, the concentration of solutes increases proportionally (Equation 9a) to cause two separable effects of approximately equal importance for CO_2. First, the salinity (S) of seawater rises by almost 1 salinity unit (a δS/S of +2.7%, including a +2.7% increase in total boron), with effects on the carbonate chemistry equilibrium constants—K_0, K_1, and K_2 in Equations 2 and 9b—that raise CO_2 by about +6 ppm (+2.15%, Table 1). Second, ocean DIC and alkalinity are concentrated by approximately 2.7%, with the effect of increasing carbonic acid, bicarbonate, carbonate, borate, and boric acid proportionally by 2.7%. This, by itself, raises CO_2 by +4 ppm (i.e., +1%, Table 1; the δS/S term in Equation 9b includes the effect of the+2.7% increase in borate alkalinity; see also Equations 5c and 5d).

$$\frac{\delta V_{oc}}{V_{oc}} = \frac{A_{oc}}{V_{oc}} * \delta SL \approx \frac{\delta m_{oc}}{m_{oc}} = -\frac{\delta S}{S} = -\frac{\delta DIC}{DIC} = -\frac{\delta ALK}{ALK} \quad (9a)$$

$$\frac{\delta_S CO_2}{CO_2} \cong \Phi * \left(\frac{1}{K_2}\frac{\delta_S K_2}{\delta S} - \frac{1}{K_0}\frac{\delta_S K_0}{\delta S} - \frac{1}{K_1}\frac{\delta_S K_1}{\delta S} + \frac{1}{S}\right) * \delta S$$

$$= \Phi * \left(2.15\% + \frac{1}{S}\right) * \delta S \approx 4\% * \delta S \quad (9b)$$

The combined fractional CO_2 effects of higher salinity and carbonate and borate species concentrations (Equation 9b) can be reframed as a linear function of ocean volume change and sea-level change (Equation 9c), which is useful because sea-level reconstructions (e.g., Figure 1) are the primary observational constraint on ocean volume changes. Integrating this sea-level CO_2 sensitivity while accounting for equilibration with the atmosphere (Φ = 0.85; Equation 6) results in a +10 ppm (+4%) atmospheric CO_2 increase for 100 m of sea-level lowering (Equation 9d, where S = 34.7, ocean area A_{oc} is 3.58×10^{14} m^2, and ocean volume V_{oc} is 1.34×10^{18} m^3; Table A.1 in Sarmiento & Gruber, 2006). To clarify the dS/S term: (a) raising total boron without alkalinity change lowers *p*H and raises CO_2, (b) proportionally raising total boron and borate alkalinity has no effects on *p*H and CO_2, (c) proportionally raising DIC and carbonate alkalinity has no effect on pH but HCO_3^-, CO_3^{2-} and CO_2 all rise by dS/S.

$$\frac{\delta_{SL} CO_2}{CO_2} = \Phi * (-2.15\% * S - 1) * \frac{\delta V_{oc}}{V_{oc}} \approx \Phi * -1.75 * \frac{A_{oc}}{V_{oc}} * \delta SL \quad (9c)$$

$$\Delta_{SL} ln CO_2 \approx \Phi * \int_{0m}^{-100m} -0.047 \frac{\%}{m} \delta SL = +4\% \quad (9d)$$

Thus, taking all of the above effects together, the atmospheric CO_2 rise for an ocean volume decline equivalent to 125 m of sea-level fall is approximately 5%, in good agreement with carbonate chemistry solver results (+5%, +13 ppm; Table 2) and with numerical carbon cycle model integrations yielding a 12- to 16-ppm CO_2 increase for simulations isolating the sea-level effect at low stand (Kohfeld & Ridgwell, 2009; see also Lhardy et al., 2021a). As with the temperature and land carbon storage changes, this projected CO_2 change is before taking into account the response of $CaCO_3$ burial and thus ocean alkalinity. When the alkalinity change (due to "$CaCO_3$ compensation") is included, the ocean volume-driven CO_2 increase almost doubles (to +8%, +23 ppm; Table 2).

Biological Pump

Productivity, Export, and Regeneration

Photosynthesis by phytoplankton floating in the sunlit surface ocean converts CO_2 into the organic carbon of biomass. This reduces DIC, which lowers the dissolved CO_2 concentration of surface waters largely by raising its *p*H (Equations 3, 5; Figure 2). Phytoplankton metabolism, decomposition and metabolism by microbes and grazing and respiration by zooplankton and higher trophic levels oxidize the organic carbon of the phytoplankton biomass back to DIC, reversing the carbonate chemistry effects of (and consuming the oxygen produced by) biomass growth. These processes can be represented by the following chemical equation, in which flow to the right represents photosynthesis by phytoplankton and flow to the left represents respiration by all organisms:

$$106 * H_2CO_3 + 16 * NO_3^- + HPO_4^{2-} + 16 * H_2O + 18 * H^+ \Leftrightarrow (CH_2O)_{106}(NH_3)_{16}(H_3PO_4) + 138 * O_2 \quad (10a)$$

This formulation includes on its left-hand side the dominant inorganic forms of the major nutrients nitrogen and phosphorus—nitrate (NO_3^-) and singly protonated phosphate (HPO_4^{2-})—as well as protons to balance the charge. The right-hand side represents soft-tissue biomass with a C:N:P ratio of 106:16:1, following the canonical major nutrient-to-carbon stoichiometry of marine plankton derived by Alfred Redfield (1934), although subsequent work indicates a slightly higher average carbon content and substantial biogeographic variation in the C:N:P ratios of phytoplankton (Anderson & Sarmiento, 1994; Li & Peng, 2002; Martiny et al., 2013; Paulmier et al., 2009; Takahashi et al., 1985; Teng et al.,

2014). In photosynthetic growth, the consumption of protons associated with the assimilation of nitrate and phosphate into biomass corresponds to a small increase in ALK, further lowering CO_2 (Morel & Hering, 1993, see also Wolf-Gladrow et al., 2007). Hence, Equation 10b, where the fractional CO_2 drawdown ($\delta_{STP}CO_2/CO_2$; STP referring to "soft-tissue pump") is a linear function of photosynthetic growth of "soft-tissue" biomass and where the concentration equivalent of that biomass is usefully framed in terms of the net conversion from dissolved phosphate to organic matter–bound phosphorus (δP referring to a differential conversion from phosphate to organic P):

$$\frac{\delta_{STP}CO_2}{CO_2} = \Phi * \left(-106 * \frac{\delta_{DIC}CO_2}{CO_2} - 18 * \frac{\delta_{ALK}CO_2}{CO_2}\right) * \delta P$$

$$\approx \Phi * \frac{-70\%-10\%}{\mu molP/kg} * \delta P = \Phi * \frac{-80\%}{\mu molP/kg} * \delta P \quad (10b)$$

That is, if phytoplankton draw down phosphate (positive δP), nitrate, and CO_2 according to a given stoichiometry, then the DIC decrease and ALK increase associated with that growth act to lower surface ocean CO_2 and drive ocean carbon uptake from the atmosphere in a predictable ratio to the phosphate drawdown. For example, if 0.1 μmol/kg of phosphate is utilized with the C:N:P stoichiometry of 106:16:1, the corresponding net carbon fixation in surface waters (ΔC_P, where C_P refers to biological pump C storage) is 178 PgC (Equation 10c).

$$\Delta C_P = 106 * \frac{12gC}{\mu molP/kg} * M_{oc} * \Delta P = 1781 \frac{PgC}{\mu molP/kg} \quad (10c)$$

A common misconception about the ocean's biological pump is that the amount of biological pump C storage (C_P) equates to the amount of CO_2 removed from the atmosphere. However, the 178 PgC of carbon storage associated with 0.1 μmol/kg phosphate drawdown from surface waters integrates to a 6.5% reduction in atmospheric CO_2 once the surface ocean has equilibrated with the atmosphere (Equation 10d) and hence only causes an approximately 40-PgC (~19 ppm) reduction in atmospheric CO_2.

$$\Delta_{STP} lnCO_2 \approx \Phi * \int_0^{0.1\mu\frac{mol}{kg}} \frac{\delta_{STP}CO_2}{CO_2} = -6.5\% \quad (10d)$$

Alternatively, when using the 117:16:1 C:N:P stoichiometry of Anderson and Sarmiento (1994), an approximate 7.1% CO_2 reduction is found, which is marginally greater than accurate carbonate chemistry solver results in Table 1 (−6%, −18 ppm). The small proportion of carbon removed from the atmosphere can be understood by considering where inorganic carbon would go if an equivalent amount of carbon were to be released from land carbon reservoirs. Most would end up as DIC in the voluminous deep ocean, leaving only about 15% of this carbon as CO_2 in the atmosphere (i.e., 1 − Φ as in Equation 6).

A second misconception regarding the ocean's biological pump is that it involves the accumulation of organic matter. Unlike the forests and permafrost on land that store thousands of PgC, the total open ocean planktonic carbon inventory is estimated at only about 1 PgC (Falkowski, 1994). Most of that standing stock of plankton and nekton in surface waters is decomposed within the surface mixed layer so as to regenerate the carbon and nutrients to their inorganic forms and undo the chemical effects of biomass production. This decomposition back to DIC in the surface ocean occurs almost entirely within months of the organic carbon having been produced by photosynthesis. The critical aspect of surface ocean biological production for atmospheric CO_2 is that a fraction of the organic matter is exported out of the surface mixed layer and into the ocean interior ("export production"), mostly as sinking particles (Bender et al., 1987; Dugdale & Goering, 1967). This exported organic matter is also almost entirely remineralized, but in the ocean interior, with the respiration of the organic carbon producing a stoichiometric amount of DIC and (acidic) nutrients while also consuming dissolved oxygen (Equation 10a, the leftward reaction; Anderson, 1995; Anderson & Sarmiento, 1994; Redfield, 1934; Redfield et al., 1963; Sarmiento & Gruber, 2006). The transfer of carbon, (negative) alkalinity, and nutrients from the surface mixed layer to the ocean interior has no immediate effect on the global ocean's inventory or mean concentration of these constituents. However, it causes the carbonate chemistry of surface waters to be different from the mean ocean, and it is only the surface that equilibrates with the atmosphere. Hence, export production changes surface carbonate chemistry relative to the mean ocean, maintaining a lower surface ocean's concentration of CO_2 as it continuously "pumps" carbon and other constituents into the ocean interior. This, in turn, causes a net uptake of atmospheric CO_2. This set of processes is

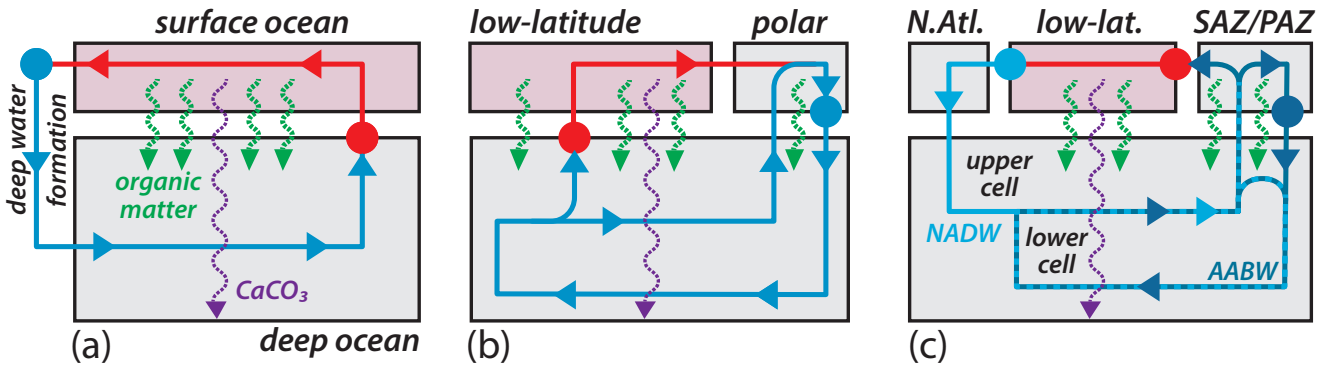

Figure 4. Conceptual models of the ocean's biological pump. The development of the understanding of the biological pump can be summarized as a succession of three major conceptual advances. (a) Nutrient-limited export production sequesters carbon (but also alkalinity) from the surface ocean into the deep ocean interior (Broecker, 1982a, 1982b; Volk & Hoffert, 1985). When first proposed, it was implicitly assumed that surface water returns to the deep ocean through deep water formation largely sourced from the low latitude surface, in the form of modern NADW. In this context, a rise in ocean nutrient inventories was proposed to enhance the biological pump during ice ages. In a more accurate view of the modern ocean (b), the biological pump does not operate at maximal efficiency with respect to its nutrient inventory because most of the deep ocean is filled from the polar ocean surface where nutrients are not completely utilized for export production. In the first studies to represent this (Knox & McElroy, 1984; Sarmiento & Toggweiler, 1984; Siegenthaler & Wenk, 1984; see also Keeling & Bolin, 1968), the polar region was implicitly the Southern Ocean, although the polar surface box was fed in part from low latitude surface, unlike in the modern Southern Ocean. In the context of (b), drawdown of unused Southern Ocean nutrients was proposed to drive ice age atmospheric CO 2 reductions. More recent conceptions (c) combine (a) and (b): The low-nutrient North Atlantic and the high-nutrient Antarctic Zone compete to fill the deep ocean with distinct water masses (NADW, AABW) that differ in their burden of preformed (unused) nutrients (Bolin & Stommel, 1961; Sigman & Haug, 2003; Stommel & Arons, 1959; Toggweiler, 1999; Toggweiler et al., 2003). The dashing of the lower cell overturning loop in (c) is to indicate that AABW is an admixture of dense water formed in the Antarctic Zone surface (especially the Polar Antarctic Zone, PAZ) and deep water formed in the North Atlantic and the Subantarctic Zone (SAZ) of the Southern Ocean (Gebbie & Huybers, 2010). In this context, it has been proposed that, during the ice ages, reduced overturning or additional sea ice introduced barriers to the release of sequestered carbon from the Antarctic Zone to the atmosphere, effectively leaving the North Atlantic and Subantarctic Zone to indirectly ventilate the abyssal ocean, which strengthens both the soft-tissue and carbonate components of the biological pump. In all mechanisms, whole ocean alkalinity responds to the forced change in deep ocean $CaCO_3$ saturation state, further changing atmospheric CO_2. This effect is more pronounced with explicit separation of the interior into mid-depth and abyssal layers (Boyle, 1988b; Keir, 1988; Hain et al., 2010; Toggweiler, 1999).

commonly referred to as the *biological pump* (Volk & Hoffert, 1985). The term "soft-tissue pump" specifically refers to the effects of organic biomass alone (Equation 10a), excluding the biomineral hard parts (Equations 12 and 13). As discussed later, the biomineral flux out of the surface ocean includes $CaCO_3$, which extracts both DIC and alkalinity from the surface, and its effects on the ocean's DIC and ALK distribution are referred to as the "carbonate pump" (see Box 1).

Finally, addressing a third misconception, an increase in export production from the surface is not strictly required for the biological pump to sequester more carbon in the ocean interior. The strength of the biological pump in any given region is controlled by the ratio of (a) the rate at which organic carbon is exported from the surface to (b) the rate at which CO_2- and nutrient-rich deep water is returned to the ocean surface; the higher the ratio, the stronger the pump. As described later, this ratio is reflected in the degree to which the major nutrients are consumed in surface waters.

The biological pump in the ocean was recognized early in the search for the origin of glacial/interglacial CO_2 change (Broecker, 1982a, 1982b; Figure 4a). Biological pump hypotheses first revolved around the low latitude ocean, where, to first approximation, the major nutrients are (and will essentially always be) completely consumed from surface waters. These hypotheses necessarily revolved around the ocean major nutrient reservoirs and/or the carbon-to-nutrient ratios of organic matter export from the surface ocean. The critical role of the high latitude ocean (and specifically the "Southern Ocean" around Antarctica) in the biological pump then came into focus, broadening the range of mechanisms by which oceanic changes could enhance the biological pump so as to lower atmospheric CO_2 during ice ages (e.g., Knox & McElroy, 1984; Sarmiento & Toggweiler, 1984; Siegenthaler & Wenk, 1984; Figure 4b).

The sinking flux of soft-tissue organic matter consists of particles that undergo decomposition as they sink, leading to a progressive decline in the particle flux with increasing depth, with most of the sinking flux respired near the surface and only a small proportion reaching the deep ocean (Buesseler et al., 2007, 2020; Karl et al., 1988; Martin et al., 1987; Pavia et al., 2019). Due to the temperature sensitivity of respiration rates, sinking particles may reach less deeply into the ocean before being decomposed under global warming (Boscolo-Galazzo et al., 2018, 2021; López-Urrutia et al., 2006; Marsay et al., 2015; Passow & Carlson, 2012; Sarmento et al., 2010; Wohlers et al., 2009) and may have sunk to greater depths during the ice ages (Kwon et al., 2009; Matsumoto, 2007), with other probable changes likely also affecting the attenuation of particle flux with depth (Taucher et al., 2014) and organic carbon flux to the seafloor (Jeltsch- Thömmes et al., 2019; Roth et al., 2014; Tschumi et al., 2011). Under most scenarios, a deepening of remineralization lowers atmospheric CO_2. However, the amplitude of this effect (i.e., the degree of change in the soft-tissue pump) depends on the response of surface nutrient

distributions, which, in turn, depends on the response of surface ocean phytoplankton production. Thus, different assumptions about the phytoplankton response lead to starkly different sensitivities of atmospheric CO_2 to a deepening of organic matter remineralization, ranging from minimal change to up to nearly half of the ice age decline (Kwon et al., 2009; Matsumoto, 2007; Sigman et al., 1998). There are also dynamics related to the calcium carbonate described in the section "Mean Ocean Alkalinity Change," about which there is more confidence: An increase in the sinking depth of soft-tissue organic matter should concentrate biological CO_2 sequestration in the deep ocean, driving a transient reduction in seafloor $CaCO_3$ burial, which increases mean ocean alkalinity and thus lowers atmospheric CO_2 (Boyle, 1988a, 1988b; Sigman et al., 1998; Toggweiler, 1999).

Preformed Versus Regenerated Nutrients and Ocean Carbon Storage

Because of the known stoichiometry of organic matter and the measurement of apparent oxygen utilization (AOU), which refers to the observed oxygen depletion relative to saturation with the atmosphere and serves as an estimate of true oxygen utilization (Arons & Stommel, 1967; Redfield, 1934), it is possible to map out the distribution of respired carbon and the corresponding regenerated nutrients in the ocean (Broecker, 1974; Broecker et al., 1985). The average ocean concentrations of phosphate and AOU are approximately 2.2 μmol/kg and 154 μmol/kg, respectively (see Table A.3 in Sarmiento & Gruber, 2006), suggesting that only about half of the ocean's total phosphate is *regenerated* from organic matter. Accordingly, the other half of the phosphate (known as *preformed*) was not utilized in the surface but was instead carried from the sea surface into the ocean interior by ocean circulation and mixing:

$$P_{total} = P_{preformed} + P_{regenerated} \approx P_{preformed} + \frac{AOU}{138} \quad (11)$$

The modern ocean holds almost 2,000 PgC of respired (i.e., regenerated) carbon sequestered via the soft-tissue component of the biological pump (Box 1), on par with the quantity of organic carbon in all forests on land or locked away in permafrost. If marine productivity and carbon export were to stop, atmospheric CO_2 would almost double (e.g., Kwon et al., 2011). Preformed nutrients reflect a missed opportunity for biological carbon sequestration—a measure of the inefficiency of the modern biological pump. This important distinction is relevant to the early hypothesis of an increase in the ocean's total phosphate inventory as the cause for a stronger biological pump (Broecker, 1982a, 1982b; Jeltsch-Thömmes & Joos, 2023; Roth et al., 2014; Tsandev et al., 2008; Wallmann, 2003; Wallmann et al., 2016). Only in the low- and mid-latitude ocean does the supply of the major nutrients phosphate and nitrate appear to represent the ultimate limiting factor for biological productivity (Figure 4a). Thus, in calculating the CO_2 drawdown expected from an increase in the ocean's phosphate reservoir, it should be taken into account that this phosphate inventory increase is unlikely to be met by a proportional increase in high latitude biological production, with a substantial portion of the added phosphate becoming preformed (Sigman et al., 1998; cf., Lauderdale et al., 2020).

Polar ocean productivity appears to be co-limited by "trace" nutrient supply (chiefly iron; e.g., Boyd et al., 2007) and photosynthetically active radiation from sunlight in the surface mixed layer, such that polar surface water is replete in unused (i.e., preformed) "major" nutrients phosphate and nitrate (Figure 4b). Converting some of the polar ocean preformed phosphate into regenerated phosphate during the ice ages would increase the ocean interior inventory of sequestered DIC, lowering atmospheric CO_2 (Knox & McElroy, 1984; Sarmiento & Toggweiler, 1984; Siegenthaler & Wenk, 1984). The mechanism that is shared by this hypothesis and that of an ice age increase in the whole ocean phosphate inventory (Broecker, 1982a, 1982b) is an increase in the quantity of regenerated phosphate, which would be accompanied by a decline in ocean interior oxygenation (Equation 11). All else equal, the expectations are that (a) an increase in phosphate inventory would strengthen the soft-tissue pump by increasing low- and mid-latitude productivity, while (b) a relative increase in trace nutrient (e.g., iron) supply to the polar surface would raise polar productivity so as to strengthen the soft- tissue pump. The effect of a decrease in the gross supply of phosphate from the ocean interior, a third mechanism put forward for enhancing the biological pump during ice ages (François et al.,1997; Sarmiento & Toggweiler, 1984), requires more careful consideration. Deep water upwelling is an important iron source to the polar ocean surface, but it is stoichiometrically deficient relative to nitrate and phosphate. Atmospheric and coastal iron inputs can compensate for this deficiency, and a reduction in polar upwelling would tend to make that compensation more important (e.g., Lefèvre & Watson, 1999; Moore, 2016; Moore et al., 2013; Sigman & Hain, 2012). Moreover, even without any decoupling of the phosphate and iron supply, a longer residence time of water at the sunlit surface may lead to iron recycling and thus more complete phosphate drawdown in those surface waters (e.g., Rafter et al., 2017). As a result, a reduction in polar upwelling is expected to tend to lower productivity but enhance major nutrient consumption, strengthening the biological pump.

Box 1. Soft-Tissue and Carbonate Pumps

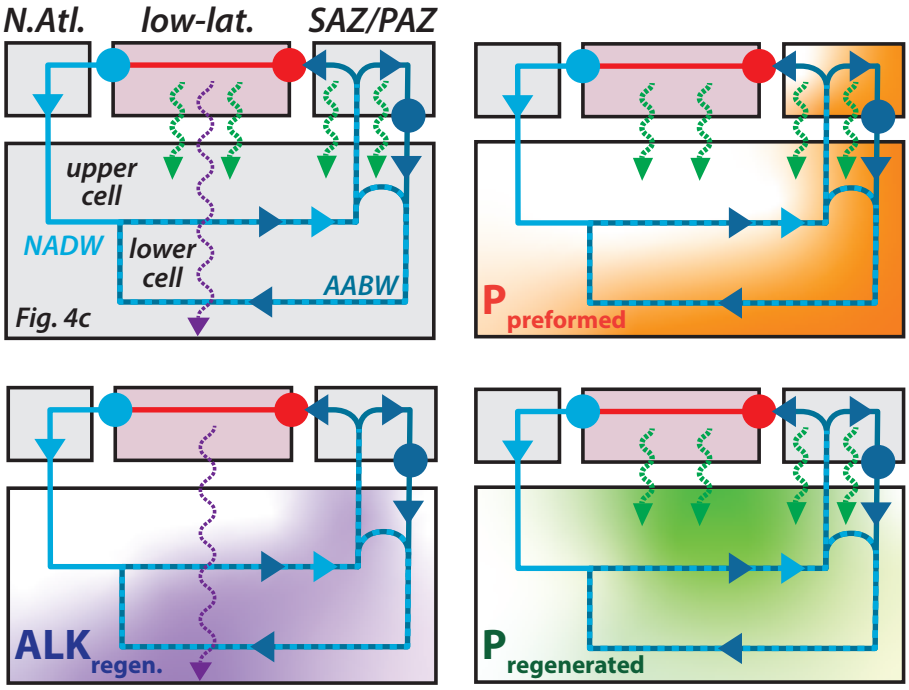

The soft-tissue and $CaCO_3$ components of the biological pump both operate through the sinking ("rain") of biogenic material produced by the surface planktonic ecosystems, but the soft-tissue pump (STP, shown as green) and carbonate pump (CP, shown as purple) differ in three important ways. First, the STP primarily acts to sequester DIC (alongside regenerated phosphorus nutrient, $P_{regenerated}$) and thus acts to draw down atmospheric CO_2, whereas the CP primarily sequesters alkalinity ($ALK_{regenerated}$) so as to raise atmospheric CO_2. Second, microbial heterotrophy in the dark ocean interior rapidly decomposes the organic matter rain, thereby releasing respired carbon (i.e., regenerated DIC) and regenerated nutrients shallow in the water column (green shading) whereas $CaCO_3$ is more resistant to losses while sinking, is buried on the shelf and shallow to mid-depth seafloor, and dissolves mostly when it rains onto the deep seafloor, below about 3.7 km (purple shading). Third, calcifying plankton such as coccolithophores thrive in low-nutrient, low-latitude settings while silicifying diatoms dominate productivity in the polar ocean, where the concentration of unused nutrients is high at the surface. For these reasons, the STP and CP are effectively decoupled, and their respective scaling relationships for their integrated effect on the Earth System differ, yielding different carbon cycle feedbacks. The STP is closely tied to the total available phosphate inventory and the nutrient conditions in the polar ocean surface, where nutrients can go unused in the surface (such as phosphate, $P_{preformed}$), a missed opportunity for biological carbon storage (orange shading). Alkalinity sequestration in the ocean interior by the CP depends on $CaCO_3$ production (and thus biological productivity) in the low latitude ocean and on the approximate 1,000-year timescale with which abyssal bottom water is circulated to the Southern Ocean surface. Thus, (1) more complete nutrient consumption in the polar ocean strengthens the STP but not the CP, (2) more nutrient supply to the low-latitude surface strengthens the CP but not the STP, and (3) a slowdown in deep ocean overturning strengthens the CP. North Atlantic Deep Water (NADW), the deep water formed in the North Atlantic, is fed from the low-nutrient, low-latitude surface. As a result, NADW formation strengthens both the STP and the CP. In contrast, deep water formation in the nutrient-rich Southern Ocean (which occurs mostly in the Antarctic Zone (AZ), especially in the Polar Antarctic Zone (PAZ), as opposed to the lower-latitude Subantarctic Zone (SAZ)) weakens both the STP and the CP. This cartoon highlights the competition to fill the global abyssal ocean between the North Atlantic and the Antarctic Zone, but the Subantarctic Zone and other regions also contribute to ocean ventilation, especially at intermediate depths. Despite its great size, the Pacific basin is not explicitly represented in the figure because it contributes little to the ventilation of the deep ocean and, thus, affects its properties less directly. Here and elsewhere, colored circles indicate water temperature change (red for warming, blue for cooling).

It is the standing stock of regenerated CO_2 (i.e., respired from organic matter) that the ocean holds that defines the atmospheric CO_2 impact of the soft-tissue pump (Equation 10; Volk & Hoffert, 1985), not the particular rates or pathways of export and ocean circulation or the locus of carbon storage in the ocean interior (Hain et al., 2010; Ito & Follows, 2005;

Kwon et al., 2011; Marinov, Follows, et al., 2008; Marinov, Gnanadesikan, et al., 2008; Sigman & Haug, 2003; Toggweiler et al., 2003). That is, the soft-tissue pump CO_2 effect is determined by the ocean mean regenerated phosphate, which is the difference between mean ocean phosphate and the unused phosphate concentration at the ocean surface, weighted by the fractions of the ocean interior water that originate from distinct ocean surface areas. Just three regions dominate the ventilation of the ocean interior (Broecker et al., 1985, 1998; deVries & Primeau, 2011; Gebbie & Huybers, 2010; Rae & Broecker, 2018). Roughly 35% of the modern ocean is filled from the polar Antarctic surface, with a preformed phosphate of 2.1 μmol/kg; this is referred to as Antarctic Bottom Water (AABW), although AABW is more precisely a mixture of polar Antarctic surface water and entrained subsurface water with different ventilation origins (compare Figure 4c). About 25% is filled from the polar-to-subpolar North Atlantic by North Atlantic Deep Water (NADW) with a preformed phosphate of 0.8 μmol/kg. Another 20% is filled from the Southern Ocean north of the Antarctic Zone, by Antarctic Intermediate Water (AAIW) and Subantarctic Mode Water (SAMW), with an approximate average preformed phosphate of 1.2 μmol/kg. The residual 20% is filled by the rest of the ocean surface, with an average preformed phosphate concentration of 0.5 μmol/kg. These estimates yield an ocean average preformed phosphate concentration of 1.1 μmol/kg (relative to a mean total phosphate concentration of 2.17 μmol/kg; see Table A.3 in Sarmiento & Gruber, 2006).

Much of the complexity in discussions of soft-tissue pump hypotheses for glacial/interglacial CO_2 change involves the dynamic interactions among nutrient supply by upwelling, biological productivity, and ocean ventilation by deep water formation. The following scenarios illustrate this complexity. If biological nutrient consumption increases in the Antarctic so as to cause a decline in the preformed phosphate of AABW from 2.1 to 0.8 μmol/kg, the mean ocean value declines by 0.46 μmol/kg, an additional 810 PgC of regenerated carbon is sequestered by the biological pump, and atmospheric CO_2 declines by about 27% (Equations 10 and 11; Table 3e–g). Alternatively, if circulation changes so that NADW is eliminated and AABW instead fills the vacated 25% of the ocean, the 1.3 μmol/kg difference between these deep water sources increases mean ocean preformed phosphate by 0.33 μmol/kg, regenerated carbon sequestration by the biological pump declines by 580 PgC, and atmospheric CO_2 rises by about 25% (Equations 10 and 11; Table 3l,m). If these two scenarios are combined, rather than canceling each other's CO_2 effects, atmospheric CO_2 is still expected to be reduced by about 27% because, with a lowered preformed phosphate for AABW, there is no longer a difference from NADW, and thus, the same circulation change has no effect. If the NADW is first eliminated, prior to any change in the preformed phosphate of AABW, atmospheric CO_2 rises by 25%. Thereafter, AABW is filling 60% of the ocean interior, such that atmospheric CO_2 has become much more sensitive to the preformed phosphate of AABW. If, then, the preformed phosphate of AABW is lowered from 2.1 to 0.8 μmol/kg, mean preformed phosphate declines by 0.78 μmol/kg (from +0.33 to −0.46 μmol/kg) and atmospheric CO_2 decreases by 42% (from +25% to −27%). Hence, atmospheric CO_2 is sensitive to the combination of changes in deep ocean circulation and in Southern Ocean nutrient cycling, biological productivity, and organic matter export (Hain et al., 2010; Sigman et al., 2010). Across all these changes, the global ocean's regenerated phosphate content provides an integrated measure of soft-tissue pump change to estimate or diagnose the soft-tissue pump CO_2 effect (Hain et al., 2010; Ito & Follows, 2005; Kwon et al., 2011; Marinov, Follows, et al., 2008; Marinov, Gnanadesikan, et al., 2008; Sigman & Haug, 2003; Toggweiler et al., 2003).

A critical complication, which is explored in the section on Antarctic-based hypotheses, is air–sea CO_2 disequilibrium in polar ocean regions, caused by either ice cover or very high rates of surface–subsurface water exchange. This factor can be thought of in two mathematically equivalent ways. In one view, limitations on gas exchange reduce the ventilation from a surface region relative to its role as a source of water in the ocean interior, which is the view taken in this treatment. Alternatively, gas exchange restriction can be framed as causing "disequilibrium carbon storage," recognizing that the disequilibrium requires preexisting CO_2 oversaturation of deep water due to the action of the global ocean's biological pump or other processes (e.g., Galbraith & Skinner, 2020; Khatiwala et al., 2019).

Carbonate Export and Regenerated Alkalinity

Some plankton build hard parts from either opal (SiO_2) or calcium carbonate ($CaCO_3$), and these components have a high propensity to sink from the surface, perhaps even ballasting some soft-tissue organic matter to sink deeper into the ocean (Armstrong et al., 2001; Boyd & Trull, 2007; Klaas & Archer, 2002). The effects of this hard part construction in surface waters can be summarized by these simplified chemical equations:

$$Si(OH)_4 \Leftrightarrow SiO_2 + 2H_2O \quad (12)$$

$$Ca^{2+} + CO_2 + H_2O \Leftrightarrow CaCO_3 + 2H^+ \quad (13a)$$

The conversion between silicic acid and opal does not affect seawater carbonate chemistry, because neither carbon nor protons are part of the reaction. In contrast, the production and export of $CaCO_3$ from the surface ocean has the overall effect of lowering *p*H and therefore raising the CO_2 of surface water and atmosphere (Figures 2 and 3). This is because, even though the export of $CaCO_3$ contains carbon and lowers DIC by 1 unit (raising *p*H), the production of $CaCO_3$ adds 2 units of protons so as to reduce surface alkalinity (decreasing *p*H, Equation 13a, 13b). As with the soft-tissue pump (Equation 10b; Box 1), the CO_2 effect of $CaCO_3$ export scales with the inventory of sequestered DIC and ALK "regenerated"

from $CaCO_3$ dissolution held in the ocean interior, which is framed here as the mean ocean concentration of regenerated $CaCO_3$, δCa_{reg}:

$$\frac{\delta_{CP}CO_2}{CO_2} = \left(\frac{\delta_{DIC}CO_2}{CO_2} + 2 * \frac{\delta_{ALK}CO_2}{CO_2}\right) \approx \Phi * \frac{-0.66\%+2*0.56\%}{\mu mol/kg} * \delta Ca_{reg} \quad (13b)$$

where CP refers to the carbonate pump. This term has been used to highlight the qualitative similarity to the soft-tissue pump, but specifically referring to the export of $CaCO_3$ from the surface ocean and its sequestration of DIC and ALK in the deep ocean (Hain et al., 2010, 2014; Kwon et al., 2011; Sarmiento & Gruber, 2006; Box 1). In opposition to the soft-tissue pump, its effect is to raise CO_2 in the surface waters and thus the atmosphere. The concentration of alkalinity regenerated from $CaCO_3$ dissolution in the ocean interior is roughly 50 µmol/kg (Chung et al., 2003; Feely et al., 2002; Fry et al., 2015; Sabine et al., 2002), suggesting an inventory in the ocean interior of 420 PgC carbon (and 1,400 Pg of calcium). For every 10-µmol/kg increase in regenerated $CaCO_3$, atmospheric CO_2 would rise by about 4%:

$$\Delta_{CP} lnCO_2 \approx \Phi * \int_0^{10\frac{\mu mol}{kg}} \frac{\delta_{CP}CO_2}{CO_2} = +4\% \quad (13c)$$

This estimate is only for the direct CO_2 effect of "dissolved $CaCO_3$" that has been removed from the surface, transferred to, and sequestered in the ocean interior (i.e., the *closed system* effect of the carbonate pump). The *open system* effect, which arises from temporary imbalances that it causes between alkalinity sources from weathering and $CaCO_3$ burial on the seafloor, is categorized in section "Mean Ocean Alkalinity Change." A hypothesis for lowering atmospheric CO_2 that involves strengthening of the biological (soft-tissue) pump will be less effective if it also strengthens the carbonate pump (Hain et al., 2010; Kwon et al., 2011; Sigman et al., 1998).

Mean Ocean Alkalinity Change

Because charge is conserved in a *closed system*, a 3% reduction in ocean volume due to ice sheet growth would raise mean ocean alkalinity proportionally, by approximately 81 µmol/kg (as included in Equation 9, Tables 1–3). However, on the multi-millennial timescale of the ice age cycles, the ocean operates as an *open system* for alkalinity. By far the largest input flux of alkalinity to the ocean is the weathering of marine limestone on land (which adds two units of ALK for each unit of DIC), and the largest output flux is seafloor $CaCO_3$ burial, these opposing fluxes comprising the ocean's $CaCO_3$ "budget." Hence, any change in mean ocean alkalinity above and beyond the ocean volume effect is caused by an imbalance between $CaCO_3$ burial and weathering (primarily of $CaCO_3$): an increase in weathering or a decrease in burial tends to raise mean ocean alkalinity (and DIC in a 2:1 ratio) and thereby reduce atmospheric CO_2 (Figure 2). $CaCO_3$ burial responds to mean ocean alkalinity change by minimizing the weathering/burial imbalance to yield a balanced $CaCO_3$ budget. To understand the role of this feedback and because support is lacking for a significant ice age increase in weathering (as outlined in the next section on Lysocline Constraints), the focus here is on the controls on $CaCO_3$ burial.

Land carbon release (i.e., a decrease in land carbon storage) during glacial times would have driven CO_2 into the ocean, which would cause ocean *p*H to drop, reducing the concentration of carbonate ion and thus the saturation state of $CaCO_3$ (Ω; Ω>1 for oversaturation and Ω<1 for undersaturation):

$$CaCO_3 \overset{K_{sp}}{\Leftrightarrow} Ca^{2+} * CO_3^{2-} \quad (14a)$$

$$\Delta CO_3^{2-} = -CPF * \frac{\Delta C_{land}}{M_{oc}} = CPF * \frac{\Delta C_{CaCO_3}}{M_{oc}} \quad (14b)$$

$$\Delta\Omega = \frac{Ca^{2+} * \Delta CO_3^{2-}}{K_{sp}(T,S,p)} \quad (14c)$$

Broecker (1982a, 1982b) pointed out that deep ocean sediment cores indicate rather similar $CaCO_3$ saturation during the LGM and modern conditions, and he proposed the dynamic of $CaCO_3$ *compensation*—where any forced change in deep ocean DIC would dissolve an equivalent amount of $CaCO_3$ from the deep ocean seafloor (ΔC_{CaCO3} in Equation 14d and Tables 1–3; see Equation 5; Hain et al., 2018) to re-establish balance between weathering on land and $CaCO_3$ burial in the ocean (Broecker & Peng, 1987; see also Högbom, 1894). For example, land carbon release during ice ages would cause CO_2 uptake by the ocean, including the deep ocean, which would lower deep ocean carbonate ion concentration and thus temporarily reduce $CaCO_3$ burial. As $CaCO_3$ burial is the main removal flux of alkalinity from the ocean, its decline would cause a transient surplus of alkalinity delivered to the ocean by weathering on land. That surplus would diminish over time as the ocean accumulates excess alkalinity, returning deep ocean carbonate ion concentration and thus $CaCO_3$ burial to pre-perturbation levels. Within roughly 4,000 years (e-folding timescale; see Equation 19), the ocean $CaCO_3$ budget is restored to a balance between weathering and burial:

$$\Delta\overline{CO_3^{2-}} \approx \frac{-CPF}{\frac{12g}{molC} * M_{oc}} * (-\Delta C_{CaCO3} + \Delta C_{Land}) \approx 0 \quad (14d)$$

The mean ocean alkalinity rise due to the transient net addition of dissolved $CaCO_3$, in itself, causes atmospheric CO_2 to decline. Hence, the direct effect on atmospheric CO_2 of land carbon change ($\delta_{Land}CO_2/CO_2$) and the indirect effect that arises over time from the $CaCO_3$ compensation response ($\delta_{CaCO3}CO_2/CO_2$) must be distinguished:

$$\frac{\delta_{Land,comp.}CO_2}{CO_2} = \frac{\delta_{Land}CO_2}{CO_2} + \frac{\delta_{CaCO3}CO_2}{CO_2} \approx \left(\frac{-3.2\%}{100PgC} + \frac{-3.2\%+5\%}{100PgC}\right) * \delta C_{Land} = \frac{-1.4\%}{100PgC} * \delta C_{Land} \quad (14e)$$

For example, if there was a net release of 350 PgC from land carbon shrinkage during the LGM (e.g., Crowley, 1995; Curry et al., 1988; Duplessy et al., 1984, 1988; Menviel et al., 2017; Oliver et al., 2010; Peterson et al., 2014; Shackleton, 1977)—sufficient to instantaneously raise CO_2 by 165 ppm (+59%)—an about 32-ppm CO_2 increase (+11%) would be expected after the added carbon fully equilibrates between atmosphere and ocean (Equation 6) and only a 10-ppm (+3%) CO_2 increase after mean ocean alkalinity is increased by 38 µmol/kg through net open-system dissolved $CaCO_3$ addition (Table 2). That is, after $CaCO_3$ compensation, less than one-fifteenth of the carbon released from land would remain in the atmosphere. Thus, only large changes in land carbon can drive notable changes in atmospheric CO_2 that persist for thousands of years, exactly as Högbom (1894) predicted.

Carbon cycle box model studies (e.g., Boyle, 1988a, 1988b; Broecker & Peng, 1987; Hain et al., 2010; Keir, 1988; Sigman et al., 1998; Toggweiler, 1999) have argued that any

Figure 5. Lysocline, CSH, and deep sea $CaCO_3$ dissolution. $CaCO_3$ production by plankton is typically greater than the rate of mineral dust blown onto the open ocean, such that mineral particle rain from the open ocean surface into the ocean interior can be approximately 80%–90% $CaCO_3$. That particle rain is intercepted by and preserved on shallow seafloor (shown in beige, top axis), where both calcite and aragonite forms of $CaCO_3$ are oversaturated in the water column ($\Omega > 1$, calcite in green, aragonite in purple), leading to the preservation and burial of the $CaCO_3$ rain (shown in blue). The solubility of $CaCO_3$ increases with pressure, and, hence, saturation (Ω) declines significantly with water depth (green for calcite and purple dashed for aragonite), first driving the more soluble aragonite to undersaturation ($\Omega_a < 1$ below the aragonite saturation horizon, ASH) and then calcite undersaturation in the deeper ocean ($\Omega_c < 1$ below the calcite saturation horizon, CSH). The respiration of organic matter on the seafloor tends to drive sediment porewaters toward undersaturation, but diffusion of carbonate ions from seawater into the sediment can neutralize the carbonic acid from respiration and protect seafloor $CaCO_3$ from respiration-driven dissolution if bottom water is sufficiently oversaturated ($\Omega >> 1$). In contrast, if bottom water is undersaturated ($\Omega < 1$), $CaCO_3$ dissolution proceeds readily and rapidly, up to the point that the $CaCO_3$ rain to the sediment is entirely dissolved. For example, at the CSH, all the aragonite and half of the calcite rain may dissolve (F_{diss} = 60%), but the residual 40% of preservation still yields a $CaCO_3$ ooze composed of >60% $CaCO_3$ because of the low non-carbonate sediment flux. Because of increasing calcite solubility with pressure (and thus depth), F_{diss} may reach 90% on the order of 500 m below the CSH, where the character of the sediment begins to change to deep sea aluminoslicate clay with minor $CaCO_3$. The carbonate compensation depth (CCD) is defined as the depth where dissolution is essentially complete (F_{diss} ~ 99%) and seafloor sediments are composed of approximately 95% non-carbonate. More relevant to the ocean's $CaCO_3$ burial budget is the lysocline (horizontal gray shading bounded by dashed red lines)—referring to the depth interval spanning across the CSH where the degree of dissolution (F_{diss}) increases rapidly with depth. Any change in temperature, salinity, pressure, or carbonate chemistry of the bottom water near the depth of the lysocline will change the depths of the CSH and lysocline (see Equation 15; Box 1), thereby changing the area of seafloor on which $CaCO_3$ is buried. This affects the ocean's alkalinity budget, causing atmospheric CO_2 change while feeding back on the deep ocean's $CaCO_3$ saturation state.

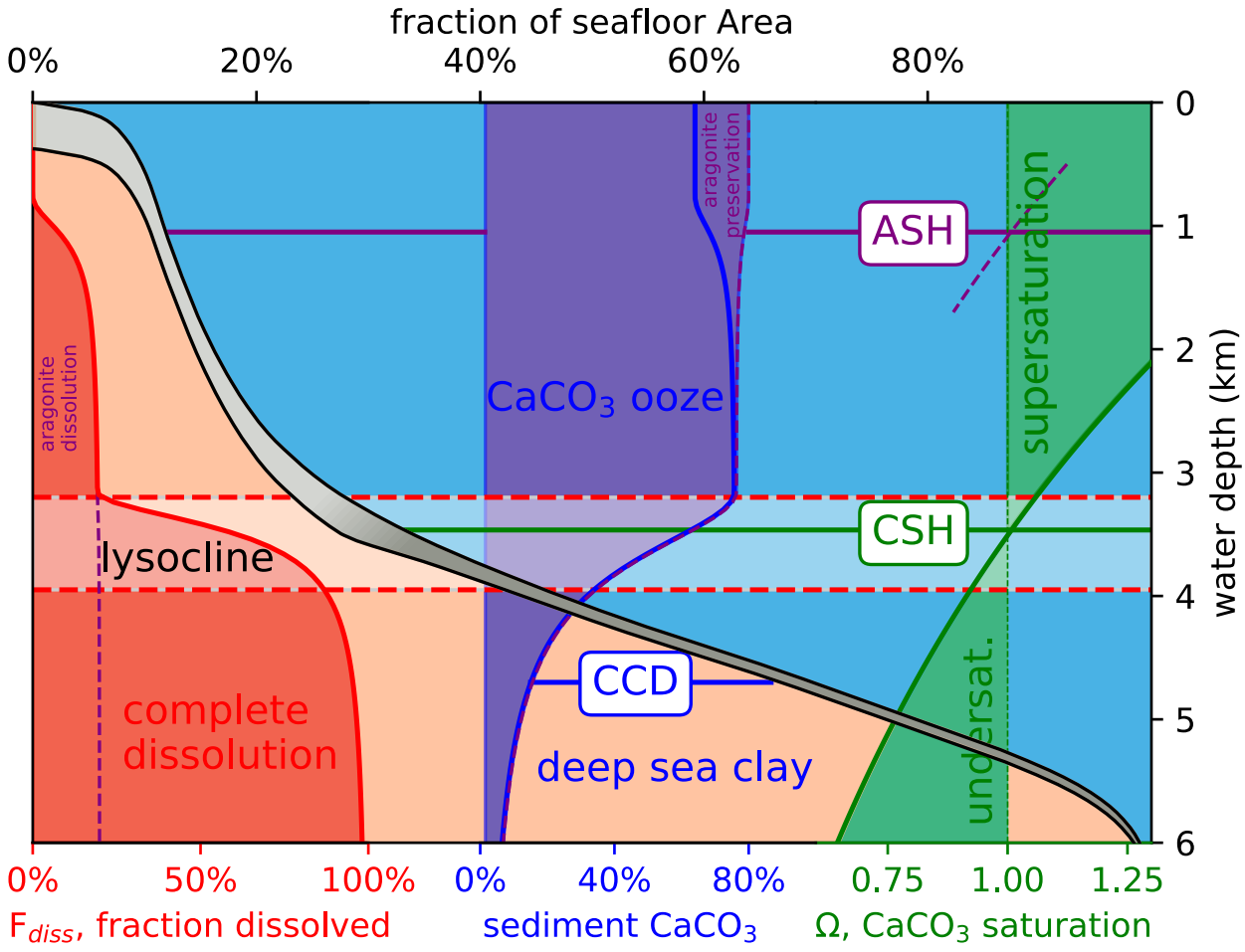

process affecting the saturation state of $CaCO_3$ on the deep ocean seafloor ($\delta\Omega_{forced}$, Equation 15a) would cause a $CaCO_3$ compensation response ($\delta\Omega_{CaCO3}$), extending the purview of $CaCO_3$ compensation to nearly all possible glacial/interglacial changes in the carbon cycle. This response restores any perturbation to deep ocean $CaCO_3$ saturation through a transient imbalance in the ocean $CaCO_3$ budget (not just land carbon as in Equation 14d)—excess burial or excess weathering—that changes mean ocean alkalinity. That is, an increment of net $CaCO_3$ exchange between seawater and solid Earth ($\delta CaCO_3$, positive in the case of dissolved $CaCO_3$ addition to seawater) causes a saturation effect toward restoring alkalinity mass balance (Equation 15b). The resulting 2-to-1 change in seawater ALK and DIC affects CO_2 in proportion to any forced disturbance of the deep ocean saturation state (Equation 15c). Thus, the direct CO_2 effect of any forced change ($\delta_{forced}CO_2$) is complemented by an indirect effect of changing mean ocean alkalinity (and DIC) by net $CaCO_3$ dissolution, yielding the net (i.e., "$CaCO_3$ compensated") CO_2 change ($\delta_{comp.}CO_2$; Equation 15d).

$$0 = \frac{\delta\Omega_{forced}+\delta\Omega_{comp.}}{\Omega} = \frac{\delta K_{sp}}{K_{sp}} - \frac{\delta_{SL}Ca^{2+}}{Ca^{2+}} - \frac{\delta CO_3^{2-}|_{forced}+\delta CO_3^{2-}|_{comp.}}{CO_3^{2-}} \quad (15a)$$

$$\frac{\delta\Omega_{CaCO3}}{\Omega} = \frac{\delta_{CaCO3}CO_3^{2-}}{CO_3^{2-}} = \frac{-CPF}{CO_3^{2-}} * \frac{\delta CaCO_3}{M_{oc}} \quad (15b)$$

$$\frac{\delta_{CaCO3}CO_2}{CO_2} = \Phi * \frac{-0.46\%}{\mu mol/kg} * \frac{\delta CaCO_3}{M_{oc}} \approx \Phi * 0.6 * \frac{\delta\Omega_{forced}}{\Omega} \quad (15c)$$

$$\frac{\delta_{comp.}CO_2}{CO_2} \approx \frac{\delta_{forced}CO_2}{CO_2} + \frac{\delta_{CaCO3}CO_2}{CO_2} \quad (15d)$$

Ocean temperature, salinity, volume, and hydrostatic pressure changes directly affect the deep ocean saturation with respect to $CaCO_3$, mainly through the fractional change in the solubility product ($\delta K_{sp}/K_{sp}$) and the ocean's calcium concentration ($\delta Ca/Ca$). In response, a predictable quantity of $CaCO_3$ is dissolved or preserved ($\delta CaCO_3$) to restore the carbonate ion concentration to return the ocean to a balance between the weathering input of dissolved $CaCO_3$ and the precipitation and burial of $CaCO_3$. For example, a 3.3 °C LGM cooling would cause +7 µmol/kg net $CaCO_3$ dissolution, with the resulting 2:1 mean ocean increase in ALK and DIC reducing atmospheric CO_2 by about -3% (−6 ppm, Table 2). The approximate 125-m LGM sea-level lowering would reduce Ksp due to the pressure drop, increase Ksp due to the higher salinity, and raise the concentrations of calcium, bicarbonate, carbonate and borate ions, which in net would cause a +7.4% increase in Ω ($\delta\Omega/\Omega_{forced}$). This ocean volume effect would drive about 8 µmol/kg of net disolved $CaCO_3$ loss (negative $\delta CaCO_3$ divided by the mass of the ocean, M_{oc}) until the ocean's $CaCO_3$ budget is restored—equivalent to the net preservation of about 130 PgC of $CaCO_3$ and a +3% increase in atmospheric CO_2 due to $CaCO_3$ compensation. That is, the reduction in LGM ocean volume concentrates mean ocean alkalinity by +81 µmol/kg (a closed system effect), and the alkalinity changes from the $CaCO_3$ compensation (i.e., open-system) responses to LGM ocean cooling (+7 µmol/kg) and volume loss (−10 µmol/kg) nearly cancel one another (Table 2). If temperature and volume effects are combined with 350 PgC reduction in LGM land carbon storage (causing +38 µmol/kg net $CaCO_3$ dissolution), the $CaCO_3$ compensation in response to these combined factors would have increased mean ocean alkalinity by +115 µmol/kg (from 2,364 to 2,479 µmol/kg, see Table 2; dashed vertical line in Figures 3 and 6).

When considering $CaCO_3$ compensation of the biological pump, it is important to note that the atmosphere and surface ocean are very small reservoirs for inorganic carbon in comparison to the voluminous ocean interior. As a result, changes in the regenerated CO_2 and alkalinity from soft-tissue organic matter degradation and $CaCO_3$ dissolution have no immediate, significant effect on the total DIC or alkalinity of the ocean interior. That is, the mean concentrations of bicarbonate and carbonate ions in the ocean interior are nearly unchanged, despite the input of inorganic carbon from the atmosphere and surface ocean in the case of a stronger biological pump. As a consequence, the soft- tissue and carbonate components of the biological pump have no significant effect on mean ocean $CaCO_3$ saturation ($\delta\Omega/\Omega = 0$) and thus fail to cause significant $CaCO_3$ compensation. This is consistent with box model results where the ocean interior is represented by one large reservoir (Toggweiler, 1999). It also explains the lack of significant $CaCO_3$ compensation in model experiments in which the ocean's phosphate reservoir is increased, driving an increase in the low-latitude biological productivity (Keir, 1988; Sigman et al., 1998).

Instead, $CaCO_3$ compensation of soft-tissue or carbonate pump changes is important when DIC and ALK are redistributed among the large volumes of the ocean interior. $CaCO_3$ compensation is largely achieved by changes in the depth of the *lysocline* (Broecker, 2003), the carbonate saturation-driven depth transition between shallower seafloor that hosts $CaCO_3$ burial and deeper seafloor on which the $CaCO_3$ rain is nearly entirely dissolved (Figure 5). Accordingly, significant $CaCO_3$ compensation is caused if there is preferential accumulation, relative to the ocean mean, of regenerated DIC and/or ALK, in the deeper portion of the ocean near the lysocline (i.e., by factors X_{STP} and X_{CP}; see Figure 5; Equations 16e and 16f). For example, if a strengthening of the soft-tissue pump increases mean ocean P_{reg} by 0.1 µM and if the additional carbon storage is concentrated in the deeper half of the ocean by a factor X_{STP}= 2 over the mean change, then a 10% reduction in deep Ω should occur. This deep Ω reduction is then compensated by a net addition of dissolved $CaCO_3$ of 12 µmol/kg that reduces atmospheric CO_2 by about 4% in addition to

Box 2. Effects on Deep Ocean $CaCO_3$ Saturation

Ocean volume effect, expressed in terms of meters of sea-level (SL) change: A reduction in SL causes a fractional reduction in ocean volume as determined by ocean surface area and ocean volume (A_{oc}/V_{oc} term), which proportionally raises seawater Ca^{2+} and CO_3^{2-} so as to raise deep ocean $CaCO_3$ saturation (Ω) by +6.4%/100 m. Moreover, per 100 m of sea-level lowering, seawater salinity rises and the hydrostatic pressure declines so as to change the $CaCO_3$ solubility product K_{sp} by +3% and −1.8%, respectively, for a combined −1.2%/100 m decrease in deep ocean $CaCO_3$ saturation from K_{sp}. Compounding all changes, $CaCO_3$ saturation increases by +5.2% per 100 m of sea-level fall.

$$\frac{\delta_{SL}\Omega}{\Omega} = \left(\frac{A_{oc}}{V_{oc}} * \left(1 + \frac{CPF*(DIC-ALK)}{CO_3^{2-}}\right) - \frac{\delta_{SL}K_{sp}}{K_{sp}*\delta SL}\right) * \delta SL \cong \frac{+5.2\%}{100m} * \delta SL \qquad (16a)$$

Deep ocean temperature effect: In a closed parcel of seawater, a temperature 2increase causes an incremental *p*H decrease but almost no change in CO_3^{2-}. Rather, the main effect is a −1.5% decrease in K sp that causes a +1.5% increase in $CaCO_3$ saturation per degree of warming (and the opposite for cooling).

$$\frac{\delta_T\Omega}{\Omega} \cong \frac{\delta_T K_{sp}}{K_{sp}*\delta T} * \delta T \cong \frac{+1.5\%}{^{\circ}C} * \delta T \qquad (16b)$$

Neutralization of land (or fossil) carbon release: Once dispersed through the ocean/atmosphere system, the CO_2 released from a reduction in land carbon storage titrates seawater $B(OH)_4^-$ and CO_3^{2-}, lowering $CaCO_3$ saturation by about 3.4% per 100 PgC land carbon release.

$$\frac{\delta_{Land}\Omega}{\Omega} \cong \frac{-CPF}{CO_3^{2-}} * \frac{1}{M_{oc}} * \frac{\delta C_{land}}{12gC/molC} \cong \frac{-3.4\%}{100PgC} * \delta C_{land} \qquad (16c)$$

Soft-tissue pump effect, expressed in terms of mean ocean regenerated phosphate ($\overline{P_{reg}}$): The production, sinking, and respiration of organic matter effectively redistributes CO_3^{2-} within the ocean. Ocean carbonate ion decreases at the depth of the lysocline (the key depth for carbonate compensation) if additional sequestration at the lysocline depth (δP_{reg}^{lys}) exceeds the mean ocean change in sequestration ($\delta\overline{P_{reg}}$) by a factor X_{STP}. For a +0.1-µmol/kg increase in regenerated phosphate concentrated at the lysocline by a factor of 2, deep ocean saturation declines by about 7.9%.

$$\frac{\delta_{STP}\Omega}{\Omega} \cong \frac{CPF}{CO_3^{2-}} * (106+18) * \left(\delta P_{reg}^{lys} - \delta\overline{P_{reg}}\right) = \frac{CPF}{CO_3^{2-}} * 124 * (X_{STP}-1) * \delta\overline{P_{reg}} \cong \frac{-7.9\%}{0.1\mu mol/kg} * \delta\overline{P_{reg}} \qquad (16d)$$

Carbonate pump effect, expressed in terms of mean ocean alkalinity regenerated from $CaCO_3$ dissolution ($\overline{ALK_{reg}}$): The precipitation, sinking, and dissolution of $CaCO_3$ effectively redistributes CO_3^{2-} within the ocean. Ocean carbonate ion increases at the depth of the lysocline (the key depth for carbonate compensation) if additional regenerated alkalinity sequestration at that depth (δALK_{reg}^{lys}) exceeds the mean ocean change in sequestration ($\delta\overline{ALK_{reg}}$) by a factor X_{CP}. For a +10-µmol/kg increase in mean ocean regenerated alkalinity concentrated at the lysocline by a factor 2, deep ocean saturation rises by about 6.1%.

$$\frac{\delta_{CP}\Omega}{\Omega} \cong \frac{CPF}{CO_3^{2-}} * \frac{(1-2)}{2} * \left(\delta ALK_{reg}^{lys} - \delta\overline{ALK_{reg}}\right) = \frac{-CPF}{2*CO_3^{2-}} * (X_{CP}-1) * \delta\overline{ALK_{reg}} \cong \frac{+6.1\%}{10\mu mol/kg} * \delta\overline{ALK_{reg}} \qquad (16e)$$

Carbonate compensation effect, expressed in terms of mean ocean alkalinity change (δALK): An increase in mean ocean alkalinity and DIC from net dissolution of $CaCO_3$ raises deep ocean CO_3^{2-} and $CaCO_3$ saturation by raising preformed ALK and DIC in a 2:1 ratio. Per +10 µmol/kg of alkalinity increase, deep $CaCO_3$ saturation rises by about 3.3%.

$$\frac{\delta_{comp.}\Omega}{\Omega} \cong \frac{CPF}{2*CO_3^{2-}} * \delta ALK \cong \frac{+3.3\%}{10\mu mol/kg} * \delta ALK \qquad (16f)$$

Atmospheric compensation effect, expressed in terms of net change in atmospheric carbon "storage" (δC_{atm}), which is known from ice core CO_2 reconstructions to be almost −200 PgC for the LGM relative to the preindustrial period. This is the sum of a minor recursive term that has been neglected in all the other effects described earlier (Equations 16a–16f), and it accounts for the fact that the 600 PgC in the preindustrial atmosphere are not trivial compared to the less than 4,000 PgC ocean carbonate ion inventory. A net 200 PgC transfer distributed throughout the bulk ocean mass (M_{oc}) would titrate roughly 3.4% of the ocean's existing carbonate ion content to drive its own small compensation event that slightly amplifies the net open-system CO_2 effects of the other compensation mechanisms. This term is not included in Tables 1–3 or Figures 3 and 6. This term helps further lower CO_2 levels, but it is much smaller than the changes in deep ocean saturation caused directly by changes in land carbon storage, temperature, ice sheets, and the biological pump (Figure 6; Table 2).

$$\frac{\delta_{comp.}\Omega}{\Omega} \cong \frac{CPF}{CO_3^{2-}} * \frac{1}{M_{oc}} * \frac{\delta C_{atm}}{12gC/molC} \cong \frac{+3.4\%}{100PgC} * \delta C_{atm} \qquad (1)$$

the 6% direct CO_2 reduction due to the closed-system CO_2 effect of the soft-tissue pump, nearly doubling the net CO_2 reduction (Table 1; Hain et al., 2010; Keir, 1988; Toggweiler, 1999). Likewise, a 10-µmol/kg strengthening of dissolved $CaCO_3$ sequestration by the carbonate pump, when concentrated by X_{CP} = 2 in the deep ocean, causes $CaCO_3$ burial to temporarily exceed dissolved $CaCO_3$ supply from weathering, decreasing oceanic dissolved $CaCO_3$ by 10 µmol/kg. This causes a 20-µmol/kg decrease in mean ocean alkalinity that raises atmospheric CO_2 by 4%, in addition to the 4% direct CO_2 increase due to the closed- system CO_2 effect of the stronger carbonate pump (Table 1).

In summary, mean ocean alkalinity change caused by the open-system dynamic of $CaCO_3$ compensation can significantly amplify the direct atmospheric CO_2 effect of both the biological pump's soft-tissue and carbonate components. Moreover, $CaCO_3$ compensation largely cancels the direct closed-system CO_2 effect of reduced land carbon storage by making the ocean more alkaline. Finally, the $CaCO_3$ compensation responses to the lower temperature and reduced volume of the LGM ocean largely cancel each other, such that the mean ocean alkalinity increase is dominated by the closed-system effect of the ocean volume reduction. Taken together, it seems plausible that LGM mean ocean alkalinity was up to 200 µmol/kg greater than in the modern ocean (Tables 2 and 3, and Figure 6), including approximately 81 µmol/kg from the closed-system ocean volume effect, approximately 40 µmol/kg from the $CaCO_3$ compensation of 350-PgC LGM land carbon reduction, and perhaps up to 100 µmol/kg from the $CaCO_3$ compensation of a stronger LGM biological pump, the regenerated products of which were concentrated in the deeper half of the ocean (X_{STP} = X_{CP} = 2; e.g., Boyle, 1988a, 1988b; Cartapanis et al., 2016; Hain et al., 2010; Jaccard et al., 2009; Toggweiler, 1999). In these calculations, no shift has been assumed in the ocean's steady-state lysocline depth that is overlain on the process of $CaCO_3$ compensation. The following section addresses the possibility of an ice age change in the steady-state lysocline depth, that is, the lysocline depth expected once the ocean had arrived at its new steady-state balanced ALK budget under ice age conditions.

Lysocline Constraints

Because $CaCO_3$ compensation is a transient dynamic that restores the balance between weathering on land and $CaCO_3$ burial in the ocean, there are a number of potential carbon cycle changes that would lead to a change in the steady-state deep ocean saturation state (and thus lysocline depth) after $CaCO_3$ compensation is complete (e.g., Archer, 1991, 1996a, 1996b; Archer & Maier-Reimer, 1994; Archer et al, 2000; Keir, 1988; Sigman & Boyle, 2000; Sigman et al., 1998). However, observational constraints on the seafloor depth distribution of $CaCO_3$ preservation for the LGM ocean suggest that the global ocean saturation horizon depth was similar to the modern (e.g., Berger, 1982a, 1982b; Catubig et al., 1998; Chalk et al., 2019; Farrell & Prell, 1989, 1991; Yu et al., 2010, 2014; see also Cartapanis et al., 2016; Rickaby et al., 2010; Wood et al., 2023). Biological $CaCO_3$ production (F_{prod}) and the dissolution of that $CaCO_3$ (F_{diss}) are much greater than the rate of carbonate weathering on land (F_{weath}) or the preservation and burial of $CaCO_3$ in ocean sediments (F_{burial}). However, the recycling of alkalinity within the ocean has no effect on the ocean's mean alkalinity, a change in which requires an imbalance between carbonate weathering and burial (Equation 16a). If, for example, weathering increases, a transient surplus of alkalinity supply over burial that leads the ocean to become more alkaline could be expected until its $CaCO_3$ saturation state has increased sufficiently to permit adequate preservation to balance the elevated weathering supply with elevated burial:

$$0 = \frac{\delta CaCO3}{\delta t} = F_{weath.} - \left(F_{prod.} - F_{diss.}\right) = F_{weath.} - F_{burial} \qquad (17)$$

Provisionally assuming that $CaCO_3$ production is constant (until considering hypotheses; Table 3), these interactions define a negative feedback between $CaCO_3$ saturation state and seafloor dissolution that restores weathering and burial toward a balanced steady state, forming the basis for the assertion that deep ocean $CaCO_3$ saturation is to be restored by $CaCO_3$ compensation (e.g., Sigman et al., 1998; Toggweiler, 1999; Equation 15a). To explain why saturation state in the deep ocean is specifically critical in the operation of this feedback and how deep-sea sediment cores record deep ocean saturation, a brief review of the controls on seafloor $CaCO_3$ dissolution is needed.

Two controls on seafloor $CaCO_3$ dissolution fluxes warrant attention. The first is the degree of $CaCO_3$ saturation of the overlying bottom seawater (Archer, 1996a; Archer, 1996b; Boudreau, 1987; Broecker & Takahashi, 1978; Emerson & Bender, 1981; Honjo & Erez, 1978; Li et al., 1969; Takahashi, 1975; Broecker & Takahashi, 1977). Due to hydrostatic pressure, $CaCO_3$ saturation declines approximately 1.8% for each 100 m of water depth (Equation 18c), and hence, preservation generally occurs on seafloor shallower than 3.5 km and complete dissolution on seafloor deeper than 4.5 km, placing the transition zone in the deep-to-abyssal ocean. This transition zone is typically apparent as a strong gradient in sedimentary $CaCO_3$ percentage and is often referred to as the "lysocline." The top of the lysocline is often near the depth of the "calcite saturation horizon" (CSH), the crossover from $CaCO_3$ supersaturation to undersaturation (Figure 5). Second, CO_2 evolved from organic matter respiration within the sediment efficiently lowers the saturation state within the sediment porewaters and thereby promotes dissolution unless the bottom water is sufficiently oversaturated to allow for the diffusion of carbonate ion from the bottom water into the sediment (Archer, 1991; Archer et al., 1989; Berger, 1970; Boudreau, 1987; Emerson & Bender, 1981; Hales, 2003; Hales & Emerson, 1996, 1997a, 1997b). The relationship between the lysocline and the CSH can be complicated by respiration

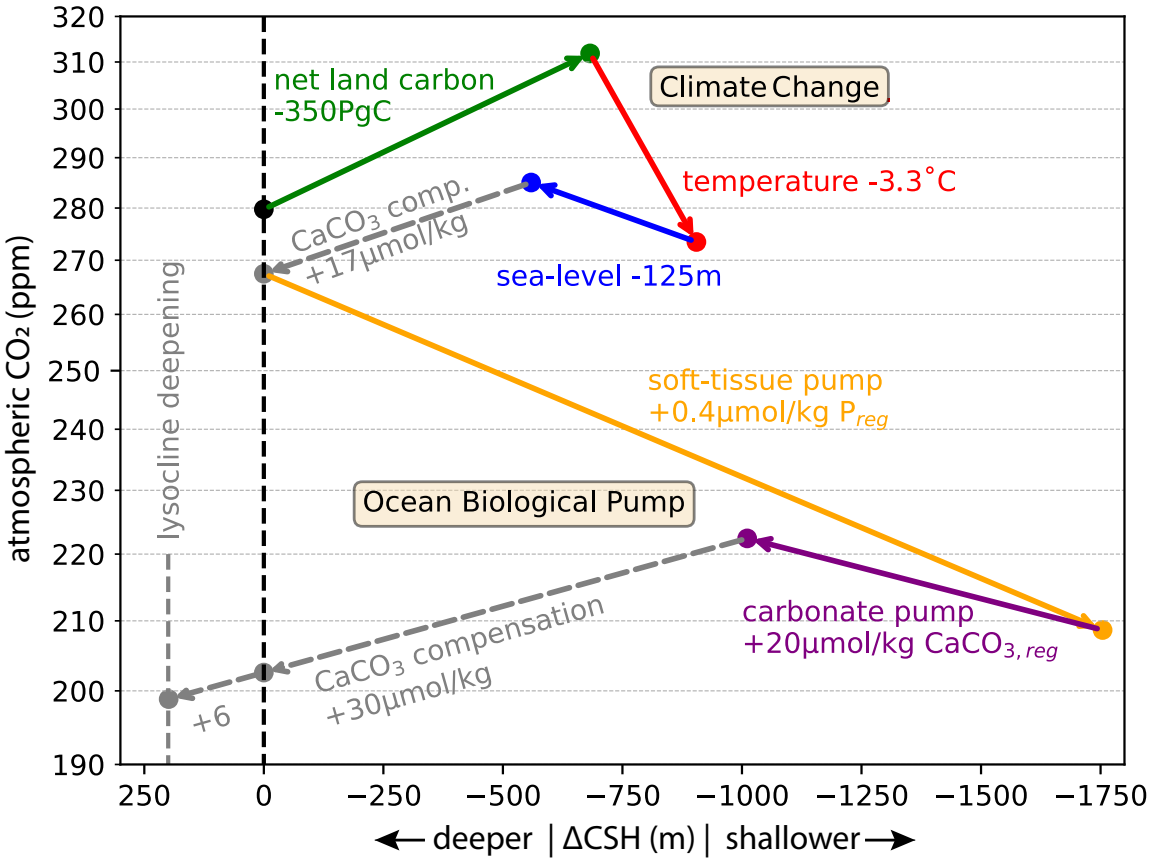

Figure 6. Composite CO_2 scenario for the Last Glacial Maximum. When assessing the drivers of observed CO_2 drawdown during the Last Glacial Maximum, processes centered outside the ocean are considered first: 350 PgC net land carbon release (green), 3.3 °C ocean cooling (red), and ice growth that lowered sea-level by 125 m (blue). The direct effect of land carbon release to raise CO_2 is nearly canceled by carbonate compensation, while the reduction in ocean volume offsets a significant portion of the effects of cooling. Compounding these three drivers (green, red, and blue) raises CO_2 from 280 to 285 ppm and shoals the calcite saturation horizon by approximately 600 m, but CO_2 is then reduced to 267 ppm (−4%) if carbonate compensation adds +17 µmol/kg of dissolved $CaCO_3$ to the ocean in order to restore the CSH to its initial depth (upper gray dashed arrow). At this point, the initial mean ocean alkalinity has been concentrated by approximately 3% (+83 µmol/kg, closed-system mean ocean alkalinity increase) and added to by carbonate compensation (+34 µmol/kg open-system alkalinity increase from +17 µmol/kg net $CaCO_3$ dissolution), but atmospheric CO 2 has declined by only 4%. Thus, the ocean's biological pump is thought to drive most of the residual CO_2 drawdown. For example, if an additional 0.4 µmol/kg of regenerated phosphorus and an additional 20 µmol/kg regenerated CaCO 3 were stored in the deeper half of the ocean (i.e., $X_{STP} = X_{CP} = 2$; Equations 16d/e), atmospheric CO_2 would decline from 280 to 231 ppm (−17%), and the CSH would shoal by about 1 km, driving carbonate compensation to add +30 µmol/kg of dissolved $CaCO_3$ to the ocean in order to restore the initial CSH (lower gray dashed arrow) and thereby further lowering CO_2 to 221 ppm (from −17% to −25%; in addition to the already compensated 4% CO_2 decrease from changes in land carbon, ocean temperature, and ocean volume). Reconstructed patterns of deep seafloor $CaCO_3$ preservation allow for minor ocean-average CSH deepening during the LGM, with an addition of +6 µmol/kg dissolved $CaCO_3$ to the ocean and its associated atmospheric CO_2 drawdown (−2%) for approximately 200 m of steady-state CSH deepening relative to the modern reference. Compounding the effects of ocean temperature, ocean volume, land carbon, and biological pump hence directly reduces CO_2 to 235 ppm (−16%), shoals the CSH dramatically, and thereby causes +53 µmol/kg net $CaCO_3$ dissolution for carbonate compensation to yield slight steady-state lysocline deepening. This rough observational lysocline constraint limits the contribution of low-latitude ocean processes to CO_2 drawdown because hypotheses of reductions in $CaCO_3$ export production, reductions in coral reef $CaCO_3$ burial in shallow waters, increases in weathering from land and exposed marine sediments, and nutrient deepening all depend in part on steady-state CSH deepening to raise ocean alkalinity and reduce atmospheric CO_2. Instead, it favors an increased efficiency of the biological pump — due to polar ocean changes in deep water formation, degree of surface nutrient consumption, and/or air–sea gas exchange — as the dominant cause of lower atmospheric CO_2 during the LGM and other ice ages. The initial temperature, DIC, and ALK are taken from Table A.3 in Sarmiento and Gruber (2006), and carbonate chemistry is solved using PyCO2sys (Humphreys et al., 2022) assuming a constant Φ of 0.85 to account for equilibration with the atmosphere. For the so"-tissue and carbonate pumps, increases in regenerated DIC and ALK are assumed to be concentrated in the deeper half of the ocean (X = 2; see Box 2), as is appropriate for polar ocean mechanisms. Detailed results are given in Table 2, and a collection of mechanistic scenarios for changes in the biological pump is given in Table 3.

within the sediments (which can shoal the top of the lysocline relative to the saturation horizon; idealized in Figure 5) as well as at locations with high $CaCO_3$ rain rate to the seabed (which can deepen the lysocline relative to the saturation horizon). While the CSH and lysocline may be offset, a change in deep ocean carbonate ion concentration tends to shift the CSH and the lysocline by similar magnitudes (Sigman et al., 1998).

The net effect of these two dynamics is to separate the deep ocean seafloor into three preservation zones: (a) a burial zone where oversaturation of the seawater is sufficient to neutralize the respired CO_2 and protect most of the $CaCO_3$

from corrosion, (b) a dissolution zone where combined undersaturation and sediment respiration are sufficient to dissolve effectively all seafloor $CaCO_3$, and (c) the *lysocline*, the transition zone between (a) and (b) where dissolution is substantial but not sufficient to dissolve all $CaCO_3$ sinking from the surface ocean to the seafloor (Archer, 1991, 1996b; Archer et al., 1989; Broecker & Takahashi, 1977; Jahnke et al., 1994).

A lysocline shift would change the seafloor area above the lysocline where $CaCO_3$ is preserved and buried and would thus affect the total deep ocean flux of $CaCO_3$ preservation and burial:

$$F_{burial} \approx \frac{F_{prod.}}{A_{oc}} * A^{\uparrow}_{lyso.} + 0 * A^{\downarrow}_{lyso.} \quad (18a)$$

$$\delta F_{burial} \approx \frac{\delta F_{prod.}}{A_{oc}} * A^{\uparrow}_{lyso.} + \frac{F_{prod.}}{A_{oc}} * \frac{\delta A^{\uparrow}_{lyso.}}{\delta z} * \delta CSH \quad (18b)$$

where $A^{\uparrow}_{lyso.}$ and $A^{\downarrow}_{lyso.}$ are the seafloor areas above and below the ocean depth of the lysocline (and thus also, approximately, the CSH) and $A^{\uparrow}_{lyso.}/\delta z$ reflects the depth distribution of the seafloor (i.e., its "hypsometry"). This simplified formulation has three important implications: First, any change in $CaCO_3$ export from the surface to the deep ocean ($\delta F_{prod.}$) directly affects global $CaCO_3$ burial because of the large area of seafloor above the lysocline, where $CaCO_3$ is preserved and buried. Second, every forced 1% decrease/increase in abyssal ocean Ω would shoal/deepen the calcite saturation horizon by about 55 m, so as to decrease/increase the area of deep ocean $CaCO_3$ burial by about 2%, corresponding to approximately 6.5 million km2 or 1.3% of Earth's total surface area—a transient dissolution/preservation event that facilitates $CaCO_3$ compensation (Broecker & Peng, 1987). Third, for every 1% reduction in $CaCO_3$ export— or for roughly a 4% increase in weathering, or for a roughly 2% decrease in net shelf carbonate burial, a major contributor to total ocean carbonate burial—the steady state lysocline must deepen by about 27 m to achieve balance between weathering and preservation so as to increase the seafloor area above the lysocline by about 1%.

$$\delta CSH \cong \left(\frac{-1}{K_{sp}} * \frac{\delta_z K_{sp}}{\delta z}\right)^{-1} * \left(\frac{-CPF}{CO_3^{2-}}\right) * \frac{\delta CaCO_3}{M_{oc}}$$

$$\cong \left(\frac{-1}{K_{sp}} * \frac{\delta_z K_{sp}}{\delta z}\right)^{-1} * \left(\frac{-CPF}{CO_3^{2-}}\right) * \left(\frac{+0.66\% - 2*0.56\%}{\frac{\mu mol}{kg}}\right)^{-1} * \Phi^{-1} * \frac{\delta_{lyso.}CO_2}{CO_2} \quad (18c)$$

$$\frac{\delta_{lyso.}CO_2}{CO_2} \approx \Phi * \left(\frac{-0.46\%}{\frac{\mu mol}{kg}}\right) * \frac{\delta CaCO_3}{M_{oc}}$$

$$= \Phi * -0.6 * \frac{\delta\Omega}{\Omega} = \Phi * -0.6 * \left(\frac{1.8\%}{100m}\right) * \delta CSH \quad (18d)$$

That is, a deepening of the lysocline (a positive δCSH in Equations 18b, 18c) is achieved by the net dissolution of $CaCO_3$ ($\delta CaCO_3$), which raises deep ocean $CaCO_3$ saturation ($\delta\Omega/\Omega$) by about 1.8% per 100 m of CSH deepening (Equation 18d). For every unit of net addition of dissolved $CaCO_3$, mean ocean ALK and DIC concentration increase by 2 units and 1 unit, respectively ($\delta CaCO_3/M_{oc}$ term reflects these concentration changes, shown as $\Delta CaCO_3$ in Tables 1–3), which together cause a fractional change in bulk ocean carbonate ion concentration (-CPF/CO_3^{2-} term reflects the buffering of the bulk ocean; see Equation 5). Because the solubility of $CaCO_3$ increases exponentially with pressure and water depth z ($-\delta_z K/K$ term), a linear increase in CSH depth (positive δCSH) corresponds to a fractional increase in bulk ocean carbonate ion that causes a fractional reduction in atmospheric CO_2 ($\delta_{lyso}CO_2/CO_2$). This expression can be reframed to highlight the fundamental sensitivities of atmospheric CO_2 to the open-system $CaCO_3$ cycle (Equation 18d): CO_2 declines by 0.46% per each 1-μmol/kg net $CaCO_3$ dissolution, by 0.6% for every 1% increase in deep ocean saturation due to net $CaCO_3$ dissolution, and by about 1.1% ($0.6 * 1.8\%$, or ~3 ppm) for every 100 m of CSH deepening due to net $CaCO_3$ dissolution. This relationship between CO_2 and CSH sets the slopes of the dashed arrows projecting to ΔCSH = 0 in Figure 3 and Figure 6, representing the $CaCO_3$ compensation that restores the lysocline back to its current steady-state depth.

A number of hypotheses for lowering ice age CO_2 are based on a proposed rise in ocean alkalinity associated with a deepening of the steady-state lysocline relative to its modern depth (positive ΔCSH in Figure 3 and Figure 6). These include (a) a glacial increase in continental weathering, (b) a glacial reduction in $CaCO_3$ export production either because of lower low-latitude ocean productivity (Kwon et al., 2009; Matsumoto et al., 2002) or less $CaCO_3$ production per unit of productivity (Archer & Maier-Reimer, 1994; Chikamoto et al., 2009; Matsumoto and Sarmiento, 2008), and (c) a glacial reduction in coral reef growth (Berger, 1982a, 1982b; Opdyke & Walker, 1992; Wood et al., 2023). However, the CO_2 reduction is only about 1% (~3 ppm, Table 1) per 100 m of steady-state lysocline deepening (Figure 3). Reconstructions of deep-sea $CaCO_3$ burial (e.g., Cartapanis et al., 2016; Hays et al., 2021; Wood et al., 2023) and saturation (e.g., Chalk et al., 2019; Yu et al., 2010, 2014) allow for no more than a few hundred meters of LGM lysocline deepening relative to the modern, which would imply a maximal CO_2 reduction of less than 10 ppm associated with lysocline deepening. All the preceding hypotheses for atmospheric CO_2 reduction that lead to lysocline deepening must compete to cause this maximal CO_2 reduction.

Conversely, hypotheses that invoke glacial increases in low- and mid-latitude biological production by increasing the overall nutrient (nitrogen and phosphorus) inventory of the ocean (Broecker, 1982a, 1982b; Broecker & Henderson, 1998; Falkowski, 1997) suffer from the possibility of raising $CaCO_3$ production (Box 1), which would force a decline in ocean alkalinity due to a shoaling of the steady state lysocline, which works to raise atmospheric CO_2 and thus offsets a component of CO_2 drawdown due to the

biological pump (Sigman & Boyle, 2000; Sigman et al., 1998). In contrast, because polar biological productivity is associated with proportionally less $CaCO_3$ production, polar ocean changes in productivity and nutrient consumption do not cause substantial steady-state lysocline changes, except to the degree that they alter $CaCO_3$ production in the low-latitude ocean (Archer et al., 2000; Hain et al., 2010, 2014; Keir, 1988; Sigman et al., 1998). Moreover, the polar regions have great leverage over the global efficiency of the soft-tissue pump, and their sinking organic matter is efficiently routed into deep waters at the depth of the lysocline. Thus, hypothesized polar biogeochemical changes discussed later can drive a significant portion of their atmospheric CO_2 drawdown through $CaCO_3$ compensation and without causing large changes in the steady-state lysocline depth (Hain et al., 2010; Sigman & Boyle, 2000; Sigman et al., 1998).

Any imbalance in the ocean's $CaCO_3$ budget can be framed as the vertical offset ΔCSH between the current CSH and the depth it would need to be at to yield a balanced the $CaCO_3$ budget—the steady-state CSH depth. The carbonate compensation feedback will over time reduce the imbalance so that CSH and lysocline relax towards their steady state depths, where ΔCSH is zero. Making the simplifying assumptions of (a) constant $CaCO_3$ rain per area (F_{prod}/A_{deep}) and (b) a constant slope for deep ocean seafloor ($\delta A_z^{\uparrow}/\delta z$), the timescale of lysocline adjustment is solved for analytically:

$$\frac{\delta CaCO_3}{\delta t} \approx \frac{\delta A_z^{\uparrow}}{\delta z} * \frac{F_{prod.}}{A_{deep}} * \Delta CSH \qquad (19a)$$

$$\frac{\delta \Delta CSH}{\delta t} = \left(\frac{\delta A_z^{\uparrow}}{\delta z} * \frac{K_{sp} * \delta z}{\delta_z K_{sp}} * \frac{F_{prod.}}{A_{deep}} * \frac{CPF}{M_{oc}} * \frac{Ca^{2+}}{K_{sp}}\right) * \Delta CSH = \frac{\Delta CSH}{\tau_{lysocline}} \qquad (19b)$$

$$\tau_{lysocline} = \left(\frac{\delta A_z^{\uparrow}}{A_{deep} * \delta z} * \frac{K_{sp} * \delta z}{\delta_z K_{sp}} * \frac{CPF * F_{prod.}}{M_{oc}} * \frac{Ca^{2+}}{K_{sp}}\right)^{-1}$$

$$= \left(\frac{2\%}{100m} * \frac{100m}{1.8\%} \frac{-0.65 * \frac{40 * 10^{12} mol}{yr}}{1.4 * 10^{21} kg} * \frac{0.01 mol/kg}{8 * 10^{-7} mol^2/kg^2}\right)^{-1} = 3877\ yr \qquad (19c)$$

That is, any change in weathering or $CaCO_3$ production or other perturbation to deep ocean $CaCO_3$ saturation (see Box 2) would offset the CSH from its eventual steady state depth (by the amplitude of ΔCSH), with lysocline adjustment relaxing ΔCSH over time to yield the new steady-state CSH. The adjustment is achieved through a transient imbalance between the weathering input and seafloor preservation ($\delta CaCO_3/\delta t$), which reduces ΔCSH with an e-folding timescale $\tau_{lysocline}$ of about 3,900 years. This is lower than previous estimates (Archer et al., 1997; Broecker, 1982a, 1982b; Jeltsch-Thömmes & Joos, 2023), but uncertainties are high, for example, due to uncertainty in modern weathering and burial rates. Whatever imbalances may exist in the ocean *open-system* $CaCO_3$ *cycle* will be compensated by lysocline adjustments that restore deep ocean carbonate ion concentration toward a level set by weathering and marine $CaCO_3$ production. Hence, for any change in the global carbon cycle, while the direct CO_2 effect is likely to be established after a few centuries of ocean overturning, the indirect open- system CO_2 effect from transient and steady-state lysocline adjustments is expected to require thousands of years to unfold.

Table 2. LGM Scenario for Atmospheric CO_2 Drawdown

forcing	effect	value	direct CO_2	compensated CO_2	$\Delta CaCO_3$	direct ΔCSH	compensated ΔCSH	mean ocean DIC	mean ocean ALK	deep ocean O_2
			(ppm)	(ppm)	(µmol/kg)	(m)	(m)	(µmol/kg)	(µmol/kg)	(µmol/kg)
modern reference			280	280	+0	3656	3656	2249	2364	165
land C uptake		150 PgC	267 (−4%)	276 (−1%)	-8	277	0	2232	2348	165
land C release		−500 PgC	327 (+17%)	294 (+5%)	+27	−990	−0	2306	2418	165
net land C change		−350 PgC	312 (+11%)	290 (+3%)	+19	−682	−0	2289	2402	165
temperature	DIC speciation (K_0, K_1, K_2)	−3.3 °C	245 (−12%)	245 (−12%)	+0	0	0	2249	2364	193
temperature	$CaCO_3$ saturation (K_{sp})	−3.3 °C	280 (0%)	272 (-3%)	+7	−243	0	2256	2379	165
temperature	combined	−3.3 °C	245 (-12%)	239 (-15%)	+7	−243	0	2256	2379	193
ice volume	DIC, ALK, & AOU concentration	−125 m	285 (+2%)	292 (+5%)	−7	241	0	2320	2431	160
ice volume	salinity & Ca concentration	−125 m	287 (+3%)	286 (+2%)	+2	−58	-0	2251	2367	163
ice volume	seafloor pressure (K_{sp})	−125 m	280 (+0%)	284 (+2%)	-4	138	0	2245	2356	165
ice volume	all combined	−125 m	293 (+5%)	303 (+8%)	-10	322	0	2317	2427	157
lysocline change	steady-state deepening	+179 m	280 (+0%)	274 (−2%)	+6	−20	179	2255	2376	165
biological pump	organic matter (P_{reg})	+0.4 µmol/kg	217 (-23%)	188 (-33%)	+50	−1883	-0	2299	2463	29
biological pump	regenerated $CaCO_3$	+20 µmol/kg	302 (+8%)	329 (+18%)	−20	663	0	2229	2324	165
land,T,SL combined		as above	285 (+2%)	267 (−4%)	+17	−559	-0	2364	2479	185
biological pump	combined P_{reg}, $CaCO_3$	as above	231 (−17%)	210 (−25%)	+30	−1083	179	2279	2423	29
all combined		as above	235 (−16%)	199 (−29%)	+53	-1660	179	2400	2551	49

Note: This scenario for atmospheric CO_2 reduction during the Last Glacial Maximum (LGM) is computed in the same way and from the same modern reference point as Table 1, but using reconstruction-based estimates for net land carbon storage change, ocean cooling, sea-level lowering, and a Southern Ocean–focused scenario of biological pump change (Hain et al., 2010). Compounding the changes in land carbon storage, temperature, and sea-level lowering yields little net CO_2 reduction, and hence Southern Ocean changes, making the ocean's biological pump more efficient, appear central to the lower atmospheric CO_2 of the ice ages. This scenario for the LGM can account for 81-ppm (−29%) CO_2 drawdown without deepening the global steady-state CSH beyond observational constraints. All output parameters are as in Table 1.

Hypotheses for Ice Age CO_2 Drawdown

The physicochemical, biogeochemical, and alkalinity budget-related mechanisms for altering atmospheric CO_2 outlined above comprise the geochemical possibilities for the origin of ice age CO_2 drawdown. However, this gallery of CO_2 sensitivities does not, by itself, offer a mechanistic explanation for why CO_2 tracked the ice age cycle, in rhythm with relatively minor changes in Earth's orbit. Any such explanation must identify climate-driven environmental changes that, through these sensitivities, caused atmospheric CO_2 to change. Even in the case of some otherwise external dynamic, such as CO_2 release from the solid Earth (Stott and Timmermann, 2011) or from terrestrial organic C deposits (Wadham et al., 2019; Zeng, 2003), the ocean's carbon cycle sensitivities are of central importance.
The drawdown of atmospheric CO_2 during glacial maxima has become an important target in climate science that has prompted a range of mechanistic hypotheses and spurred a concerted effort by the scientific community to produce observational constraints and evidence for or against these. In the following discussion, these hypotheses are grouped by geographic region. First, causal mechanisms of CO_2 change centered outside the ocean are considered. Then ocean-based mechanisms are discussed, first those centered on the low latitudes and then those centered on the high latitudes. This structure helps to clarify why high-latitude ocean changes appear to be critical in CO_2 regulation during the ice ages. This finding, in turn, motivates an in- depth account of the various high-latitude ocean-centered hypotheses and their observational support.

Certain changes in the ice age ocean seem unavoidable as contributors to the atmospheric CO_2 changes of the glacial cycles. These include ocean cooling as a driver of ice age CO_2 decrease and ice volume increase and arguably terrestrial carbon loss as drivers of CO_2 increase. Having accounted for these "background" effects, there is not consensus as to whether the ice age CO_2 reductions are the result of many overlapping mechanisms or are dominated by one or a few central mechanisms. The following review of potential mechanisms ultimately favors two distinct changes in the Southern Ocean, one focused in its Subantarctic Zone and the other in its Antarctic Zone.

Effects of Background Ice Age Conditions

Global surface temperature, land ice volume, terrestrial carbon storage, and land surface processes such as rock weathering have changed in association with the glacial cycles. These conditions and processes are not (or not dominantly) controlled by the ocean; nevertheless, due to the centrality of the ocean in the global carbon cycle, ocean carbon chemistry mediates their effects on atmospheric CO_2.

A net increase in carbon storage on land would reduce the combined carbon inventory of the ocean and atmosphere, lowering atmospheric CO_2. However, with only 1 of 15 carbon atoms derived from the atmosphere after ocean $CaCO_3$ compensation (Box 2), a very large increase in land carbon would be required to explain the ice age decline in atmospheric CO_2. In contrast, studies of marine carbonate carbon isotopes and lake pollen have led to the conclusion that the terrestrial biosphere *lost* roughly 300–400 PgC during ice ages (Adams et al., 1990; Crowley, 1991, 1995; Duplessy et al., 1988; Lindgren et al., 2018; Peterson et al., 2014; Prentice et al., 1993; Shackleton, 1977), a change that would have increased atmospheric CO_2 by about 10 ppm (+3%, Table 2). Arguments for as much as 1,250 PgC LGM of land carbon reduction (Jeltsch-Thömmes et al., 2019) would raise CO_2 significantly more and represent a major challenge for explaining low LGM CO_2. An important caveat comes with episodes of abrupt destabilization of permafrost carbon and the associated CO_2 release to the atmosphere (Crichton et al., 2016; Köhler et al., 2014; Winterfeld et al., 2018), which may have caused temporary speed-ups in atmospheric CO_2 rise during the last deglaciation (e.g., Marcott et al., 2014; Monnin et al., 2001). Abrupt deglacial reductions in the carbon inventory of permafrost might result from continental warming that reduces the geographic extent of frozen ground and increases the active layer depth of summer-season thawing as well as from erosion of coastal permafrost soils with rising sea-levels. However, on longer timescales, ice sheet retreat exposes barren mineral soils, allowing biological growth to sequester soil carbon over time (e.g., Lindgren et al., 2018). Estimates of changes in organic carbon storage based on the global ocean carbon isotope change (i.e., Jeltsch-Thömmes et al., 2019; Shackleton, 1977) integrate the changes in permafrost and terrestrial biosphere carbon storage as well as those in organic carbon storage within shallow marine sediments, pointing to net carbon release during ice ages (Cartapanis et al., 2016). This comes with the caveat that ice age conditions may have advantaged C4 plants over C3 plants, which fractionate carbon isotopes differently (Hobbie & Werner, 2004). In general, significant uncertainties persist for the ice age changes in individual terrestrial organic carbon stocks as well as for the combined (net) change in land-and- shelf organic carbon storage.

Ocean water temperatures decline with the global cooling of ice ages (e.g., Baggenstos et al., 2019), thereby increasing the seawater solubilities of CO_2 and $CaCO_3$ as well as shifting seawater carbon speciation and pH, with a 3.4% CO_2 reduction and about 75-m CSH shoaling per 1 °C of cooling (Figure 3; Table 1). Observation-based estimates of deep ocean cooling from marine microfossil and porefluid data suggest 2–4 °C of ocean cooling during the LGM (e.g., Adkins et al., 2002; Cutler et al., 2003; Labeyrie et al., 1987; Martin et al., 2002; Schrag et al., 1996; Waelbroeck et al., 2002), and ice core noble gas estimates for the last three glacial maxima suggest 3.3 ± 0.4 °C of mean ocean cooling (Baggenstos et al., 2019; Haeberli et al., 2021; Headly & Severinghaus, 2007; cf., Pöppelmeier et al., 2023). Taken at face value, the closed-system response to 3.3 °C of cooling corresponds to a −12% (~35-ppm) reduction in atmospheric

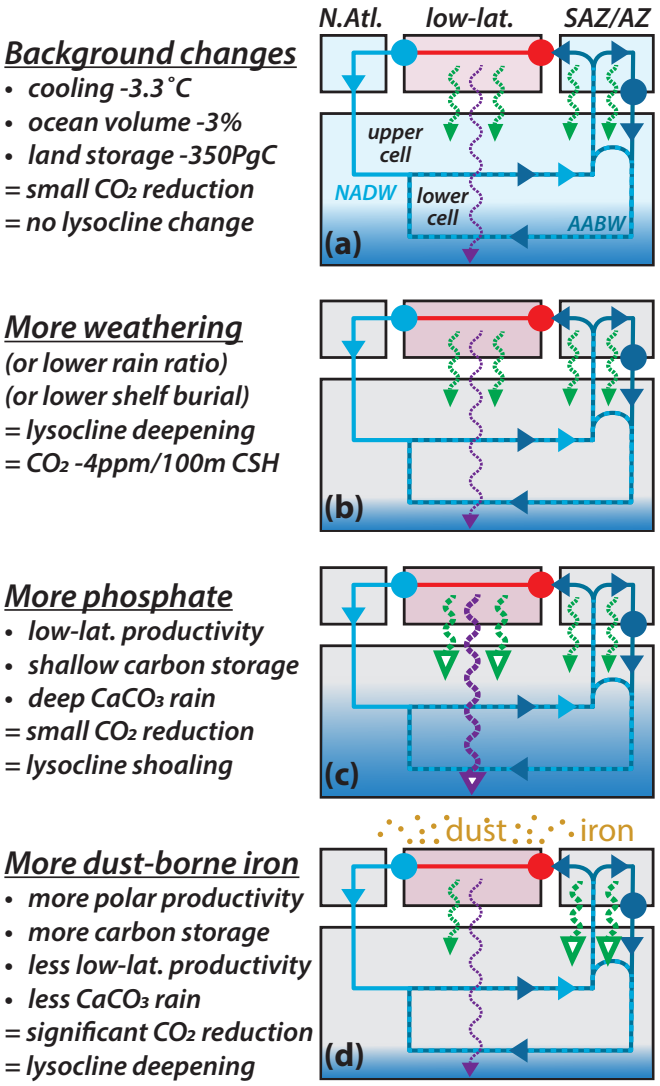

Figure 7. Global-scale hypotheses for ice age atmospheric CO_2 reduction. (a) Background conditions associated with ice ages, when combined, yield little net CO_2 change, even after carbonate compensation restores the steady state lysocline to its original depth (bottom shading). (b) Hypotheses focused on the ocean's alkalinity budget. If weathering on land increased and/or the burial of $CaCO_3$ in the ocean decreased, the resulting imbalance would make the ocean more alkaline, increasing its carbon storage capacity and absorbing CO_2 from the atmosphere—but either change would cause deepening of the steady-state lysocline. (c) Hypotheses focused on the ocean's major nutrient budgets. An increase in the ocean's phosphate inventory would raise the inventory of nitrogen, the other major nutrient, and the two would spur biological productivity in the low-latitude surface ocean, driving additional biological carbon storage. However, the associated increase in $CaCO_3$ rain from the surface would increase carbonate burial, reduce ocean alkalinity, and shoal the steady state lysocline so as to yield little net CO_2 change. (d) Hypotheses focused on dust-borne iron fertilization of the ocean. As the micronutrient iron often limits biological productivity in higher latitude ocean regions, the reconstructed increase in dust-borne iron input to the ocean under cold and dry glacial climates may have fertilized phytoplankton growth in these regions. The reconstructed iron fertilization of the Subantarctic Zone in the Southern Ocean (Figure 9) draws down unused major nutrients, storing more carbon in the deep ocean. It also reduces the supply of major nutrients to the upper cell and the low-latitude ocean, thus reducing low- latitude productivity and $CaCO_3$ rain, which, in turn, causes ocean alkalinity to rise so as to deepen the steady state lysocline, causing additional CO_2 reduction in the process. Observations suggest that the steady-state lysocline changed little between the ice ages and the interglacials, offering a constraint that limits how much of the atmospheric CO_2 reduction may have been caused by the combination of these hypothesized mechanisms (Table 3). Moreover, neither of these hypotheses accounts for reconstructed changes in deep ocean circulation or the ice age reduction in productivity of the Antarctic Zone of the Southern Ocean (Figure 8), the major surface water source for the lower cell of the ocean's overturning circulation.

CO_2 and a 243 m shoaling of the CSH. To restore deep ocean CSH requires the net dissolution of 7 µmol/kg $CaCO_3$, causing an open-system CO_2 decrease of −3% in addition to the −12% closed- system CO_2 decrease (for a net decrease of −41 ppm, −15%; Figures 3 and 6; Table 2).

The massive continental ice sheets of glacial times sequestered water and thereby reduced the ocean mass and volume and lowered global sea-level by about 125 m during the LGM, which corresponds to a CO_2 rise of +13 ppm (+5%, Table 2) and 322 m of CSH deepening for peak glacial conditions (Figure 3). This closed-system sensitivity includes a +3% increase in the concentrations of calcium, DIC, and ALK (e.g., increases in mean ocean alkalinity of +83 µmol/kg and in deep ocean carbonate ion of +3%, Table 2) and the effects of salinity and seafloor pressure on the carbonate chemistry equilibrium constants (Box 2). To restore deep ocean CSH requires the net burial of 10 µmol/kg $CaCO_3$, causing an open-system CO_2 increase of +3% in addition to the +5% closed- system CO_2 increase (yielding a net increase of +23 ppm, +8%; Table 2; Figure 6).

These "background" ice age changes—land carbon release, ocean cooling, and ocean volume reduction—when taken together, probably only modestly affected CO_2 during ice ages because (Figure 7a): (a) net land carbon release to the atmosphere is overwhelmingly buffered by ocean carbon uptake and $CaCO_3$ compensation, and (b) the CO_2 reduction driven by ocean cooling is significantly offset by the sequestration of ocean water into land ice (Tables 1 and 2, Figure 6). All of these changes are caused by global climate change, and so their CO_2 effects are climate feedbacks associated with the glacial cycles. However, in the aggregate, they fail to cause the observed CO_2 change: The combined closed-system driven CO_2 change is +5 ppm, while the net CO_2 reduction when including open-system effects is −13 ppm (Table 2, Figure 6). Ocean biogeochemical mechanisms related to the biological pump are thus implicated as the main driver of the ice age CO_2 cycles (Broecker, 1982a, 1982b; Table 3).

Nevertheless, the "background" changes caused a substantial net LGM increase in Earth's albedo—the fraction of incoming sunlight that is reflected back to space— related to the expansion of ice and snow cover, the contraction of forests, the expansion of land area, and greater dustiness of the atmosphere during peak glacial conditions (e.g., Hansen

et al., 1985; Köhler et al., 2010). This positive feedback between ice age surface changes, albedo increase, and radiative cooling is estimated to roughly double the global temperature response to the radiative forcing from observed changes in CO_2 and other greenhouse gases (Sherwood et al., 2020, Figure 1). Moreover, the increase in dust inputs has the potential to enhance global ocean CO_2 storage during the ice ages (Martin, 1990).

Low-Latitude Ocean Hypotheses

Most of the ocean surface and seafloor is situated at low- and mid-latitudes, between 45° N and 45° S, where strong insolation forms a warm and thus buoyant surface water mixed layer that only slowly exchanges with colder and denser subsurface water. In these settings, the slow nutrient supply to the surface from depth leads to nearly complete surface nutrient consumption and a balance between nutrient supply and the export of organic matter with average nutrient-to-carbon ratios of 1:16:106 (P:N:C)— the "Redfield ratios" (Redfield, 1934). Furthermore, the low latitudes dominate $CaCO_3$ production and burial, both on the continental shelves and by calcifying plankton in the open ocean. Both the complete consumption of the nutrient supply and the extensive precipitation of $CaCO_3$ are in contrast to characteristics of biological productivity in polar ocean surface waters, as described below. These differences yield distinct sets of hypotheses for ice age CO_2 drawdown that are mechanistically linked to one or the other of these surface ocean environments. The low-latitude ocean-based hypotheses are organized into those that entirely relate to $CaCO_3$ cycling versus those hypotheses in which organic matter and nutrient cycling are central but with knock-on effects from $CaCO_3$.

Reef-, Weathering-, and Rain Ratio-Driven Ocean Alkalinity Change

With the discoveries of orbitally paced glacial/interglacial cycles with major sea-level change (e.g., Broecker & Thurber, 1965; Hays et al., 1976) and abrupt CO_2 rise at the end of the last ice age, Berger (1982a, 1982b) noted the importance of $CaCO_3$ burial by coral reefs for the ocean's alkalinity budget. He proposed that glacial sea-level lowering would expose shallow water reefs to reduce carbonate burial on the continental shelves and/or increase the weathering of newly emergent shelf carbonate deposits, reducing the ocean's alkalinity output or driving a net alkalinity input, deepening the steady state lysocline and lowering atmospheric CO_2 (Opdyke & Walker, 1992), with about −1% (−2- to −3-ppm) atmospheric CO_2 decline per 100 m of steady-state lysocline deepening (see Equations 15c, 18d; Table 1). While the scenario is intuitive (Figure 7b), the requisite proportional increase in deep ocean $CaCO_3$ burial is not borne out by the observations (e.g., Archer & Maier-Reimer, 1994), which implies that the global average depth of the lysocline changed little (deepened by ~200 m in Table 2 and Figure 6) during peak glacials (e.g., Catubig et al., 1998; Yu et al., 2010), requiring that the difference between weathering and shelf $CaCO_3$ burial remained constant (Cartapanis et al., 2016; Hays et al., 2021; Wood et al., 2023) or was offset by other changes.

The attempt to overcome the constraint of the ocean's lysocline depth led to the proposal of a glacial reduction in the proportion of open ocean export of $CaCO_3$ relative to organic carbon: the "rain ratio hypothesis" (Archer & Maier-Reimer, 1994; Ridgwell et al., 2002). In this line of argument, the greater proportion of organic matter to $CaCO_3$ reaching the deepest seafloor would enhance porewater-driven seafloor $CaCO_3$ dissolution (Archer, 1991; Emerson & Bender, 1981) and thereby shoal the lysocline relative to the CSH (Figure 5). However, such decoupling of lysocline and CSH was found implausible for the LGM (Anderson & Archer, 2002; Ridgwell, 2003a; Sigman et al., 1998). Furthermore, reconstructions of deep-sea carbonate ion concentrations (Allen et al., 2015; Broecker & Clark, 2003; Marchitto et al., 2005; Yu et al., 2010) do not differ greatly between glacial and interglacial intervals, with the notable exception of significant glacial stage shoalings of CSH and lysocline in the Atlantic (e.g., Chalk et al., 2019; Francois et al., 1990) that have long been thought to counterbalance minor lysocline deepening in the Pacific (Emerson & Archer, 1990; Farrell & Prell, 1989). Hence, while the lysocline depth constraint allows for large changes in ocean alkalinity driven by $CaCO_3$ compensation (which affects the CSH only transiently), it effectively eliminates hypotheses that rely on steady-state CSH deepening to increase ocean alkalinity and lower CO_2 (Sigman et al., 1998). This includes scenarios in which changes in low-latitude surface $CaCO_3$ export are driven by changes in the $CaCO_3$–to–organic carbon rain ratio or in the rate of nutrient supply to, and thus biological export production from, low-latitude surface waters.

Ocean Nutrient Inventory and the Biological Pump

In his first attempt to explain the newly discovered ice age CO_2 drawdown, Broecker (1982a, 1982b) recognized the potential of the ocean's biological pump (more specifically, its soft-tissue pump) to store more carbon in the ocean interior. He considered three observational tests of this possibility, all focused on the ice age deep ocean: (a) a stronger surface–to–deep carbon isotopic gradient, (b) lower deep ocean oxygen concentrations, and (c) a deep seafloor $CaCO_3$ dissolution event upon glaciation and a $CaCO_3$ preservation event upon deglaciation. With some caveats, there is now compelling support for each of these tests (e.g., Anderson et al., 2019; Curry & Oppo, 2005; François et al.,1997; Galbraith & Jaccard, 2015; Hoogakker et al., 2018; Jaccard et al., 2009, 2016; Jacobel et al., 2020; Marchitto et al., 2005; Vollmer et al., 2022). These findings have motivated the ongoing search for a mechanism by which the biological pump was strengthened during ice ages.

Broecker's (1982a, 1982b) focus was on the low-latitude ocean (Figure 7c), where the supply of nitrogen and phosphorus, the two "major nutrients" required universally and in large quantities by phytoplankton, are fully consumed

and ultimately converted to export production. An increase in the ocean's inventory of the major nutrients would increase their supply to the surface, drive an increase in export production, and hence sequester additional carbon away from the atmosphere. This first-order description of sustained biological carbon sequestration in the ocean interior was the first paradigm of the biological pump (Figure 4a).

Phosphorus is delivered to the ocean by rivers, and it spends on average >16 kyr in the ocean between entering from the continents and being buried in sediment, mainly along the continental margin (Froelich et al., 1982; Ruttenberg, 2003). Yet, during the major deglaciations, CO_2 rises by >80 ppm in less than 10 kyr, which requires a major excess in phosphorus removal during these periods. Broecker suggested the deposition of phosphorus-containing marine organic matter on coastal sediments upon deglacial sea-level rise as the special process that drove the hypothesized rapid deglacial decline in ocean phosphorus, but phosphorus would have declined by less than 40% even if burial had somehow doubled over the approximate 10 kyr of deglacial sea-level rise. Critically, since Broecker's proposal, it was determined that sea-level rise lags the increase in atmospheric CO_2 at deglaciations (Bard et al., 1990; Fairbanks, 1989), which rules out Broecker's shelf sediment-based hypothesis in its original form. Still, climate-related changes in shelf phosphorus storage appear possible and warrant continued investigation (Wallmann, 2010).

Phytoplankton in the tropical to subtropical ocean are most frequently found to be limited by biologically available ("fixed") nitrogen (Moore et al., 2013). Accordingly, it has been proposed that changes in the ocean fixed nitrogen reservoir might strengthen the biological pump so as to explain part of the ice age CO_2 drawdown (Broecker & Henderson, 1998; Falkowski, 1997; McElroy, 1983). Dinitrogen (N_2), a gas that composes most of the atmosphere and is abundant in ocean water, is converted to oceanic fixed nitrogen through biological nitrogen fixation, and it spends on average 2–3 kyr in the ocean before being "denitrified" (converted from nitrate back to N_2) by bacteria that thrive under oxygen depletion, mainly in sediments on the continental shelf and in oxygen-deficient zones of the ocean's water column (Brandes & Devol, 2002). On average, nitrogen and phosphorus are consumed in the Redfield ratio of 16:1 during the production of open ocean biomass and released back into the water column in that ratio during its remineralization (Equation 9a). Denitrification, by removing oceanic fixed N but not P, generates a nitrogen deficit (or phosphorus excess) relative to the stoichiometric requirements of plankton (Broecker & Peng, 1982; Deutsch et

Table 3. Comparing CO_2 Effects of Different Hypotheses

	scenario	P_{prf} PAZ/NA/SAZ	volume ventilated PAZ/NA/SAZ	ΔP_{reg}	$\Delta CaCO_{3,reg}$	SAZ export	AZ export	Low lat. export	direct ΔCSH	lysocline deepening	deep O_2	direct CO_2	$\Delta CaCO_3$	compensated CO_2
		µmol/kg	%	µmol/kg	µmol/kg	Δ%	Δ%	Δ%	meters	meters	µmol/kg	ppm (Δ%)	µmol/kg	ppm (Δ%)
a)	T, SL, and land carbon combined	2.10/0.80/1.2	35%/25%/20%	0.000	+0	+0%	+0%	+0%	−559 m	0 m	165	285	17	267
b)	P_{total} +0.4 µmol/kg (+18%)	2.50/1.00/1.6	35%/25%/20%	0.130	+4	-0%	+0%	+18%	664 m	−498 m	143	247(−7%)	−20	266(+0%)
c)	Subantarctic P_{prf} −0.3 µmol/kg	2.25/0.65/0.9	35%/25%/20%	0.045	−3	+50%	+0%	-14%	-693 m	373 m	150	255(−4%)	21	237(−11%)
d)	Subantarctic P_{prf} −0.6 µmol/kg	2.40/0.50/0.6	35%/25%/20%	0.090	-6	+100%	+0%	−28%	−1407 m	747 m	135	246(−7%)	43	214(−20%)
e)	Antarctic P_{prf} −0.4 µmol/kg	1.70/0.80/1.2	35%/25%/20%	0.140	+0	+0%	+200%	+0%	−580 m	0 m	118	243(−9%)	17	229(−14%)
f)	Antarctic P_{prf} −0.8 µmol/kg	1.30/0.80/1.2	35%/25%/20%	0.280	+0	+0%	+400%	+0%	−1198 m	0 m	70	223(−16%)	35	200(−25%)
g)	Antarctic P_{prf} −1.2 µmol/kg	0.90/0.80/1.2	35%/25%/20%	0.420	+0	+0%	+600%	+0%	−1849 m	0 m	23	205(−23%)	52	177(−34%)
h)	Antarctic isolation (10Sv)	2.10/0.80/1.2	25%/30%/25%	0.110	+10	+0%	−49%	+0%	−119 m	0 m	128	256(−3%)	4	253(−5%)
i)	Antarctic isolation (3.5Sv)	2.10/0.80/1.2	15%/35%/30%	0.220	+20	+0%	−82%	+0%	−240 m	0 m	91	247(−7%)	7	241(−9%)
j)	Antarctic isolation (0Sv)	2.10/0.80/1.2	0%/45%/35%	0.395	+40	+0%	-100%	+0%	-298 m	0 m	31	237(−11%)	9	230(−13%)
k)	complete Antarctic sea ice	2.20/0.80/1.2	0%/45%/35%	0.395	+40	+0%	−100%	+0%	−298 m	0 m	31	237(−11%)	9	230(−13%)
l)	cell decoupling (40Sv)	2.10/0.80/1.2	50%/15%/15%	−0.175	-10	+0%	+104%	+0%	−1306 m	0 m	180	309(+11%)	38	268(−4%)
m)	cell decoupling (20Sv)	2.10/0.80/1.2	50%/15%/15%	−0.175	+0	+0%	+0%	+0%	−941 m	0 m	180	322(+15%)	28	288(+3%)
n)	cell decoupling with P deepening	2.20/0.70/1.1	50%/15%/15%	−0.175	-2	+0%	+0%	−9%	−1292 m	249 m	180	320(+14%)	38	275(−2%)
o)	Antarctic (-0.4 µmol/kg, 3.5Sv)	1.70/0.80/1.2	15%/35%/30%	0.280	+20	+0%	−45%	+0%	−491 m	0 m	70	238(−10%)	15	226(−15%)
p)	Subantarctic & Antarctic	1.85/0.65/0.9	15%/35%/30%	0.400	+14	+50%	−45%	−14%	−1642 m	373 m	29	217(−18%)	48	188(−29%)
q)	Subantarctic, Antarctic & P_{total} +9%	2.05/0.75/1.1	15%/35%/30%	0.475	+18	+50%	−45%	−5%	−888 m	124 m	29	210(−21%)	27	193(−27%)
r)	decoupled, Sub/Antarctic & P_{total} +9%	2.15/0.65/1.0	25%/30%/25%	0.413	+14	+50%	−48%	−14%	−1876 m	373 m	19	215(−19%)	55	183(−31%)

Note: Based on the results in Tables 1 and 2, the CO_2 effects are given for different hypotheses for the cause of peak atmospheric CO_2 drawdown, such as during the Last Glacial Maximum (LGM, Table 2). The various indicative scenarios shown here are called out by letter throughout the third part of the text. Table 3a indicates the minor effect of the combined changes in temperature (3.3 °C cooling), sea-level (125-m drop), and land carbon storage (350 PgC decrease). Table 3b indicates the potential for a whole-ocean phosphate (P_{total}) increase to shoal the steady state lysocline to counter lysocline deepening from other hypotheses. Table 3c–r summarize the effects of changes in the Southern Ocean that have been proposed to be central to ice age

al., 2001). It has long been expected that N_2 fixation would increase in the face of fixed nitrogen deficits, acting as a negative feedback to stabilize the ocean's fixed N reservoir at a given relationship to the P reservoir (Broecker, 1982a, 1982b; Deutsch et al., 2004; Schindler, 1977; Tyrrell, 1999). The ocean's spatial distribution of N_2 fixation (Deutsch et al., 2007; Marconi et al., 2017) and regional changes in N_2 fixation over glacial cycles (Ren et al., 2009, 2012, 2017; Straub et al., 2013) suggest that this feedback acts on adequately short spatial and temporal scales to maintain a consistent relationship between nitrogen and phosphorus reservoirs on glacial/interglacial time scales. This argues against N reservoir change as a major, independent driver of glacial/interglacial CO_2 change, refocusing attention on the oceanic dissolved phosphorus inventory.

Based on Broecker's first paradigm for the biological pump (Figure 4a), a mean ocean dissolved phosphate concentration increase of approximately 1 µmol/kg (+45%) could explain LGM CO_2 drawdown. However, the quasi-global increase in export production required in this hypothesis (Figure 7c) is inconsistent with available reconstructions of export production proxy records from the low latitudes (Sigman & Haug, 2003 and references therein). Moreover, complete consumption of the major nutrients only applies to the low-latitude surface because phytoplankton in high-latitude surface regions tend to be limited by some combination of light and trace nutrients (most importantly, iron). As a result, a given increase in ocean phosphate would not lead to a proportionally equivalent strengthening of the soft-tissue pump (Sigman et al., 1998). For the example given in Table 3b, a 0.4 µmol/kg (+18%) ocean phosphate increase raises regenerated phosphate by only 0.13 µmol/kg, with preformed phosphate increasing by 0.27 µmol/kg.

Moreover, because the low-latitude ocean hosts most of the surface $CaCO_3$ production and seafloor burial in the global ocean, an increase in low-latitude biological production would likely strengthen not just the soft-tissue pump but also the carbonate pump. The strengthening of the carbonate pump would counteract the decrease in atmospheric CO_2 due to the soft-tissue pump. For the example given in Table 3b, a 0.4-µmol/kg (+18%) phosphate increase raises regenerated $CaCO_3$ by +4 µmol/kg (+16%) in proportion to productivity; as a result, the CO_2 reduction due to the combined direct effects of soft- tissue and carbonate pump is only −20 ppm (−7%, Table 3b). Because the "rain ratio" of $CaCO_3$ and soft-tissue organic carbon (Corg) from the low-latitude surface to the deep ocean is roughly 1:1, any proportional change in export would fail to cause a transient seafloor $CaCO_3$ dissolution event (Box 2), resulting in only a negligible additional CO_2 decline from $CaCO_3$ compensation in this same example scenario (Equation 18d; Table 3b). Finally, an increase in surface $CaCO_3$ export also raises the burial of $CaCO_3$ on the seafloor above the lysocline, causing excess $CaCO_3$ burial and ocean alkalinity loss until the CSH and lysocline have adjusted to a shallower steady-state depth (Sigman & Boyle, 2000; Sigman et al., 1998; Equation 19b). In the example in Table 3b, because $CaCO_3$ rain is 18% greater, the ocean must lose 20 µmol/kg of dissolved $CaCO_3$ for the steady-state lysocline to shoal by approximately 500 m so as to rebalance the ocean's $CaCO_3$ budget. The loss of ocean alkalinity from this process works to raise atmospheric CO_2. Taking all processes into consideration, the net atmospheric CO_2 reduction is only about 1 ppm (−0%; Table 3b). This simplified scaling relationship assumes a constant deep ocean $CaCO_3$-to-Corg rain ratio near 1 (see Table 9.4.1 in Sarmiento & Gruber, 2006; Milliman et al., 1999), and ocean models can show larger net CO_2 decreases depending on their respective representations of the soft-tissue and carbonate components of the biological pump (Box 1; Hain et al., 2010, 2014). However, under the reasonable assumption that productivity in nutrient-rich high-latitude ocean regions would not respond to an increase in the ocean phosphate reservoir (because of a lack of phosphate limitation in those waters), it captures the limited capacity of an ocean phosphate change to lower atmospheric CO_2 (Sigman et al., 1998).

Other changes, as well as combinations of changes, in low-latitude biological production have been considered as possible drivers of CO_2 reduction during ice ages. One such proposal is that organic matter decomposed more slowly as it was sinking through a colder ice age water column (Boyle, 1988a, 1988b; Kwon et al., 2009; Matsumoto, 2007), thereby reaching greater depth and differentially concentrating respired carbon and nutrients at the depth of the lysocline, causing a $CaCO_3$ compensation event in which deep seafloor $CaCO_3$ burial transiently decreases. Deeper remineralization of the organic matter sinking flux would have shifted nutrients out of the upper ocean, reducing low-latitude biological production and thus the $CaCO_3$ sinking flux, in which case this change would have caused a deepening of the steady-state lysocline (Sigman et al., 1998), which is not observed. This violation of observations could be avoided if deeper organic matter remineralization (e.g., Table 3c,d,n) is somehow paired with some mechanism for an increase in low latitude biological production (e.g., due to an increase in ocean phosphate), in which case the observation of a relatively conserved steady-state lysocline is not violated (Table 3q,3r). As a similar example, enhanced low latitude biological production could be paired with a reduction in the $CaCO_3$-to-Corg rain ratio, effectively holding constant the per area rate of $CaCO_3$ rain (Equations 18a, 18b, and 19) and thus the steady-state lysocline depth (Sigman et al., 1998). However, as described earlier, there is not compelling evidence for such low-latitude biological changes (Hernández-Almeida et al., 2019; Sigman & Haug, 2003).

High-Latitude Ocean Hypotheses

For the purposes of this article, the "polar ocean" refers to the high-latitude regions where surface waters are cold and dense enough to readily exchange with water masses of the deep ocean and even form new deep-water masses, in contrast to the warm low/mid-latitude regions where the exchange between surface and interior waters is slow (Figure

4b). Furthermore, the rapid rate of nutrient supply to the surface in the polar ocean typically outstrips the capacity of the surface ocean ecosystem to consume it, with phytoplankton growth often limited by light and/or the trace metal nutrient iron (e.g., Moore et al., 2013). As a result, the major nutrients N and P go unused for carbon sequestration by the biological pump, leading them to elevate the ratio of preformed to regenerated nutrients in the ocean interior, allowing regenerated CO_2 to leak back to the atmosphere, and thus raising atmospheric CO_2. Any change in the ratio of polar nutrient upwelling to export production modifies the degree of surface nutrient consumption, the preformed nutrient concentration of the deep ocean, and hence the overall efficiency of the biological pump, separate from any change in the ocean's overall nutrient inventory (Keir, 1988; Knox & McElroy, 1984; Marinov et al., 2006; Marinov, Follows, et al., 2008; Marinov, Gnanadesikan, et al., 2008; Sarmiento & Toggweiler, 1984; Siegenthaler & Wenk, 1984; Toggweiler, 1999; Toggweiler & Sarmiento, 1985). These concepts have become the cornerstone for the development of detailed polar ocean- centered hypotheses for glacial CO_2 drawdown (reviews by Fischer et al., 2010; Galbraith & Skinner, 2020; Hain et al., 2014; Kohfeld & Ridgwell, 2009; Sigman & Boyle, 2000; Sigman & Haug, 2003; Sigman et al., 2010, 2021). Moreover, they have motivated paleoproxy reconstructions of the conditions in polar ocean surface waters and the deep ocean over glacial-interglacial cycles (Figure 9).

Subantarctic Iron Fertilization

Two discoveries—(a) that polar ocean productivity in the early 21st century is in part limited by the deficiency of the trace nutrient iron (Landing & Bruland, 1987; Martin & Fitzwater, 1988; Martin & Gordon, 1988) and (b) that the ice age atmosphere was dustier (De Angelis et al., 1987)—led John Martin to propose that iron-bearing dust fertilized the Southern Ocean so as to draw down CO_2 during the ice ages (Martin, 1990; Figure 7d). Subsequent work confirmed a much dustier ice age atmosphere (Kohfeld & Harrison, 2001; Lambert et al., 2008, 2021; Maher et al., 2010; Mahowald et al., 1999; Vallelonga et al., 2013). Coupled reconstructions of dust-borne iron supply, biological productivity, and the degree of nitrate consumption have yielded strong support for the iron fertilization hypothesis (Chase et al., 2001; Kumar et al., 1995; Martinez-Garcia et al., 2009, 2014; Robinson, Sigman, et al., 2005; Figure 9f). However, the region of enhanced productivity during peak ice ages was found to be only the Subantarctic Zone, the northern portion of the Southern Ocean that is under the strong westerly winds and directly downwind of dust sources in Patagonia and Australia (Kohfeld et al., 2005, and references therein).

The Subantarctic is an important pathway by which nutrients from the deep ocean are supplied to the low-latitude surface ocean (Fripiat et al., 2021; Marinov et al., 2006; Palter et al., 2010; Sarmiento et al., 2004), as part of the "upper cell" of ocean overturning that ultimately feeds NADW formation (Figure 4c). Subantarctic nutrient drawdown would therefore reduce the preformed nutrient burden of the ocean volume ventilated by the Subantarctic (~20% of ocean volume in the early 21st century) and, to some degree, also the volume ventilated by the North Atlantic (~25%). However, by concentrating the ocean's nutrient inventory in the deep ocean, it would also increase nutrient supply via the "lower cell" of ocean overturning to the more poleward Antarctic zone of the Southern Ocean surface, raising the unused nutrient concentration where AABW is formed (Table 3c,d). Including these downstream effects, the capacity of Subantarctic iron fertilization to make the soft-tissue pump more efficient is limited. At the same time, the reduction in upper ocean nutrients would cause a reduction in low- latitude biological productivity (Figure 7d; Marinov et al., 2006), which may also reduce the low-latitude $CaCO_3$ rain, weakening the carbonate pump, such that a Subantarctic phosphate drawdown of 0.3–0.6 µmol/kg would yield a net direct CO_2 drawdown of 12– 22 ppm (−4 to −7%) before $CaCO_3$ compensation (Table 3c,d). In addition, the reduction in low-latitude productivity and $CaCO_3$ rain to the seafloor would reduce $CaCO_3$ burial to make the global ocean more alkaline until the steady-state lysocline had deepened by approximately 370–750 m, decreasing atmospheric CO_2 in the process. Including alkalinity changes from the $CaCO_3$ compensation of the biological pump (Equations 16d, 16e) and from steady-state lysocline deepening results in the potential for 34–62 ppm CO_2 drawdown (−11% to −20%; Table 3). Similar sensitivities of CO_2

Subantarctic nutrient drawdown in carbon cycle models that include some or all of these effects (Hain et al., 2010; Joos et al., 1991; Marinov et al., 2006; Parekh et al., 2008; Ridgwell, 2003b; Sarmiento et al., 2004; Watson et al., 2000) support the view that the dust-borne Subantarctic iron fertilization hypothesis as envisaged by Martin (1990) can explain a significant part—although probably not more than half—of the peak ice age CO_2 drawdown (e.g., Röthlisberger, 2004). The steady-state lysocline deepening arguably risks violating the observational constraint of little steady-state lysocline change. However, low-latitude changes that might have offset this effect, such as a modest ocean nutrient inventory increase (Figure 7c), have been described.

Antarctic Mechanisms of CO_2 Drawdown

The Antarctic Zone of the Southern Ocean is the surface source region for about 35% of the global ocean's interior volume including through the formation of AABW (Broecker et al., 1985; Gebbie & Huybers, 2010; Primeau et al., 2013; Rae & Broecker, 2018; Table 3a). Due to this role of the Antarctic Zone in ventilating the deep ocean, if iron fertilization is also applied to spur productivity in the Antarctic Zone (i.e., Figure 7d), the full ice age CO_2 drawdown would easily be in reach (Marinov et al., 2006; Table 3e,f). However, in contrast to the evident increase in biogenic fluxes in the ice age Subantarctic Zone, available reconstructions consistently indicate lower productivity

across the ice age Antarctic Zone (François et al.,1997; Jaccard et al., 2013; Kohfeld et al., 2005; Mortlock et al., 1991; Weber et al., 2022), although some researchers have questioned this interpretation (Abelmann et al., 2006; DiTullio et al., 2000; Moore et al., 2000). Remarkably, nitrogen isotopic measurements of bulk sediment and fossil-bound organic matter indicate that Antarctic Zone nitrate consumption was more complete during the ice ages, despite the apparently lower productivity. The combination of more complete nitrate consumption and lower productivity suggests that gross nitrate supply was reduced (Ai et al., 2020; François et al.,1997; Robinson & Sigman, 2008; Sigman et al., 1999, 2021; Studer et al., 2015; Wang et al., 2017; Figure 9e). That is, major nutrient supply declined, as did productivity, but productivity declined less, so as to yield more complete nutrient consumption and lower surface nutrient concentrations relative to deep water. The reduction in nutrient supply appears to require slowed input of subsurface water into the Antarctic surface (Kemeny et al., 2018) and has been referred to as Antarctic surface "stratification" (François et al.,1997) or "isolation" (Sigman et al., 2021; Figure 8a). Why productivity would decline less than the major nutrient supply in the ice age Antarctic is an important question, likely involving the role of iron as a limiting nutrient in the region (Boyd & Ellwood 2010; Lefèvre & Watson, 1999; Rafter et al., 2017; Studer et al., 2015).

There is great potential for CO_2 drawdown associated with changing the Antarctic surface water entering the deep ocean from its Holocene condition of nutrient-richness to being nutrient-poor: All else equal, an Antarctic surface phosphate decrease from 2.1 to 1.3 µmol/kg lowers atmospheric CO_2 by 66 ppm (−24%, Table 3f). This potential is due to several considerations. First, there is little $CaCO_3$ production in the Antarctic Zone, so the enhanced nutrient drawdown is not associated with enhanced surface alkalinity drawdown (i.e., no strengthening of the carbonate pump) or with significantly higher $CaCO_3$ flux to the deep ocean (i.e., no forced shoaling of the steady state lysocline; cf. Broecker & Peng, 1989; Hain et al., 2010). Second, the organic carbon flux is regenerated in waters that communicate readily with the abyssal water that bathes the global lysocline, maximizing the $CaCO_3$ compensation-driven CO_2 decline (Box 2). These factors are in contrast with an enhancement of the low latitude biological pump, which (a) would tend to strengthen the carbonate pump due to an associated increase in $CaCO_3$ rain, which in itself raises atmospheric CO_2, and (b) would send sinking matter to the deep ocean with a $CaCO_3$-to-Corg ratio near 1, which prevents it from driving significant CO_2 reduction through $CaCO_3$ compensation (Hain et al., 2011; Sigman et al., 1998).

However, significant Antarctic nutrient drawdown requires either (a) a large increase in Antarctic productivity (Table 3e,f,g; Figure 7d) or (b) a substantial decline in gross nutrient supply from the ocean interior to the Antarctic surface (François et al.,1997; Kemeny et al., 2018; Figure 8a). The first option, when considered alone, is counter to the observations of an ice age reduction in export production. As described above, there is a scenario that is, in some sense, a composite of the two options: Both nutrient supply and productivity declined, but nutrient supply declined more, yielding both a reduction in the nutrient content of Antarctic surface waters and the importance of this water in ventilating the ocean interior. This scenario (Table 3o; cf., Hain et al., 2010) involves large reductions in Antarctic overturning (−82%), Antarctic deep ocean ventilation (−20% of ocean volume vacated), productivity (−45%), and Antarctic preformed phosphate (from 2.1 to 1.7 µmol/kg), resulting in a net atmospheric CO_2 reduction of 41 ppm (−15%).

Importantly, in this calculation, the circulation-driven reduction in nutrient supply to the Antarctic surface must be coupled to a reduction in the flux of the Antarctic surface waters back into the deep ocean, such as in the process of AABW formation. Otherwise, its CO_2 effects would be similar to, and redundant with, those of Subantarctic iron fertilization, such that their respective CO_2 drawdown terms would not be additive (Hain et al., 2010). Much of the CO_2 decline associated with the scenario of Table 3o derives from this reduction in deep ocean ventilation. If the rate of exchange between the Antarctic surface and the deep Southern Ocean declines, more of the global deep ocean water is ventilated by (i.e., "comes from") the North Atlantic and Subantarctic surface— a framing of ocean ventilation as the competition between preformed nutrient-rich and -poor ventilation sources (Figure 4c; Bolin & Stommel, 1961; Hain et al., 2010, 2014; Kwon et at., 2012; Sigman & Haug, 2003; Sigman et al., 2010; Stommel & Arons, 1959; Toggweiler et al., 2003). The proposed change has been categorized as an "Antarctic barrier mechanism" (Archer et al., 2003), in which the communication between the deep ocean and the atmosphere through the Antarctic surface undergoes an ice age reduction.

In isolation, eliminating Antarctic overturning and deep ventilation (from 35% to 0%) lowers the preformed nutrient content of the ocean by almost 0.4 µmol/kg phosphate, thus strengthening the soft tissue pump (Figure 6) so as to lower atmospheric CO_2 by 36 ppm (−13%, Table 3h–j). This mechanism is less effective at lowering atmospheric CO_2 than is Antarctic surface nutrient decline alone, as shown earlier (Table 3e–g *versus* 3h– j). This is because the reduced Antarctic ventilation strengthens the carbonate pump in step with the soft-tissue pump and leads to a weaker $CaCO_3$ compensation response (Hain et al., 2010; Kwon et al., 2012; Table 3h–j). Moreover, it is not additive with the surface nutrient depletion mechanism (Table 3e–g): In the end-member limit where the Antarctic surface does not ventilate the ocean interior, Antarctic surface nutrient conditions do not affect the soft-tissue pump (Hain et al., 2010; e.g., Table 3o). That is, Antarctic nutrient drawdown and reduction in Antarctic ventilation of the ocean interior undercut each other's leverage to set the deep ocean's preformed nutrient burden. As a result, given

the observational constraint of reduced Antarctic productivity during the ice ages, it appears unlikely that the composite Antarctic CO_2 drawdown exceeded 35–40 ppm (−10% to −15%; Hain et al., 2010; Table 3h–j,o).

Antarctic Hypotheses: Ocean Circulation *Versus* Air–Sea Gas Exchange

A number of physical mechanisms have been proposed to change ocean circulation so as to yield Antarctic surface "isolation" during the ice ages. These mechanisms operate by altering the vertical density structure of the Antarctic water column (de Boer et al., 2007; Sigman et al., 2004), with increased sea ice cover (Bouttes et al., 2010; Watson et al., 2015) or reduced wind-driven upwelling often proposed as the instigator (Ai et al., 2020; Anderson et al., 2009; Menviel et al., 2018; Sigman & Boyle, 2000; Sigman et al., 2021; Toggweiler et al., 2006). Changes in deep ocean conditions have also been proposed to reduce the rate of deep ocean ventilation by the Antarctic Zone, largely by slowing the loss of dense water from the abyssal ocean (de Boer & Hogg, 2014; Lund et al., 2011; Watson & Naveira Garabato, 2006). The critical challenge for all of these hypotheses is that they are not supported by ocean general circulation models: Under ice age boundary conditions, most models have the tendency to increase the exchange of water between the Antarctic surface and the underlying deep ocean, not decrease that exchange (Galbraith & Lavergne, 2019; Jansen, 2017; Jansen et al., 2018; Otto-Bliesner et al., 2007; Stouffer & Manabe, 2003; see also Lhardy et al., 2021b; Figure 8d).

An alternative Antarctic "barrier mechanism" for reducing CO_2 leakage from the deep ocean to the atmosphere is that of reduced air–sea CO_2 exchange due to enhanced sea- ice cover (Stephens & Keeling, 2000; Figures 8c and 9e). If sea ice cover was nearly complete in the region of the Antarctic forming deep water during the ice ages, then it could have reduced CO_2 outgassing and thus the concentration of atmospheric CO_2. In this hypothesis, the CO_2 was sequestered in another part of the ocean by the soft-tissue component of the biological pump, but it was retained in the sea ice–covered Antarctic surface water even as its nutrients went unused. The potential for CO_2 storage by this hypothesis, taken to completion, is effectively equivalent to that of complete isolation of the Antarctic surface from the underlying ocean interior (Table 3j *vs.* Table 3k), sharing the same limited and mutually exclusive potential to effect atmospheric CO_2 drawdown, unlikely more than 37 ppm (−13%; Table 3). The main difference between these two Antarctic barrier mechanisms—reduced surface-deep exchange and sea ice–induced reduction in gas exchange—is that the barrier to communication with the atmosphere is at the top or bottom of the Antarctic surface mixed layer, respectively (Figure 8a *vs*. 8c). This difference has few implications for the carbon chemistry of the atmosphere and ocean at the large scale. Similarly, Antarctic sea-ice cover and Antarctic nutrient consumption undercut each other's leverage to effect CO_2 decline (Hain et al., 2010). Sea ice retains upwelled respired carbon in Antarctic surface waters in form of "disequilibrium carbon" (e.g., Galbraith & Skinner, 2020; Khatiwala et al., 2019; Williams & Follows, 2011) whereas nutrient consumption removes disequilibrium carbon storage and would even generate negative disequilibrium carbon in the Antarctic surface under high productivity scenarios (e.g., Table 3g; Hain et al., 2010; Wu et al., 2019). Both of the Antarctic barrier mechanisms—controlled by circulation or sea ice cover (Figure 8a *vs*. Figure 8c)—suffer from the fact that the carbonate pump is strengthened along with the soft-tissue pump. As a stronger carbonate pump works to raise atmospheric CO_2, this effect reduces the net atmospheric CO_2 drawdown (Figures 3, 6; Box 1). Estimates of this effect depend strongly on how ocean models simulate $CaCO_3$ fluxes and seafloor processes. In particular, models with insufficient $CaCO_3$ sinking flux to the deep ocean underrepresent the carbonate pump and thereby overestimate the potential of the Antarctic barrier mechanisms to lower atmospheric CO_2 (supplement to Hain et al., 2010).

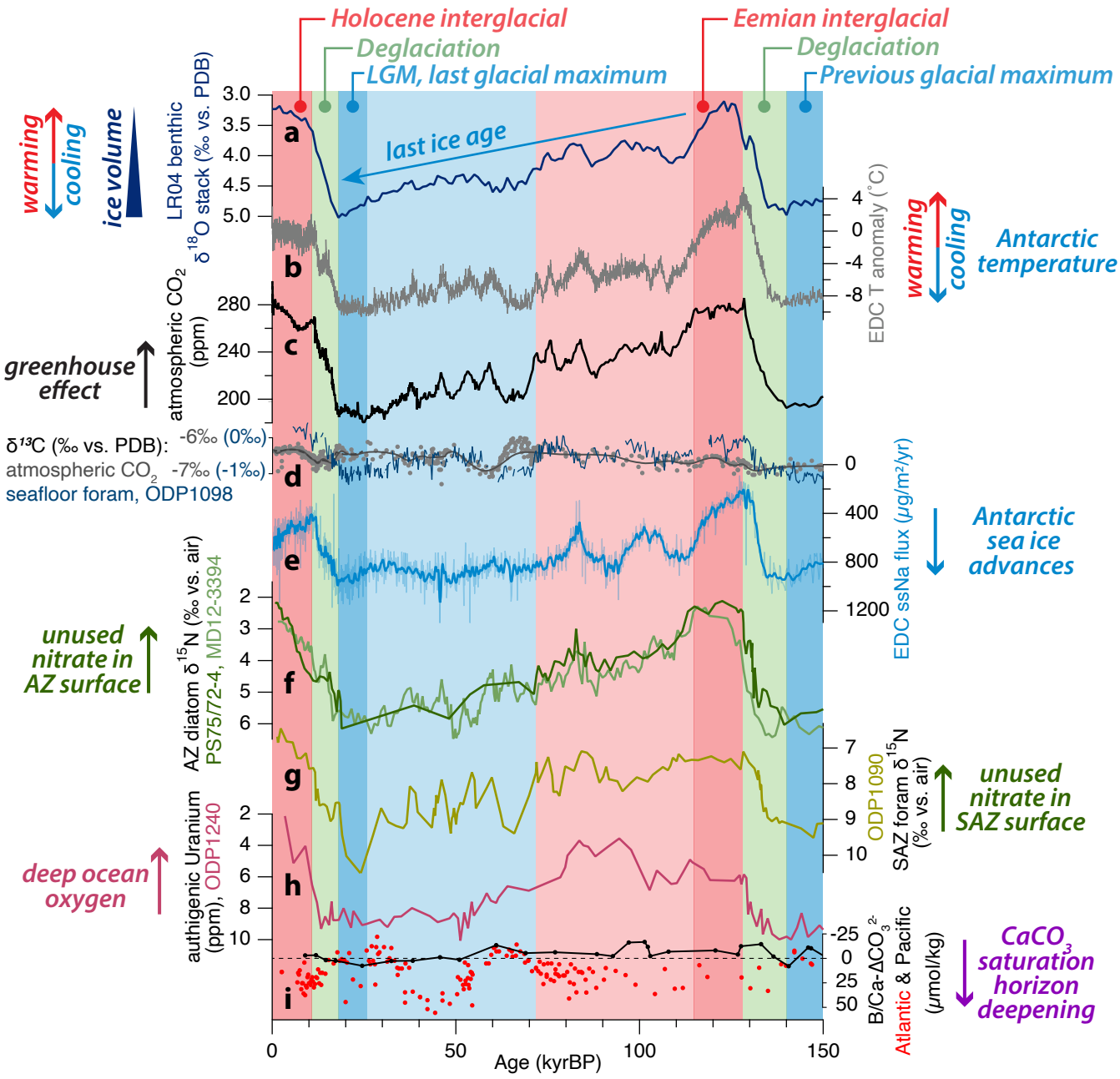

Figure 9. CO_2-relevant records over the last ice age cycle. Ice age cycles of the last million years have broadly followed a pattern of long-term cooling, ice growth, and CO_2 reduction to yield glacial maxima, which are followed by abrupt glacial terminations that yield short-lived interglacial climate conditions similar to preindustrial times (Figure 1). The best studied of these glacial cycles is the last one. The previous glacial maximum (~140 kyrBP; 140 thousand years before present) gave rise to deglaciation and ice age termination II (~125–135 kyrBP) and the Eemian interglacial (~115–125 kyrBP). The climate system then trended back toward ice age conditions, with three distinct episodes of cooling, ice sheet growth, and CO_2 reduction (at ~115, 70–80, and 20–30 kyrBP). This last glacial cycle culminated in the Last Glacial Maximum (LGM, ~20 kyrBP), followed by deglaciation and ice age termination I (~10–20 kyrBP) and then the current interglacial (the Holocene; since ~11 kyrBP). These broad global patterns are evident in reconstructions of ocean temperature and ice volume (a), Antarctic air temperature (b), and atmospheric CO_2 (c) (Bereiter et al., 2015; EPICA Community Members, 2004, 2006; Lisiecki & Raymo, 2005). The lowest recorded temperatures and CO_2 correspond to glacial maxima (dark blue background shading), after which temperature and CO_2 rise during intervals of deglaciation that terminate ice ages (light green shading), leading to the highest recorded temperatures and CO_2 during the brief warm interglacial periods (dark red shading)—with a stable climate/CO_2 relationship extending back throughout the ice core record (Figure 1; Siegenthaler et al., 2005). Shown here are several data sets relevant to the origin of the glacial/interglacial change in atmospheric CO_2 (d–i). Comparison of deep ocean (Hodell et al., 2003) and atmospheric (Eggleston et al., 2016; Elsig et al., 2009; Menking et al., 2022; Schmitt et al., 2012; Schneider et al., 2013) carbon isotope reconstructions (d) suggests there was more respired carbon (with its low $\delta^{13}C$) in the deep ocean during peak ice age conditions than during interglacial times. Many hypotheses for ice age CO_2 change involve the Southern Ocean, as the modern Southern Ocean is characterized by incomplete consumption of major nutrients (nitrogen and phosphorus) by phytoplankton, representing a “missed opportunity” for carbon sequestration via the biological pump (Box 1; Sigman et al., 2010). (continues next page)

Figure 9. (continued) The nitrogen isotopic composition ($\delta^{15}N$) of organic matter preserved within plankton fossils is a proxy for the degree of Southern Ocean surface nutrient consumption (Altabet & Francois, 1994; Shemesh et al., 1993; Sigman et al., 1999), where higher $\delta^{15}N$ reflects more complete nutrient consumption, with a smaller proportion of nutrients le" unused in the surface. Fossil-bound $\delta^{15}N$ records from the Southern Ocean, both the SAZ (g) and AZ[ii] (f), indicate a more efficient biological pump during ice ages (Ai et al., 2020; Martinez-Garcia et al., 2014; Studer et al., 2015). SAZ productivity increases during ice ages (Kumar et al., 1995; Martinez-Garcia et al., 2009), consistent with dust-borne iron fertilization driving the enhanced nutrient consumption. In contrast, even though Antarctic $\delta^{15}N$ indicates that nutrient supply to the AZ surface was more completely consumed during ice ages, it appears that AZ productivity was reduced (François et al.,1997; Mortlock et al., 1991). This combination suggests that the ice age AZ was characterized by reduced upwelling and/or overturning, leading to a reduction in the leakage of biologically stored carbon. An alternative AZ-focused mechanism for CO_2 drawdown is a sea ice–induced restriction of air–sea CO_2 exchange (Stephens & Keeling, 2000), a possibility supported by evidence for ice age sea ice expansion from sea salt-sodium concentration in Antarctic ice cores (e, Fischer et al., 2007; Fischer et al., 2021; Röthlisberger et al., 2010; Wolff et al., 2006) and other data. Findings of an ice age decline in deep ocean O 2 (h; Jacobel et al., 2020) and in preformed phosphorus (Vollmer et al., 2022) provide observational support for an ice age increase in the biologically stored carbon in the deep ocean or its conversion to disequilibrium-stored carbon by a failure to vent to the atmosphere across the AZ air-sea interface. Reconstructed changes in deep ocean $CaCO_3$ saturation (i) are significant in the Atlantic (Sosdian et al., 2018) but minimal in the Pacific (Kerr et al., 2017). The Southern Ocean-centered dynamics responsible for the progressive CO_2 decline going into long ice ages may be different from the dynamics of abrupt glacial termination, where Southern Ocean CO_2 release may have been caused by a sequence of events that began with a change in the northern ice sheets.

Deep Ocean Overturning, Ventilation, and Carbon Storage

In considering the role of the polar ocean in glacial/interglacial CO_2 decline, the focus so far has been on the conditions and fluxes of the upper ocean. This is appropriate, as the ocean surface layer and its communication with both the overlying atmosphere and the underlying ocean interior are responsible for the effect that the polar ocean has on atmospheric CO_2. Nonetheless, the ocean interior is the ultimate site of the ocean's CO_2 storage, and its physical and chemical conditions record the net outcome of the upper ocean's fluxes of heat, salt, carbon, alkalinity, and nutrients. Thus, evidence of deep ocean change is central to the effort to understand how the ocean worked to lower atmospheric CO_2 during the ice ages.

Collectively, the data have yielded a rough consensus for the geometry and composition of the deep ocean during at least the last ice age. The "upper cell" associated with NADW formation is reconstructed to have shoaled, leaving the "lower cell" sourced by AABW to take up a larger proportion of the deep ocean (e.g., Adkins, 2013; Curry & Oppo, 2005; Duplessy et al., 1988; Lynch-Stieglitz et al., 2007; Menviel et al., 2017; Figure 8b; see also Figure 4c). The upper cell appears to have been more nutrient-deplete than in the Holocene, perhaps due to a combination of Subantarctic iron fertilization and a circulation-driven reduction in the contribution of AAIW and SAMW to NADW source waters (e.g., Sigman et al., 2003). The lower cell of global ocean overturning appears to have absorbed the nutrients from the upper cell (Boyle, 1988a, 1988b). A lower oxygen concentration in the lower cell and other changes suggest that a large proportion of these nutrients were emplaced by the remineralization of sinking organic matter (François et al., 1997; Hoogaker et al., 2018; Jaccard et al., 2009; Jacobel et al., 2020; Lu et al., 2022), which would represent a strengthening of the soft-tissue pump (e.g., Kwon et al., 2009; Matsumoto, 2007; Menviel et al., 2012; Vollmer et al., 2022). Moreover, the concentrated carbon storage in the deep ocean near the lysocline depth would have driven $CaCO_3$ compensation that would have raised whole ocean alkalinity (Boyle, 1988b; Toggweiler, 1999; Yu et al., 2010; Box 2). Radiocarbon data suggest that the lower cell was ventilated only slowly (Galbraith et al., 2007; Rafter et al., 2022; Sikes et al., 2000; Skinner & Bard, 2022; Skinner et al., 2017; Zhao et al., 2018; cf. Broecker & Clark, 2010), which could be due to reduced flow rates of water into the abyssal volume, limited air– sea CO_2 isotopic equilibration in the source region for incoming abyssal water, or both. The resulting picture of the deep ocean appears strongly supportive of Southern Ocean– driven mechanisms for lowering ice age CO_2 (e.g., Anderson et al., 2019; Galbraith & Jaccard, 2015; Hoogakker et al., 2018; Jaccard et al., 2016; Jacobel et al., 2020; Menviel et al., 2017; Rae et al., 2018; Vollmer et al., 2022; e.g., Figure 9h).

Numerical models of ocean circulation would appear to support this "geometry" for the ice age ocean's water masses. In response to glacial boundary conditions (e.g., in temperature, land ice, and orbit), models often spontaneously produce an expanded lower overturning cell sourced from the Southern Ocean, with an upper cell sourced from the North Atlantic that reaches less far into the interior (e.g., Jansen, 2017; Otto-Bliesner et al., 2007; Stouffer & Manabe, 2003). Moreover, studies have suggested physical mechanisms for the "decoupling" of upper and lower overturning cells that might reinforce this tendency (de Boer & Hogg, 2014; Ferrari et al., 2014; Galbraith & Lavergne, 2019; Jansen et al., 2018; Lund et al., 2011; Figure 8b). However, expanded Antarctic ventilation of the deep ocean overturning cell tends to impose the high preformed nutrient burden of the Antarctic surface onto the deep ocean, weakening the soft-tissue component of the biological pump and thereby tending to raise atmospheric CO_2 (Cliff et al., 2021; Galbraith & Lavergne, 2019; Galbraith & Skinner, 2020; Hain et al., 2010; Khatiwala et al., 2019; Kwon et al., 2012; Marinov, Follows, et al., 2008; Marzocchi & Jansen, 2019; Sigman & Haug, 2003; Figure 8b; Table 3l–m). Hence, it is incorrect to assume—as is done commonly in the literature—that expansion of the Antarctic- ventilated lower overturning cell would, by itself, enhance ocean CO_2 sequestration. It has also been proposed that the abyssal water of the lower cell "stagnated" due to extremely slow circulation (Keigwin & Schlegel, 2002; Marchitto et al., 2007;

Sikes et al., 2000; Skinner et a l., 2010) and thus accumulated the regenerated products of biological production (Kwon et al., 2011; Skinner et al., 2017; Toggweiler, 1999). However, adding the effect of the carbonate pump associated with the biological $CaCO_3$ sinking flux into the deep ocean would yield a nearly equal sequestration of regenerated DIC and ALK in the proposed stagnant abyssal reservoir—leading to little change in atmospheric CO_2 (Hain et al., 2011; Equation 5f). In the extreme case of perfect isolation of an abyssal volume, its tendency to accumulate regenerated alkalinity and DIC at a ratio greater than 1 would lead to the unobserved phenomenon of abyssal $CaCO_3$ deposition, a decline in global ocean alkalinity, and thus a rise in atmospheric CO_2 (Hain et al., 2011), the opposite of what is required to lower ice age atmospheric CO_2. Among the physical ocean modeling community, the specific set of mechanisms that is most often favored for ice age CO_2 drawdown is that of an abyssal ocean reservoir, in which CO_2 is trapped due to sea ice cover–driven gas exchange limitation at the Antarctic surface, the "Antarctic barrier" mechanism operating through disequilibrium carbon storage (Marzocchi & Jansen, 2019; Stouffer & Manabe, 2003; Figure 8e). The discussion above has pointed out the limitations on CO_2 drawdown by this mechanism, which are in part due to $CaCO_3$ dynamics, preventing it from achieving more than half of the full ice age CO_2 drawdown (Hain et al., 2010; Kwon et al., 2011). From a physical perspective, this combination of changes also leads to a somewhat unintuitive situation: An "Antarctic-sourced" abyssal reservoir that was last ventilated outside the Antarctic, in the North Atlantic, or some other region. That is, from the perspective of air-sea CO_2 exchange, the water in the putative abyssal reservoir would need to have been ventilated largely from the North Atlantic and have entered the abyssal reservoir by ocean interior mixing, across the hydrographic boundary that separates the upper and lower overturning cells (Figure 8e; Toggweiler, 1999).

Given the inherent limitations of the CO_2 drawdown from Antarctic gas exchange limitation, some studies have combined the mechanism with enhanced nutrient drawdown by Southern Ocean iron fertilization (e.g., Brovkin et al., 2012; Stephens & Keeling, 2000). Indeed, some studies find that, even without an ice age expansion in sea ice cover, the slow rate of gas exchange in the Antarctic Zone is adequate to prevent the evasion of the additional CO_2 stored from iron fertilization (Ito & Follows, 2013; Khatiwala et al., 2019). Reciprocally, studies arguing for lower surface nutrients in the Antarctic surface have turned to reduced Antarctic surface-to-deep exchange in order to explain the lower biological export production in the region (François et al.,1997; Kemeny et al., 2018; Sigman et al., 2021). In both cases, the net result is the coupling of a biological pump mechanism with an Antarctic barrier mechanism, be it Antarctic surface "isolation" (Figure 8d) or Antarctic air-sea gas exchange limitation (Figure 8e). In summary, there is now substantial evidence that more CO_2 was stored in the deep ice age ocean and that the Southern Ocean played a major role in this, but the respective roles of the biological pump versus surface CO_2 disequilibrium are not yet clear (Sigman & Hain, 2024).

Deglaciations and Their Implications

The end of the last ice age can be viewed as an abrupt *termination* of a longer cycle or as a short period of transition between climate and carbon cycle states. The approximate 10- kyr interval containing the termination of each of the glacial maxima is known as a *deglacial period* (highlighted by green shading in Figure 9), a colloquial term referring to the age range of geomorphic features and deposits that record most ice sheet and mountain glacier retreat (i.e., deglaciation).

The timing of events at deglaciations, especially the last deglaciation, has been pursued as a source of information on the cause of the ice age cycles in ice volume, climate, and atmospheric CO_2, including the mechanistic connections among these cycles. Among the most influential findings is that Antarctica, and the southern hemisphere in general, began warming prior to the first major warming in the northern hemisphere (Jouzel et al., 1995; Sowers & Bender, 1995; WAIS Divide Project Members, 2015). This suggests either that northern hemisphere insolation change associated with deglaciations somehow remotely triggers Antarctic warming, preserving the primacy of the Milankovitch hypothesis that northern summer insolation drives ice ages (Abe-Ouchi et al., 2013; Alley et al., 2002; Broecker & Denton, 1989; Imbrie et al., 1992; Jochum et al., 2012; Kawamura et al., 2007; Figure 10) or that a southern hemisphere insolation trigger must be sought (Galbraith & Lavergne, 2019; Genthon et al., 1987; Held, 1982; Huybers & Denton, 2008; Timmermann et al., 2014; WAIS Divide Project Members, 2013). While most northern hemisphere warming and ice loss appear to occur relatively late in the deglaciation (Fairbanks, 1989), there is evidence for some northern hemisphere ice loss very early in the deglacial sequence, consistent with Milankovitch's mechanism (Clark et al., 2009). Accordingly, mechanisms have been proposed by which Milankovitch theory could be extended to explain early southern hemisphere warming (Imbrie et al., 1992). A popular proposal is that a nascent deglacial warming in the northern hemisphere triggered a "Heinrich event" at approximately 17 kyrBP, an iceberg discharge into the North Atlantic that shut down NADW formation, causing a cold event in the circum–North Atlantic until 14.7 kyrBP (Clark et al., 2002; Heinrich, 1988; Hemming, 2004; Jouzel et al., 2007; McManus et al., 2004; Robinson et al., 2005). The NADW shut-off would have reduced heat transport from the southern to the northern hemisphere, thus potentially explaining the early warming in the southern hemisphere (Blunier et al., 1998; Clark et al., 2002; Ganopolski & Rahmstorf, 2001; Manabe & Stouffer, 1988; Stocker, 1998; Zhu et al., 2022). There is tentative evidence that some amount of Southern Ocean deglacial change began prior to the onset of North Atlantic cooling associated with this

deglacial Heinrich event (Sikes et al., 2023; Stott et al., 2007; Wolff et al., 2006). If so, an additional mechanism must explain these changes, with possible implications for the pacing mechanism of the ice age cycles as a whole (Huybers & Denton, 2008; Timmermann et al., 2009).

Deglacial CO_2 rise is observed to begin nearly in step with Antarctic warming (Monnin et al., 2001). This has been interpreted to indicate a leading, early role for the greenhouse effect of CO_2 in causing global warming and deglaciation (Parrenin et al., 2013; Shakun et al., 2012). Regarding the cause of deglacial CO_2 rise, the timings suggest a direct connection to the Antarctic climate and Southern Ocean changes (Monnin et al., 2001; Schmitt et al., 2012). This might be taken to indicate that the CO_2 feedback is not strongly related to the Milankovitch northern hemisphere ice sheet–based feedback (Figure 10). However, as with southern hemisphere deglacial warming, the Milankovitch mechanism could still have triggered Southern Ocean CO_2 release to the atmosphere, with many proposals positing a role for NADW shutdown as the teleconnection between hemispheres.

Various hypotheses for this linkage call on the Southern Ocean mechanisms for reducing ice age atmospheric CO_2 discussed earlier but operating in the context of deglaciation. For example, the CO_2 increase at the onset of deglaciation might result from the waning of dust-borne iron fertilization (Martinez-Garcia et al., 2014), from declining Antarctic sea ice cover that allowed CO_2 to escape across the sea–air interface (Stephens & Keeling, 2000), or from enhanced Antarctic upwelling and/or deep overturning (Anderson et al., 2009; Burke & Robinson, 2012; Denton et al., 2010; Martínez-Botí, Marino, et al., 2015; Menviel et al., 2011; Rose et al., 2010; Schmittner & Galbraith, 2008; Sigman et al., 2007; Skinner et al., 2010; Tschumi et al., 2011). In general, the data on deglaciations are consistent with a primary role of the Southern Ocean in ice age CO_2 cycles (Figure 9). Ongoing measurement efforts seek to test the range of proposed mechanisms for ice age CO_2 reduction by assessing their potential to explain the timing of deglacial CO_2 rise (Ai et al., 2020; Anderson et al., 2009; Rae et al., 2018). Ultimately, this will require that the data be incorporated into or compared with numerical models of the proposed environmental changes (e.g., Chalk et al., 2017; Gottschalk et al., 2019; Hain et al., 2014; Menviel et al., 2018).

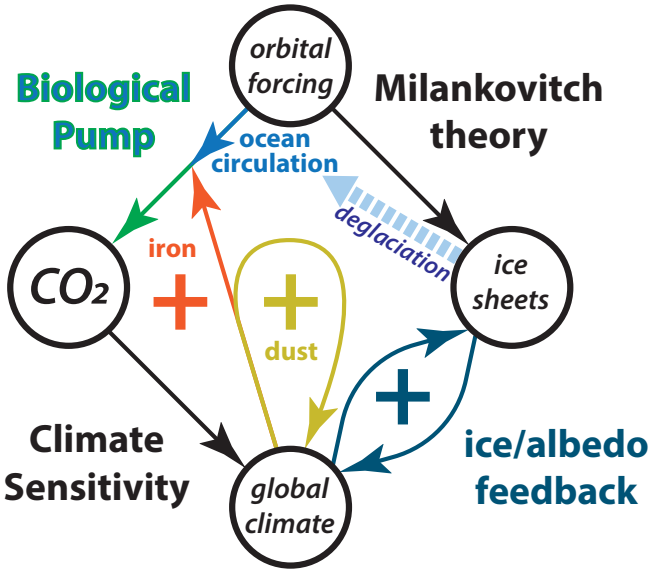

Figure 10. Interactions and feedbacks proposed for the ice age cycles. Changes in Earth's orbit gradually redistribute solar insolation between seasons and latitude bands, and this orbital forcing somehow paced the rhythm of past ice age cycles. The original proposal by Milankovitch and his associates was that low summer insolation in high northern latitudes favors accumulation of snow and hence ice sheet advance. Any expansion of high-albedo snow and ice cover would cause ice age cooling near that ice and in the global average, thereby amplifying ice sheet advance in a positive ice/albedo feedback. This paradigm was largely accepted by the 1970s. Subsequently, the discovery of glacial/interglacial changes in atmospheric carbon dioxide (CO_2) indicated a second feedback, driven by the greenhouse effect, with the potential for strong interaction between the two feedbacks. However, the insolation and/or climatic origins of the CO_2 changes remain unclear. Based on the sensitivity analysis and data reviewed here, CO_2 change was probably primarily caused by changes in the ocean's biological pump, likely mediated by the response of the Southern Ocean to orbital forcing. Any global cooling from CO_2 reduction would be amplified by the positive ice/albedo feedback, driving additional ice sheet advance. There is also evidence for a much dustier atmosphere during cold and dry ice ages, which would increase Earth's albedo in positive dust/albedo climate feedback. Moreover, data support the hypothesis that the dust fertilized Southern Ocean phytoplankton growth during peak ice age conditions, acting to strengthen the ocean's biological pump and thus lower CO_2 levels, thereby constituting a positive dust/CO_2 climate feedback. When put in this context, the Milankovitch theory and the CO_2 theory are not in competition, instead acting together to cause the ice age cycles in CO_2, global climate, and glaciation of the last million years or more. Additional feedbacks between climate, deglacial ice sheet melting, and ocean circulation appear to be important in the abrupt terminations of ice ages (dashed blue arrow), and they may also apply under anthropogenic warming.

Perspective

This article documents our evolving understanding of the regulation of atmospheric CO_2 on orbital timescales as part of the natural functioning of marine, terrestrial, and open system carbon cycling at the Earth System scale. The concepts are the product of 200 years of discovery in nearly every aspect of Earth System Science: physical, chemical, and geological oceanography; global biogeochemical cycles and atmospheric chemistry; terrestrial and marine biology; and paleoceanography, paleoclimatology, paleontology, and Earth history. Advances in geochemical, glaciological, geochronological, and sedimentological methods and in atmospheric and oceanic theory, modeling, and computation have been central to progress.

The ocean's biological pump is likely a critical factor in observed CO_2 changes, with plausible changes achieving reconstructed atmospheric CO_2 reductions during ice ages. The orbital theory and CO_2 theory for repeated ice age cycles in global climate are consistent if orbital change drives atmospheric CO_2 changes that yield positive climate

feedbacks (Figure 10). While CO_2 was clearly a key element of the ice age cycles, it remains unclear whether ice sheet–related feedbacks to orbital forcing trigger the CO_2 feedbacks, *vice versa*, or the two sets of feedbacks are largely independent. Ocean circulation appears to impact long-term CO_2 change more directly than does global climate, with the Southern Ocean surrounding Antarctica emerging as the nexus. The main exception is climate-induced enhancement of atmospheric dustiness, which has both a radiative albedo effect and an apparent CO_2 feedback through iron fertilization of the ocean's biological pump, both amplifying climate change (Figure 10).

This perspective has diverse implications for ongoing fossil fuel CO_2-driven climate change, three of which are highlighted here. First, as with land carbon release during the ice ages, the vast majority of the CO_2 emitted by humans will be taken up by the ocean (over centuries) and by net dissolution of $CaCO_3$ to achieve $CaCO_3$ compensation (over millennia). However, in the early 21st century, fossil fuel emissions far outpace ocean carbon uptake so that anthropogenic CO_2 is accumulating in the atmosphere and surface ocean, where it drives climate change and threatens marine ecosystems with its acidic properties. Both of these adverse conditions would be mitigated by emissions reductions, purposeful ocean alkalinity enhancement, and interventions that speed the transfer of carbon to the deep ocean.

Second, if CO_2 was the primary mediator of ice age climate change but climate sensitivity to CO_2 accounts for only half of ice age cooling, then the global ice sheets and their positive ice albedo feedback (Figure 10) may be more sensitive to greenhouse gas forcing than has been estimated so far. If so, important climate feedbacks may have been missed or underestimated. Continued loss of ice may beget more global warming than expected, with the potential for diverse feedbacks on different timescales.

Finally, glacial/interglacial CO_2 change likely involved the exchange of CO_2 between the atmosphere, polar ocean surface, and the deep ocean, as mediated by the physical, chemical, and biological processes of the polar oceans, especially the Southern Ocean. The questions that persist regarding the specific mechanisms at play—if answered— could plausibly alter climate models' treatment of polar ocean processes. This, in turn, might change the projections for anthropogenic carbon uptake by the ocean as climate warms in the future. In particular, the role that the Southern Ocean played in deep ocean CO_2 storage during the ice ages should clarify whether the circulation of the ocean's deepest, densest waters speeds up or slows down in response to climate warming. The answer to this question has direct implications for the rate with which the ocean will take up anthropogenic CO_2 and global warming heat.

Further Reading

Archer, D., & Maier-Reimer, E. (1994, January). Effect of deep-sea sedimentary calcite preservation on atmospheric CO_2 concentration <*https://doi.org/10.1038/367260a0*>. *Nature*, *367*(6460), 260–263.

Broecker, W. S. (1982). Glacial to interglacial changes in ocean chemistry. *Progress in Oceanography*, *11*, 151–197.

Broecker, W. S. (1982, October). Ocean chemistry during glacial time <*https://doi.org/10.1016/0016- 7037(82)90110-7*>. *Geochimica et Cosmochimica Acta*, *46*(10), 1689–1705.

Denton, G. H., Anderson, R. F., Toggweiler, J. R., Edwards, R. L., Schaefer, J. M., & Putnam, A. E. (2010, June 25). The last glacial termination <*https://doi.org/10.1126/science.1184119*>. *Science*, *328*(5986), 1652–1656.

Hain, M. P., Sigman, D. M., & Haug, G. H. (2010, December). Carbon dioxide effects of Antarctic stratification, North Atlantic Intermediate Water formation, and subantarctic nutrient drawdown during the last ice age: Diagnosis and synthesis in a geochemical box model <*https://doi.org/10.1029/2010GB003790*>. *Global Biogeochemical Cycles*, *24*(4).

Ito, T., & Follows, M. J. (2005, July 1). Preformed phosphate, soft tissue pump and atmospheric CO_2 <*https://elischolar.library.yale.edu/journal_of_marine_research/102*>. *Journal of Marine Research*, *63*(4), 813–839.

Khatiwala, S., Schmittner, A., & Muglia, J. (2019, June 7). Air-sea disequilibrium enhances ocean carbon storage during glacial periods <*https://doi.org/10.1126/sciadv.aaw4981*>. *Science Advances*, *5*(6), eaaw4981.

Kohfeld, K. E., Le Quéré, C., Harrison, S. P., & Anderson, R. F. (2005, April). Role of marine biology in glacial- interglacial CO 2 cycles <*https://doi.org/10.1126/science.1105375*>. *Science*, *308*(5718), 74–78.

Petit, J. R., Jouzel, J., Raynaud, D., Barkov, N. I., Barnola, J.-M., Basile, I., Bender, M., et al. (1999, June).

Climate and atmospheric history of the past 420,000 years from the Vostok ice core, Antarctica <*https://doi.org/10.1038/20859*>. *Nature*, *399*(6735), 429–436.

Sarmiento, J. L., & Gruber, N. (2006). *Ocean biogeochemical dynamics*. Princeton University Press. Sarmiento, J. L., & Toggweiler, J. R. (1984, April). A new model for the role of the oceans in determining atmospheric P CO_2. *Nature*, *308*(5960), 621–624.

Shackleton, N. J. (1977). Carbon-13 in Uvigerina: Tropical rainforest history and the equatorial Pacific carbonate dissolution cycles. In N. R. Andersen & A. Malahoff (Eds.), *The fate of fossil fuel* CO_2 *in the Oceans* (pp. 401–427). Plenum.

Siegenthaler, U., Stocker, T. F., Monnin, E., Luthi, D., Schwander, J., Stauffer, B., Raynaud, D., et al. (2005). Stable carbon cycle–climate relationship during the late Pleistocene, *Science*, *310*(5752), 1313–1317.

Sigman, D. M., Fripiat, F., Studer, A. S., Kemeny, P. C., Martínez-García, A., Hain, M. P., Ai, X., Wang, X., Ren, H., & Haug, G. H. (2021, February). The Southern Ocean during the ice ages: A review of the Antarctic surface isolation hypothesis, with comparison to the North Pacific <*https://doi.org/10.1016/j.quascirev.2020.106732*>. *Quaternary Science Reviews*, *254*, 106732.

Sigman, D. M., McCorkle, D. C., & Martin, W. R. (1998, September). The calcite lysocline as a constraint on glacial/interglacial low-latitude production changes <*https://doi.org/10.1029/98GB01184*>. *Global Biogeochemical Cycles*, *12*(3), 409–427.

Stephens, B. B., & Keeling, R. F. (2000, March). The influence of Antarctic Sea ice on glacial–interglacial CO_2 Variations <*https://doi.org/10.1038/35004556*>. *Nature*, *404*(6774), 171–174.

List of Symbols

Symbol	Unit	Description	Equations
T, ΔT, δT	˚C	Temperature, temperature change, incremental temperature change	1, 8, 16
F_{GHG}	W/m^2	Greenhouse gas radiative forcing	1
λ_{ECS}, $\lambda_{icesheets}$	W/m^2/˚C	Climate feedback parameters related to the radiative forcing caused by a change in global temperatures	1
H^+, H_2CO_3, HCO_3^-, CO_3^{2-}, H_3BO_3, $B(OH)_4^-$	μmol/kg	Concentrations of dissolved chemical species: total proton, carbonic acid, bicarbonate ion, carbonate ion, boric acid, borate ion	2
CO_2, δCO_2	ppm	Dry mixing ratio of carbon dioxide in air or equivalent CO_2 concentration of seawater, incremental CO_2 change	2,4,5
K_1, K_2, K_B	μmol/kg	Acid/base dissociation constants	2,16
K_0	μmol/kg /ppm	CO_2 solubility constant	2,16
α, β, R, CPF	unitless	Buffer factors: carbonate buffer, borate buffer, Revelle	2,4,5

		CO_2 buffer, fraction of total buffering by carbonate	
DIC, ALK, δDIC, δALK	μmol/kg	Concentrations of dissolved inorganic carbon species, concentration of alkalinity, incremental changes in DIC and ALK	3,4,5
pH_T, $-\log_{10}H_T^+$	unitless	Logarithm of total proton concentration	3
S, ΔS, δS	unitless	Seawater salinity, salinity change, incremental salinity change	3, 9, 16
$\delta_X CO_2/CO_2$	unitless	Incremental fractional change in CO_2 in response to a linear incremental change a given factor X, such as DIC, ALK, T, Sal	5, 14, 15
$\Delta_X \ln CO_2$	unitless	Integrated fractional CO_2 change caused by a change in a given factor X	5
N_{atm}	mol	Number of gas in the atmosphere excluding water vapor (1.773×10^{20} mol)	6
M_{oc}	kg	Mass of seawater in the modern ocean	6
$\Delta_{A-O}CO_2$, $\Delta_A CO_2$, $\Delta_O CO_2$	ppm	CO_2 difference between atmosphere and ocean taken to be some initial disequilibrium, atmospheric CO_2 change during equilibration, atmospheric CO_2 change during equilibration	6
Φ, $\Delta_A CO_2/\Delta_{A-O}CO_2$	unitless	CO_2 partition factor during atmosphere-ocean equilibration (assumed constant 85% in this chapter)	6
δC_{Land}	mol, PgC	Incremental change in land carbon stock, convertible between carbon atom number and carbon atom weight with 12 gC per mol C	7,14,16
$\delta_X K/K$	unitless	Incremental fractional change in equilibrium constants (see eq.2 and eq.14) in response to a linear incremental change a given factor X, such as T, S, pressure	8,9,18
SL, δSL	m	Sea level, incremental sea level change	9, 16
P, δP, ΔP	μmol/kg	Concentration of phosphorous nutrient, incremental and integrated P uptake during phytoplankton biomass net growth	10,16
ΔC_P	mol, PgC	Integrated change in ocean biomass carbon stock in response to integrated net P uptake, convertible between carbon atom number and carbon atom weight with 12 gC per mol C	10
P_{total}, $P_{preformed}$, $P_{regenerated}$	μmol/kg	Total concentration of phosphorous nutrient includes preformed component when unused by phytoplankton in the surface or regenerated when P is released in the ocean interior during biomass decomposition	11,16
AOU	μmol/kg	Apparent oxygen utilization refers to the deficit in seawater oxygen concentration relative to O_2 saturation with respect to the atmosphere; often referred to as oxygen depletion caused by the oxic respiration of organic matter biomass	
$Si(OH)_4$, SiO_2	μmol/kg	Seawater concentration of silicic acid, which is used by some plankton to form solid opal hard parts	12
Ca^{2+}, $CaCO_3$, δCa_{reg}	μmol/kg	Seawater concentration of calcium ion, which is used by some plankton to form solid calcium-carbonate hard parts, where Ca release of Ca during $CaCO_3$ dissolution in the ocean interior is counted as an incremental increase in regenerated Ca (analogous to regenerated P in eq.11)	13,16
K_{sp}	$(\mu mol/kg)^2$	$CaCO_3$ solubility product	14,16
Ω, ΔΩ, δΩ/Ω	unitless	$CaCO_3$ saturation index, absolute Ω change, incremental fractional Ω change	14, 15,16
ΔCO_3^{2-}	μmol/kg	Net change in bulk ocean carbonate ion concentration	14
ΔC_{CaCO3}, $\delta CaCO_3$	mol, PgC	Integrated and incremental net dissolution of $CaCO_3$ into the ocean, convertible between carbon atom number and carbon atom weight with 12 gC per mol C. In our context this refers strictly to the open system alkalinity mass balance of the ocean maintained through $CaCO_3$ burial.	14, 16
A_{oc}, A_{lyso}	m^2	Ocean area, seafloor area above or below the lysocline depth	16,18
V_{oc}	m^3	Ocean volume	16
$F_{weath.}$, $F_{prod.}$, $F_{diss.}$, F_{burial}, δF_{burial}	mol/yr, PgC/yr	$CaCO_3$ fluxes of weathering, production, dissolution, burial, and incremental change in $CaCO_3$ burial flux, convertible between carbon atom number and carbon atom weight with 12 gC per mol C	17, 18
CSH, δCSH, ΔCSH	m	Calcite saturation horizon depth with respect to modern sea level, incremental and integrated increase in CSH depth is often referred to as CSH deepening. CSH is closely tied to the depth of the lysocline	18, 19
A_{lyso}	m^2	Seafloor area above or below the lysocline depth, refers to the cumulative hypsometric curve of the deep ocean with a modern sea level datum	18
$\delta A_{lyso}/\delta z$	m^2/m	Incremental change in seafloor area above the lysocline per incremental change in the depth of the lysocline, refers to the hypsometric curve of the deep ocean with a modern sea level datum	18
$\tau_{lysocline}$	yr	e-folding timescale for lysocline shoaling/deepening to reestablish balance between alkalinity sources to the ocean and $CaCO_3$ burial	19

References

Abelmann, A., Gersonde, R., Cortese, G., Kuhn, G., & Smetacek, V. (2006, March). Extensive phytoplankton blooms in the Atlantic sector of the glacial Southern Ocean <https://doi.org/10.1029/2005PA001199>. Paleoceanography, 21(1).

Abe-Ouchi, A., Saito, F., Kawamura, K., Raymo, M. E., Okuno, J., Takahashi, K., & Blatter, H. (2013, August 8). Insolation-driven 100,000-year glacial cycles and hysteresis of ice-sheet volume <https://doi.org/10.1038/nature12374>. Nature, 500(7461), 190–193.

Adams, J. M., Faure, H., Faure-Denard, L., McGlade, J. M., & Woodward, F. I. (1990, December). Increases in terrestrial carbon storage from the last glacial maximum to the present <https://doi.org/10.1038/348711a0>. Nature, 348(6303), 711–714.

Adhémar, J. (1842). Révolutions de la mer <https://www.google.com/books/edition/R%C3%A9volutions_de_la_mer/OUNDAAAAcAAJ?hl=en&gbpv=1&pg=PP1&printsec=frontcover>. Carilian-Goeury et Vr Dalmont.

Adkins, J. F. (2013). The role of deep ocean circulation in setting glacial climates <https://doi.org/10.1002/palo.20046>. Paleoceanography, 28, 539–561.

Adkins, J. F., McIntyre, K., & Schrag, D. P. (2002, November 29). The salinity, temperature, and δ18 O of the glacial deep ocean <https://doi.org/10.1126/science.1076252>. Science, 298(5599), 1769–1773.

Agassiz, L. (1840). Etudes Sur les glaciers <https://lccn.loc.gov/12008544>. Jent et Gassmann.

Ahn, J., & Brook, E. J. (2008, October 3). Atmospheric CO 2 and climate on millennial time scales during the last glacial period <https://doi.org/10.1126/science.1160832>. Science, 322(5898), 83–85.

Ai, X. E., Studer, A. S., Sigman, D. M., Martínez-García, A., Fripiat, F., Thöle, L. M., Michel, E., et al. (2020, December 11). Southern Ocean upwelling, Earth's obliquity, and glacial-interglacial atmospheric CO 2 change <https://doi.org/10.1126/science.abd2115>. Science, 370(6522), 1348–1352.

Allen, K. A., Sikes, E. L., Hönisch, B., Elmore, A. C., Guilderson, T. P., Rosenthal, Y., & Anderson, R. F. (2015, August). Southwest Pacific deep water carbonate chemistry linked to high southern latitude climate and atmospheric CO2 during the last glacial termination <https://doi.org/10.1016/j.quascirev.2015.05.007>. Quaternary Science Reviews, 122, 180–191.

Alley, R. B., Brook, E. J., & Anandakrishnan, S. (2002, January). A northern lead in the orbital band: North–South phasing of ice-age events. <https://doi.org/10.1016/S0277-3791(01)00072-5> Quaternary Science Reviews, 21(1–3), 431–441.

Altabet, M. A., & Francois, R. (1994, March). Sedimentary nitrogen isotopic ratio as a recorder for surface ocean nitrate utilization <https://doi.org/10.1029/93GB03396>. Global Biogeochemical Cycles, 8(1), 103–116.

Anand, P., Elderfield, H., & Conte, M. H. (2003, June). Calibration of Mg/Ca thermometry in planktonic foraminifera from a sediment trap time series <https://doi.org/10.1029/2002PA000846>. Paleoceanography, 18(2).

Anderson, D. M., & Archer, D. (2002, March). Glacial–interglacial stability of ocean pH inferred from foraminifer dissolution rates <https://doi.org/10.1038/416070a>. Nature, 416(6876), 70–73.

Anderson, L. A. (1995, September). On the hydrogen and oxygen content of marine phytoplankton <https://doi.org/10.1016/0967-0637(95)00072-E>. Deep Sea Research Part I: Oceanographic Research Papers, 42(9), 1675–1680.

Anderson, L. A., & Sarmiento, J. L. (1994, March). Redfield ratios of remineralization determined by nutrient data analysis <https://doi.org/10.1029/93GB03318>. Global Biogeochemical Cycles, 8(1), 65–80.

Anderson, R. F., Ali, S., Bradtmiller, L. I., Nielsen, S. H. H., Fleisher, M. Q., Anderson, B. E., & Burckle, L. H. (2009, March 13). Wind-driven upwelling in the Southern Ocean and the deglacial rise in atmospheric CO 2 <https://doi.org/10.1126/science.1167441>. Science, 323(5920), 1443–1448.

Anderson, R. F., Sachs, J. P., Fleisher, M. Q., Allen, K. A., Jimin, Y., Koutavas, A., & Jaccard, S. L. (2019, March). Deep-sea oxygen depletion and ocean carbon sequestration during the last ice age. <https://doi.org/10.1029/2018GB006049> Global Biogeochemical Cycles, 33(3), 301–317.

Archer, D. (1991). Modeling the calcite lysocline <https://doi.org/10.1029/91JC01812>. Journal of Geophysical Research, 96(C9), 17037.

Archer, D. (1996a, September). A data-driven model of the global calcite lysocline <https://doi.org/10.1029/96GB01521>. Global Biogeochemical Cycles, 10(3), 511–526.

Archer, D., Emerson, S., & Reimers, C. (1989, November). Dissolution of calcite in deep-sea sediments: PH and O2 microelectrode results <https://doi.org/10.1016/0016-7037(89)90161-0>. Geochimica et Cosmochimica Acta, 53(11), 2831–2845.

Archer, D., Kheshgi, H., & Maier-Reimer, E. (1997, February 15). Multiple timescales for neutralization of fossil fuel CO 2 <https://doi.org/10.1029/97GL00168>. Geophysical Research Letters, 24(4), 405–408.

Archer, D., & Maier-Reimer, E. (1994, January). Effect of deep-sea sedimentary calcite preservation on atmospheric CO2 concentration <https://doi.org/10.1038/367260a0>. Nature, 367(6460), 260–263.

Archer, D. E., Martin, P. A., Milovich, J., Brovkin, V., Plattner, G.-K., & Ashendel, C. (2003). Model sensitivity in the effect of Antarctic sea ice and stratification on atmospheric pCO2 <https://doi.org/10.1029/2002PA000760>. Paleoceanography, 18, 1012.

Archer, D., Winguth, A., Lea, D., & Mahowald, N. (2000, May). What caused the glacial/interglacial atmospheric p CO 2 cycles? <https://doi.org/10.1029/1999RG000066> Reviews of Geophysics, 38(2), 159–189.

Archer, D. E. (1996b, March). An atlas of the distribution of calcium carbonate in sediments of the deep sea <https://doi.org/10.1029/95GB03016>. Global Biogeochemical Cycles, 10(1), 159–174.

Armstrong, R. A., Lee, C., Hedges, J. I., Honjo, S., & Wakeham, S. G. (2001, January). A new, mechanistic model for organic carbon fluxes in the ocean based on the quantitative association of POC with ballast minerals <https://doi.org/10.1016/S0967-0645(01)00101-1>. Deep Sea Research Part II: Topical Studies in Oceanography, 49(1–3), 219–236.

Arons, A. B., & Stommel, H. (1967, August). On the abyssal circulation of the World Ocean—III: An advectionlateral mixing model of the distribution of a tracer property in an ocean basin <https://doi.org/10.1016/0011-7471(67)90051-4>. Deep Sea Research and Oceanographic Abstracts, 14(4), 441–457.

Arrhenius, S. (1896, April). XXXI: On the Influence of carbonic acid in the air upon the temperature of the ground <https://doi.org/10.1080/14786449608620846>. The London, Edinburgh, and Dublin Philosophical Magazine and Journal of Science, 41(251), 237–276.

Baggenstos, D., Häberli, M., Schmitt, J., Shackleton, S. A., Birner, B., Severinghaus, J. P., Kellerhals, T., & Fischer, H. (2019, July 23). Earth's radiative imbalance from the last glacial maximum to the present <https://doi.org/10.1073/pnas.1905447116>. Proceedings of the National Academy of Sciences, 116(30), 14881–14886.

Bard, E., Hamelin, B., & Fairbanks, R. (1990). U-Th ages obtained by mass spectrometry in corals from Barbados: sea-level during the past 130,000 years. Nature, 346, 456–458.

Barnola, J. M., Raynaud, D., Korotkevich, Y. S., & Lorius, C. (1987, October). Vostok ice core provides 160,000year record of atmospheric CO2 <https://doi.org/10.1038/329408a0>. Nature, 329(6138), 408–414.

Bar-Yosef, O. (2011, October). Climatic fluctuations and early farming in West and East Asia <https://doi.org/10.1086/659784>. Current Anthropology, 52(S4), S175–S193.

Batchelor, C. L., Margold, M., Krapp, M., Murton, D. K., Dalton, A. S., Gibbard, P. L., Stokes, C. R., Murton, J. B., & Manica, A. (2019, December). The configuration of northern hemisphere ice sheets through the quaternary <https://doi.org/10.1038/s41467-019-11601-2>. Nature Communications, 10(1), 3713.

Bender, M., Grande, K., Johnson, K., Marra, J., Williams, P. J. LeB., Sieburth, J., Pilson, M., et al. (1987, September). A comparison of four methods for determining planktonic community production: Planktonic community production <https://doi.org/10.4319/lo.1987.32.5.1085>. Limnology and Oceanography, 32(5), 1085–1098.

Bender, M., Sowers, T., Dickson, M.-L., Orchardo, J., Grootes, P., Mayewski, P. A., & Meese, D. A. (1994, December). Climate correlations between Greenland and Antarctica during the past 100,000 years <https://doi.org/10.1038/372663a0>. Nature, 372(6507), 663–666.

Bender, M. L. (2002, November). Orbital tuning chronology for the Vostok climate record supported by trapped gas composition <https://doi.org/10.1016/S0012-821X(02)00980-9>. Earth and Planetary Science Letters, 204(1–2), 275–289.

Bender, M. L., Floch, G., Chappellaz, J., Suwa, M., Barnola, J.-M., Blunier, T., Dreyfus, G., Jouzel, J., & Parrenin, F. (2006, November 14). Gas age–ice age differences and the chronology of the Vostok ice core, 0100 Ka. <https://doi.org/10.1029/2005JD006488> Journal of Geophysical Research, 111(D21), D21115.

Bereiter, B., Eggleston, S., Schmitt, J., Nehrbass-Ahles, C., Stocker, T. F., Fischer, H., Kipfstuhl, S., & Chappellaz, J. (2015, January 28). Revision of the EPICA dome C CO 2 record from 800 to 600 Kyr before present: Analytical bias in the EDC CO2 record <https://doi.org/10.1002/2014GL061957>. Geophysical Research Letters, 42(2), 542–549.

Bereiter, B., Lüthi, D., Siegrist, M., Schüpbach, S., Stocker, T. F., & Fischer, H. (2012, June 19). Mode change of millennial CO 2 variability during the last glacial cycle associated with a bipolar marine carbon seesaw <https://doi.org/10.1073/pnas.1204069109>. Proceedings of the National Academy of Sciences, 109(25), 9755–9760.

Berger, A. (1988, November). Milankovitch theory and climate <https://doi.org/10.1029/RG026i004p00624>. Reviews of Geophysics, 26(4), 624–657.

Berger, A. L. (1977, September 1). Support for the astronomical theory of climatic change <https://doi.org/10.1038/269044a0>. Nature, 269(5623), 44–45.

Berger, A. L. (1978, December). Long-term variations of daily insolation and quaternary climatic changes <https://doi.org/10.1175/1520-0469(1978)035%3c2362:LTVODI%3e2.0.CO;2>. Journal of the Atmospheric Sciences, 35(12), 2362–2367.

Berger, W. H. (1970, February). Planktonic Foraminifera: Selective solution and the lysocline <https://doi.org/10.1016/0025-3227(70)90001-0>. Marine Geology, 8(2), 111–138.

Berger, W. H. (1982a, November). Deglacial CO 2 buildup: Constraints on the coral-reef model <https://doi.org/10.1016/0031-0182(82)90092-X>. Palaeogeography, Palaeoclimatology, Palaeoecology, 40(1–3), 235–253.

Berger, W. H. (1982b). Increase of carbon dioxide in the atmosphere during deglaciation: The coral reef hypothesis. Naturwissenschaften, 69, 87–88.

Berner, R. A. (1995, May 1). A. G. Hoegbom and the development of the concept of the geochemical carbon cycle. <https://doi.org/10.2475/ajs.295.5.491> American Journal of Science, 295(5), 491–495.

Berner, W., Stauffer, B., & Oeschger, H. (1978, November). Past atmospheric composition and climate, gas parameters measured on ice cores <https://doi.org/10.1038/276053a0>. Nature, 276(5683), 53–55.

Beschel, R. E. (1950). Flechten Als Altersmassstab Rezenter Moränen. Zeitschrift Für Gletscherkunde Und Glazialgeologie (1), 152–161.

Betti, L., Beyer, R. M., Jones, E. R., Eriksson, A., Tassi, F., Siska, V., Leonardi, M., et al. (2020, October). Climate shaped how Neolithic farmers and European hunter-gatherers interacted a"er a major slowdown from 6,100 BCE to 4,500 BCE. <https://doi.org/10.1038/s41562-020-0897-7> Nature Human Behaviour, 4(10), 10041010.

Blackburn, T., Edwards, G. H., Tulaczyk, S., Scudder, M., Piccione, G., Hallet, B., McLean, N., Zachos, J. C., Cheney, B., & Babbe, J. T. (2020, July 23). Ice retreat in Wilkes Basin of East Antarctica during a warm interglacial <https://doi.org/10.1038/s41586-020-2484-5>. Nature, 583(7817), 554–559.

Blunier, T., & Brook, E. J. (2001, January 5). Timing of millennial-scale climate change in Antarctica and Greenland during the last glacial period <https://doi.org/10.1126/science.291.5501.109>. Science, 291(5501), 109–112.

Blunier, T., Chappellaz, J., Schwander, J., Dällenbach, A., Stauffer, B., Stocker, T. F., Raynaud, D., et al. (1998, August). Asynchrony of Antarctic and Greenland climate change during the last glacial period <https://doi.org/10.1038/29447>. Nature, 394(6695), 739–743.

Bolin, B. (1960, August). On the exchange of carbon dioxide between the atmosphere and the sea <https://doi.org/10.1111/j.2153-3490.1960.tb01311.x>. Tellus, 12(3), 274–281.

Bolin, B., & Stommel, H. (1961, September). On the abyssal circulation of the world ocean—IV. <https://doi.org/10.1016/0146-6313(61)90002-8>. Deep Sea Research, 8(2), 95–110.

Boscolo-Galazzo, F., Crichton, K. A., Barker, S., & Pearson, P. N. (2018, November). Temperature dependency of metabolic rates in the upper ocean: A positive feedback to global climate change? <https://doi.org/10.1016/j.gloplacha.2018.08.017> Global and Planetary Change, 170, 201–212.

Boscolo-Galazzo, F., Crichton, K. A., Ridgwell, A., Mawbey, E. M., Wade, B. S., & Pearson, P. N. (2021, March 12). Temperature controls carbon cycling and biological evolution in the ocean twilight zone <https://doi.org/10.1126/science.abb6643>. Science, 371(6534), 1148–1152.

Boudreau, B. P. (1987, July). A steady-state diagenetic model for dissolved carbonate species and pH in the porewaters of oxic and suboxic sediments <https://doi.org/10.1016/0016-7037(87)90187-6>. Geochimica et Cosmochimica Acta, 51(7), 1985–1996.

Bouttes, N., Paillard, D., & Roche, D. M. (2010, September 15). Impact of brine-induced stratification on the glacial carbon cycle <https://doi.org/10.5194/cp-6-575-2010>. Climate of the Past, 6(5), 575–589.

Boyd, P. W., & Ellwood, M. J. (2010, October). The biogeochemical cycle of iron in the ocean <https://doi.org/10.1038/ngeo964>. Nature Geoscience, 3(10), 675–682.

Boyd, P. W., Jickells, T., Law, C. S., Blain, S., Boyle, E. A., Buesseler, K. O., Coale, K. H., et al. (2007, February 2). Mesoscale iron enrichment experiments 1993–2005: Synthesis and future directions <https://doi.org/10.1126/science.1131669>. Science, 315(5812), 612–617.

Boyd, P. W., & Trull, T. W. (2007, March). Understanding the export of biogenic particles in oceanic waters: Is there consensus? <https://doi.org/10.1016/j.pocean.2006.10.007> Progress in Oceanography, 72(4), 276–312.

Boyle, E. A. (1988a). The role of vertical chemical fractionation in controlling late quaternary atmospheric carbon dioxide <https://doi.org/10.1029/JC093iC12p15701>. Journal of Geophysical Research, 93(C12), 15701.

Boyle, E. A. (1988b, January). Vertical oceanic nutrient fractionation and glacial/interglacial CO2 cycles <https://doi.org/10.1038/331055a0>. Nature, 331(6151), 55–56.

Brandes, J. A., & Devol, A. H. (2002, December). A global marine-fixed nitrogen isotopic budget: Implications for Holocene

NITROGEN Cycling: NITROGEN ISOTOPIC BUDGET <https://doi.org/10.1029/2001GB001856>. Global Biogeochemical Cycles, 16(4), 67-1–67-14.

Brewer, P. G., & Goldman, J. C. (1976, January). Alkalinity changes generated by phytoplankton growth <https://doi.org/10.4319/lo.1976.21.1.0108>. Limnology and Oceanography, 21(1), 108–117.

Briner, J. P. (2011). Dating glacial landforms <https://doi.org/10.1007/978-90-481-2642-2_616>. In V. P. Singh, P. Singh, & U. K. Haritashya (Eds.), Encyclopedia of snow, ice and glaciers (pp. 175–176). Encyclopedia of Earth Sciences Series. Springer Netherlands.

Broecker, W., & Clark, E. (2010, July). Search for a glacial-age 14 C-depleted ocean reservoir <https://doi.org/10.1029/2010GL043969>. Geophysical Research Letters, 37(13).

Broecker, W. S. (1966, January 21). Absolute dating and the astronomical theory of glaciation: Changes in climate occur in response to periodic Variations in the Earth's tilt and precession <https://doi.org/10.1126/science.151.3708.299>. Science, 151(3708), 299–304.

Broecker, W. S. (1974, August). "NO," a conservative water-mass tracer <https://doi.org/10.1016/0012821X(74)90036-3>. Earth and Planetary Science Letters, 23(1), 100–107.

Broecker, W. S. (1982a). Glacial to interglacial changes in ocean chemistry. Progress in Oceanography, 11, 151–197.

Broecker, W. S. (1982b, October). Ocean chemistry during glacial time <https://doi.org/10.1016/00167037(82)90110-7>. Geochimica et Cosmochimica Acta, 46(10), 1689–1705.

Broecker, W. S. (2003). The oceanic CaCO3 cycle <https://doi.org/10.1016/B0-08-043751-6/06119-3>. In H. D. Holland & K. K. Turekian (Eds.), Treatise on geochemistry (pp. 529–549). Elsevier.

Broecker, W. S., & Clark, E. (2003, June). Holocene atmospheric CO 2 increase as viewed from the seafloor. <https://doi.org/10.1029/2002GB001985> Global Biogeochemical Cycles, 17(2).

Broecker, W. S., & Denton, G. H. (1989, October). The role of ocean-atmosphere reorganizations in glacial cycles <https://doi.org/10.1016/0016-7037(89)90123-3>. Geochimica et Cosmochimica Acta, 53(10), 24652501.

Broecker, W. S., & Henderson, G. M. (1998, August). The sequence of events surrounding termination II and their implications for the cause of glacial-interglacial CO 2 changes <https://doi.org/10.1029/98PA00920>. Paleoceanography, 13(4), 352–364.

Broecker, W. S., Peacock, S. L., Walker, S., Weiss, R., Fahrbach, E., Schroeder, M., Mikolajewicz, U., et al. (1998, July 15). How much deep water is formed in the Southern Ocean? <https://doi.org/10.1029/98JC00248> Journal of Geophysical Research: Oceans, 103(C8), 15833–15843.

Broecker, W. S., & Peng, T.-H. (1982). Tracers in the sea <https://doi.org/10.1017/S0033822200005221>. Lamont-Doherty Geological Observatory. Eldigo Press.

Broecker, W. S., & Peng, T.-H. (1987, March). The role of CaCO 3 compensation in the glacial to interglacial atmospheric CO 2 change <https://doi.org/10.1029/GB001i001p00015>. Global Biogeochemical Cycles, 1(1), 15–29.

Broecker, W. S., & Peng, T.-H. (1989, September). The cause of the glacial to interglacial atmospheric CO 2 change: A polar alkalinity hypothesis <https://doi.org/10.1029/GB003i003p00215>. Global Biogeochemical Cycles, 3(3), 215–239.

Broecker, W. S., & Takahashi, T. (1977). The solubility of calcite in sea water <https://doi.org/10.1007/978-94010-1252-2_18>. In D. G. Fraser (Ed.), Thermodynamics in geology (pp. 365–379). Springer Netherlands.

Broecker, W. S., & Takahashi, T. (1978, January). The relationship between lysocline depth and in situ carbonate ion concentration <https://doi.org/10.1016/S0146-6291(21)00007-2>. Deep Sea Research, 25(1), 65–95.

Broecker, W. S., Takahashi, T., & Takahashi, T. (1985). Sources and flow patterns of deep-ocean waters as deduced from potential temperature, salinity, and initial phosphate concentration <https://doi.org/10.1029/JC090iC04p06925>. Journal of Geophysical Research, 90(C4), 6925.

Broecker, W. S., & Thurber, D. L. (1965, July 2). Uranium-series dating of corals and oolites from Bahaman and Florida key limestones <https://doi.org/10.1126/science.149.3679.58>. Science, 149(3679), 58–60.

Brovkin, V., Ganopolski, A., Archer, D., & Munhoven, G. (2012, February 9). Glacial CO2 cycle as a succession of key physical and biogeochemical processes <https://doi.org/10.5194/cp-8-251-2012>. Climate of the Past, 8(1), 251–264.

Buch, K. (1929). Über Den Einfluss Der Temperatur Auf Die Ph-Bestimmung Des Meerwassers. Merentutkimuslaitoksen Julkaisu, Havsforskningsinstitutets Skri" (61), 1–23.

Buch, K. (1933). On boric acid in the sea and its influence on the carbonic acid equilibrium. Conseil Permanent International pour l'Exploration de la Mer, 8, 309–325.

Buch, K. (1951). Das Kohlensäure Gleichgewichtssystem Im Meerwasser: Kritische Durchsicht Und Neuberechnungen Der Konstituenten <https://helda.helsinki.fi/items/6a30a18f-4e5f-41f3-a1b1a174103b4572>. Merentutkimuslaitoksen Julkaisu, Havsforskningsinstitutets Skrift (151), 1–18.

Buch, K., Harvey, H. W., Wattenberg, H., & Gripenberg, S. (1932). Über Das Kohlensäuresystem Im Meerwasser. Rapports et Proces-Verbaux des Reunions, Conseil Permanent International pour l' Exploration de la Mer, 79, 1–70.

Buesseler, K. O., Boyd, P. W., Black, E. E., & Siegel, D. A. (2020, May 5). Metrics that matter for assessing the ocean biological carbon pump <https://doi.org/10.1073/pnas.1918114117>. Proceedings of the National Academy of Sciences, 117(18), 9679–9687.

Buesseler, K. O., Lamborg, C. H., Boyd, P. W., Lam, P. J., Trull, T. W., Bidigare, R. R., Bishop, J. K. B., et al. (2007, April 27). Revisiting carbon flux through the ocean's twilight zone <https://doi.org/10.1126/science.1137959>. Science, 316(5824), 567–570.

Burke, A., & Robinson, L. F. (2012, February 3). The Southern Ocean's role in carbon exchange during the last deglaciation <https://doi.org/10.1126/science.1208163>. Science, 335(6068), 557–561.

Callendar, G. S. (1938, April). The artificial production of carbon dioxide and its influence on temperature <https://doi.org/10.1002/qj.49706427503>. Quarterly Journal of the Royal Meteorological Society, 64(275), 223–240.

Callendar, G. S. (1949, October). Can carbon dioxide influence climate? <https://doi.org/10.1002/j.14778696.1949.tb00952.x> Weather, 4(10), 310–314.

Cartapanis, O., Bianchi, D., Jaccard, S. L., & Galbraith, E. D. (2016, February 29). Global pulses of organic carbon burial in deep-sea sediments during glacial maxima. <https://doi.org/10.1038/ncomms10796> Nature Communications, 7(1), 10796.

Catubig, N. R., Archer, D. E., Francois, R., deMenocal, P., Howard, W., & Yu, E.-F. (1998, June). Global deep-sea burial rate of calcium carbonate during the last glacial maximum <https://doi.org/10.1029/98PA00609>. Paleoceanography, 13(3), 298–310.

Chalk, T. B., Foster, G. L., & Wilson, P. A. (2019, March). Dynamic storage of glacial CO2 in the Atlantic Ocean revealed by boron [CO 3 2 −] and pH records <https://doi.org/10.1016/j.epsl.2018.12.022>. Earth and Planetary Science Letters, 510, 1–11.

Chalk, T. B., Hain, M. P., Foster, G. L., Rohling, E. J., Sexton, P. F., Badger, M. P. S., Cherry, S. G., et al. (2017, December 12). Causes of ice age intensification across the mid-Pleistocene transition <https://doi.org/10.1073/pnas.1702143114>. Proceedings of the National Academy of Sciences, 114(50), 13114–13119.

Chamberlin, T. C. (1899, September). An attempt to frame a working hypothesis of the cause of glacial periods on an atmospheric basis <https://doi.org/10.1086/608449>. The Journal of Geology, 7(6), 545–584.

Charpentier, J. (1841). Essai sur les glaciers et sur le terrain erratique du bassin du Rhone <https://books.google.com/books?id=mqcWAAAAQAAJ&printsec=frontcover&source=gbs_ge_summary_r&cad=0#v=onepage&q&f=false>. M.Ducloux.

Chase, Z., Anderson, R. F., & Fleisher, M. Q. (2001, October). Evidence from Authigenic uranium for increased productivity of the glacial subantarctic ocean <https://doi.org/10.1029/2000PA000542>. Paleoceanography, 16(5), 468–478.

Chikamoto, M. O., Matsumoto, K., & Yamanaka, Y. (2009, April). Influence of export rain ratio changes on atmospheric CO2 and sedimentary calcite preservation <https://doi.org/10.1007/s10872-009-0020-1>. Journal of Oceanography, 65(2), 209–221.

Chung, S.-N., Lee, K., Feely, R. A., Sabine, C. L., Millero, F. J., Wanninkhof, R., Bullister, J. L., Key, R. M., & Peng, T.-H. (2003, December). Calcium carbonate budget in the Atlantic Ocean based on water column inorganic carbon chemistry <https://doi.org/10.1029/2002GB002001>. Global Biogeochemical Cycles, 17(4).

Clapeyron, M. C. (1834). Mémoire sur la puissance motrice de la chaleur. Journal de l'École polytechnique [fr], 23, 153–190.

Clark, P. U., Dyke, A. S., Shakun, J. D., Carlson, A. E., Clark, J., Wohlfarth, B., Mitrovica, J. X., Hostetler, S. W., & Marshall McCabe, A. (2009, August 7). The last glacial maximum <https://doi.org/10.1126/science.1172873>. Science, 325(5941), 710–714.

Clark, P. U., & Mix, A. C. (2002, January). Ice sheets and sea level of the last glacial maximum <https://doi.org/10.1016/S0277-3791(01)00118-4>. Quaternary Science Reviews, 21(1–3), 1–7.

Clark, P. U., Pisias, N. G., Stocker, T. F., & Weaver, A. J. (2002, February). The role of the thermohaline circulation in abrupt climate change <https://doi.org/10.1038/415863a>. Nature, 415(6874), 863–869.

Clausius, R. (1850). Ueber die bewegende Kra" der Wärme und die Gesetze, welche sich daraus für die Wärmelehre selbst ableiten lassen. Annalen der Physik, 155(3), 368–397.

Cliff, E., Khatiwala, S., & Schmittner, A. (2021, January). Glacial deep ocean deoxygenation driven by biologically mediated air–sea disequilibrium <https://doi.org/10.1038/s41561-020-00667-z>. Nature Geoscience, 14(1), 43–50.

CLIMAP Project Members. (1976, March 19). The surface of the ice-age Earth: Quantitative geologic evidence is used to reconstruct boundary conditions for the climate 18,000 years ago <https://doi.org/10.1126/science.191.4232.1131>. Science, 191(4232), 1131–1137.

Craig, H. (1957, February). The natural distribution of radiocarbon and the exchange time of carbon dioxide between atmosphere and sea <https://doi.org/10.1111/j.2153-3490.1957.tb01848.x>. Tellus, 9(1), 1–17.

Crawford, E. (1997). Arrhenius' 1896 model of the greenhouse effect in context. Ambio, 26(1), 6–11.

Crichton, K. A., Bouttes, N., Roche, D. M., Chappellaz, J., & Krinner, G. (2016, September). Permafrost carbon as a missing link to explain CO2 changes during the last deglaciation <https://doi.org/10.1038/ngeo2793>. Nature Geoscience, 9(9), 683–686.

Croll, J. (1875). Climate and time in their geological relations: A theory of secular changes of the earth's climate. Daldy, Isbister & Company.

Crowley, T. J. (1991, August). Ice age carbon <https://doi.org/10.1038/352575b0>. Nature, 352(6336), 575576.

Crowley, T. J. (1995, September). Ice age terrestrial carbon changes revisited <https://doi.org/10.1029/95GB01107>. Global Biogeochemical Cycles, 9(3), 377–389.

Crowley, T. J. (2000, April 3). CLIMAP SSTs re-revisited <https://doi.org/10.1007/s003820050325>. Climate Dynamics, 16(4), 241–255.

Curry, W. B., Duplessy, J. C., Labeyrie, L. D., & Shackleton, N. J. (1988, June). Changes in the distribution of δ 13 C of deep water ΣCO 2 between the last glaciation and the Holocene <https://doi.org/10.1029/PA003i003p00317>. Paleoceanography, 3(3), 317–341.

Curry, W. B., & Oppo, D. W. (2005, March). Glacial water mass geometry and the distribution of δ 13 C of ΣCO 2 in the Western Atlantic Ocean <https://doi.org/10.1029/2004PA001021>. Paleoceanography, 20(1).

Cutler, K. B., Edwards, R. L., Taylor, F. W., Cheng, H., Adkins, J., Gallup, C. D., Cutler, P. M., Burr, G. S., & Bloom, A. L.. (2003, February). Rapid sea-level fall and deep-ocean temperature change since the last interglacial period <https://doi.org/10.1016/S0012-821X(02)01107-X>. Earth and Planetary Science Letters, 206(3–4), 253–271.

Dalton, J. (1802). Essay II: On the force of steam or vapour from water and various other liquids, both is a vacuum and in air. Memoirs of the Literary and Philosophical Society of Manchester, 5, 550–574.

De Angelis, M., Barkov, N. I., & Petrov, V. N. (1987, January). Aerosol concentrations over the last climatic cycle (160 Kyr) from an Antarctic ice core <https://doi.org/10.1038/325318a0>. Nature, 325(6102), 318–321.

de Boer, A. M., & Hogg, A. M. C. (2014, June 28). Control of the glacial carbon budget by topographically induced mixing <https://doi.org/10.1002/2014GL059963>. Geophysical Research Letters, 41(12), 4277–4284.

de Boer, A. M., Sigman, D. M., Toggweiler, J. R., & Russell, J. L. (2007). Effect of global ocean temperature change on deep ocean ventilation <https://doi.org/10.1029/2005PA001242>. Paleoceanography, 22, PA2210.

de Marchi, L. (1895). Le cause Dell'Era Glaciale. Fratelli Fusi.

Delmas, R. J., Ascencio, J.-M., & Legrand, M. (1980, March 13). Polar ice evidence that atmospheric CO2 20,000 Yr BP was 50% of present <https://doi.org/10.1038/284155a0>. Nature, 284(5752), 155–157.

Denton, G. H., Anderson, R. F., Toggweiler, J. R., Edwards, R. L., Schaefer, J. M., & Putnam, A. E. (2010, June 25). The last glacial termination <https://doi.org/10.1126/science.1184119>. Science, 328(5986), 1652–1656.

Deutsch, C., Gruber, N., Key, R. M., Sarmiento, J. L., & Ganachaud, A. (2001, June). Denitrification and N 2 fixation in the Pacific Ocean <https://doi.org/10.1029/2000GB001291>. Global Biogeochemical Cycles, 15(2), 483–506.

Deutsch, C., Sarmiento, J. L., Sigman, D. M., Gruber, N., & Dunne, J. P. (2007, January). Spatial coupling of nitrogen inputs and losses in the ocean <https://doi.org/10.1038/nature05392>. Nature, 445(7124), 163–167.

Deutsch, C., Sigman, D. M., Thunell, R. C., Meckler, A. N., & Haug, G. H.. (2004, December). Isotopic constraints on glacial/interglacial changes in the oceanic nitrogen budget <https://doi.org/10.1029/2003GB002189>. Global Biogeochemical Cycles, 18(4).

DeVries, T., & Primeau, F. (2011, December 1). Dynamically and observationally constrained estimates of water-mass distributions and ages in the Global Ocean <https://doi.org/10.1175/JPO-D-10-05011.1>. Journal of Physical Oceanography, 41(12), 2381–2401.

Dickson, A. G. (1984, November). pH scales and proton-transfer reactions in saline media such as sea water <https://doi.org/10.1016/0016-7037(84)90225-4>. Geochimica et Cosmochimica Acta, 48(11), 22992308.

Dickson, A. G. (1993, December). The measurement of sea water pH <https://doi.org/10.1016/03044203(93)90198-W>. Marine Chemistry, 44(2–4), 131–142.

Dickson, A. G., Christopher, L. S., Christian, J. R., Bargeron, C. P., & North Pacific Marine Science Organization. (Eds.). (2007). Guide to best practices for ocean CO2 measurements [PICES Special Publication, no. 3]. North Pacific Marine Science Organization.

Dickson, A. G., & Millero, F. J. (1987, October). A comparison of the equilibrium constants for the dissociation of carbonic acid in seawater media <https://doi.org/10.1016/0198-0149(87)90021-5>. Deep Sea Research Part A. Oceanographic Research Papers, 34(10), 1733–1743.

DiTullio, G. R., Grebmeier, J. M., Arrigo, K. R., Lizotte, M. P., Robinson, D. H., Leventer, A., Barry, J. P., VanWoert, M. L., & Dunbar, R. B. (2000, April). Rapid and early export of Phaeocystis antarctica blooms in the

Ross Sea, Antarctica <https://doi.org/10.1038/35007061>. Nature, 404(6778), 595–598.

Donn, W. L., & Ewing, M. (1966). A theory of ice ages. Science, 152(3730), 1706–1712.

Dugdale, R. C., & Goering, J. J. (1967, April). Uptake of new and regenerated forms of nitrogen in primary productivity <https://doi.org/10.4319/lo.1967.12.2.0196>. Limnology and Oceanography, 12(2), 196–206. Duplessy, J. C., Shackleton, N. J., Fairbanks, R. G., Labeyrie, L., Oppo, D., & Kallel, N. (1988, June). Deepwater source variations during the last climatic cycle and their Impact on the global deepwater circulation <https://doi.org/10.1029/PA003i003p00343>. Paleoceanography, 3(3), 343–360.

Duplessy, J.-C., Shackleton, N. J., Matthews, R. K., Prell, W., Ruddiman, W. F., Caralp, M., & Hendy, C. H. (1984, February). 13 C record of benthic foraminifera in the last interglacial ocean: Implications for the carbon cycle and the global deep water circulation <https://doi.org/10.1016/0033-5894(84)90099-1>. Quaternary Research, 21(2), 225–243.

Eggleston, S., Schmitt, J., Bereiter, B., Schneider, R., & Fischer, H. (2016, March). Evolution of the stable carbon isotope composition of atmospheric CO 2 over the last glacial cycle <https://doi.org/10.1002/2015PA002874>. Paleoceanography, 31(3), 434–452.

Egleston, E. S., Sabine, C. L., & Morel, F. M. M. (2010, March). Revelle revisited: Buffer factors that quantify the response of ocean chemistry to changes in DIC and alkalinity <https://doi.org/10.1029/2008GB003407>. Global Biogeochemical Cycles, 24(1).

Ehlers, J., Gibbard, P. L., & Hughes, P. D. (Eds.). (2011). Quaternary glaciations—Extent and chronology: A closer look. Developments in Quaternary Science 15. Elsevier.

Elderfield, H., Ferretti, P., Greaves, M., Crowhurst, S., McCave, I. N., Hodell, D., & Piotrowski, A. M. (2012, August 10). Evolution of ocean temperature and ice volume through the mid-Pleistocene climate transition <https://doi.org/10.1126/science.1221294>. Science, 337(6095), 704–709.

Elsig, J., Schmitt, J., Leuenberger, D., Schneider, R., Eyer, M., Leuenberger, M., Joos, F., Fischer, H., & Stocker, T. F. (2009, September). Stable isotope constraints on Holocene carbon cycle changes from an Antarctic ice core <https://doi.org/10.1038/nature08393>. Nature, 461(7263), 507–510.

Emerson, S., & Bender, M. L. (1981). Carbon fluxes at the sedimentwater interface of the deep sea: Calcium carbonate preservation. Journal of Marine Research, 39(1), 139–162.

Emerson, S. R., & Archer, D. (1990, June 19). Calcium carbonate preservation in the ocean <https://doi.org/10.1098/rsta.1990.0054>. Philosophical Transactions of the Royal Society of London: Series A, Mathematical and Physical Sciences, 331(1616), 29–40.

Emiliani, C. (1955). Pleistocene temperatures. The Journal of Geology, 63(6), 538–578.

Emiliani, C. (1966). Isotopic paleotemperatures. Science, 154(3751), 851–857.

EPICA Community Members. (2004, June). Eight glacial cycles from an Antarctic ice core <https://doi.org/10.1038/nature02599>. Nature, 429(6992), 623–628.

EPICA Community Members. (2006, November). One-to-one coupling of glacial climate variability in Greenland and Antarctica <https://doi.org/10.1038/nature05301>. Nature, 444(7116), 195–198.

Eriksson, E., & Welander, P. (1956, May). On a mathematical model of the carbon cycle in nature <https://doi.org/10.1111/j.2153-3490.1956.tb01207.x>. Tellus, 8(2), 155–175.

Etminan, M., Myhre, G., Highwood, E. J., & Shine, K. P. (2016, December 28). Radiative forcing of carbon dioxide, methane, and nitrous oxide: A significant revision of the methane radiative forcing <https://doi.org/10.1002/2016GL071930>. Geophysical Research Letters, 43(24), 12,614–12,623. Evans, E. P. (1887). The authorship of the glacial theory. The North American Review, 145(368), 94–97. Ewing, M., & Donn, W. L. (1956, June 15). A theory of ice ages <https://doi.org/10.1126/science.123.3207.1061>. Science, 123(3207), 1061–1066.

Fairbanks, R. G. (1989, December). A 17,000-year glacio-eustatic sea level record: Influence of glacial melting rates on the Younger Dryas event and deep-ocean circulation <https://doi.org/10.1038/342637a0>. Nature, 342(6250), 637–642.

Fairbridge, R. W. (1987). Ice age theory <https://doi.org/10.1007/0-387-30749-4_91>. In Climatology (pp. 504514). Encyclopedia of Earth Science. Kluwer Academic.

Falkowski, P. G. (1994, March). The role of phytoplankton photosynthesis in global biogeochemical cycles <https://doi.org/10.1007/BF00014586>. Photosynthesis Research, 39(3), 235–258.

Falkowski, P. G. (1997, May). Evolution of the nitrogen cycle and its influence on the biological sequestration of CO2 in the ocean <https://doi.org/10.1038/387272a0>. Nature, 387(6630), 272–275.

Farmer, J. R., Pico, T., Underwood, O. M., Stout, R. C., Granger, J., Cronin, T. M., Fripiat, F., Martínez-García, A., Haug, G. H., & Sigman, D. M. (2023, January 3). The Bering Strait was flooded 10,000 years before the last glacial maximum <https://doi.org/10.1073/pnas.2206742119>. Proceedings of the National Academy of Sciences, 120(1), e2206742119.

Farrell, J. W., & Prell, W. L. (1989, August). Climatic change and CaCO 3 preservation: An 800,000 year bathymetric reconstruction from the central equatorial Pacific Ocean <https://doi.org/10.1029/PA004i004p00447>. Paleoceanography, 4(4), 447–466.

Farrell, J. W., & Prell, W. L. (1991, August). Pacific CaCO 3 preservation and δ 18 O since 4 ma: Paleoceanic and paleoclimatic implications <https://doi.org/10.1029/91PA00877>. Paleoceanography, 6(4), 485–498. Federici, P. R., Ribolini, A., & Spagnolo, M.. (2017, January). Glacial history of the maritime Alps from the last glacial maximum to the little ice age <https://doi.org/10.1144/SP433.9>. Geological Society, London, Special Publications, 433(1), 137–159.

Feely, R. A., Sabine, C. L., Lee, K., Millero, F. J., Lamb, M. F., Greeley, D., Bullister, J. L., et al. (2002, December). In situ calcium carbonate dissolution in the Pacific Ocean <https://doi.org/10.1029/2002GB001866>. Global Biogeochemical Cycles, 16(4), 91-1–91-12.

Ferrari, R., Jansen, M. F., Adkins, J. F., Burke, A., Stewart, A. L., & Thompson, A. F. (2014, June 17). Antarctic sea ice control on ocean circulation in present and glacial climates <https://doi.org/10.1073/pnas.1323922111>. Proceedings of the National Academy of Sciences, 111(24), 8753–8758.

Fischer, H., Blunier, T., & Mulvaney, R. (2021). Ice cores: Archive of the climate system <https://doi.org/10.1007/978-3-030-42584-5_12>. In A. Fowler & F. Ng (Eds.), Glaciers and ice sheets in the climate system (pp. 279–325). Springer Textbooks in Earth Sciences, Geography and Environment. Springer International.

Fischer, H., Fundel, F., Ruth, U., Twarloh, B., Wegner, A., Udisti, R., Becagli, S., et al. (2007, August). Reconstruction of millennial changes in dust emission, transport and regional sea ice coverage using the deep EPICA ice cores from the Atlantic and Indian Ocean sector of Antarctica <https://doi.org/10.1016/j.epsl.2007.06.014>. Earth and Planetary Science Letters, 260(1–2), 340354.

Fischer, H., Schmitt, J., Lüthi, D., Stocker, T. F., Tschumi, T., Parekh, P., Joos, F., Köhler, P., Völker, C., Gersonde, R., Barbante, C., Le Floch, M., Raynaud, D., Wolff, E. (2010). The role of Southern Ocean processes in orbital and millennial CO2 variations – A synthesis <https://doi.org/10.1016/j.quascirev.2009.06.007>. Quaternary Science Reviews, 29(1–2), 193–205.

Foote, E. (1856). Circumstances Affecting the Heat of the Sun's Rays. The American Journal of Science and Arts, 22(66), 382–383.

Fourier, J.-B.-J. (1822). Theorie Analytique de La Chaleur <https://doi.org/10.1017/CBO9780511693229>. Cambridge University Press.

François, R., Altabet, M. A., Ein-Fen Y., Sigman, D. M., Bacon, M. P., Frank, M., Bohrmann, G., Bareille, G., & Labeyrie, L. D. (1997, October). Contribution of Southern Ocean surface-water stratification to low atmospheric CO2 concentrations during the last glacial period <https://doi.org/10.1038/40073>. Nature, 389(6654), 929–935.

Francois, R., Bacon, M. P., & Suman, D. O. (1990, October). Thorium 230 profiling in deep-sea sediments: High-resolution records of flux and dissolution of carbonate in the equatorial Atlantic during the last 24,000 years <https://doi.org/10.1029/PA005i005p00761>. Paleoceanography, 5(5), 761–787.

Fripiat, F., Martínez-García, A., Marconi, D., Fawcett, S. E., Kopf, S. H., Luu, V. H., Rafter, P. A., Zhang, R., Sigman, D. M., & Haug, G. H. (2021, November). Nitrogen isotopic constraints on nutrient transport to the upper ocean <https://doi.org/10.1038/s41561-021-00836-8>. Nature Geoscience, 14(11), 855–861.

Froelich, P. N., Bender, M. L., Luedtke, N. A., Heath, G. R., & DeVries, T. (1982). The marine phosphorous cycle. American Journal of Science, 282, 474–511.

Fry, C. H., Tyrrell, T., Hain, M. P., Bates, N. R., & Achterberg, E. P. (2015, August). Analysis of global surface ocean alkalinity to determine controlling processes <https://doi.org/10.1016/j.marchem.2015.05.003>. Marine Chemistry, 174, 46–57.

Galbraith, E., & de Lavergne, C. (2019, January). Response of a comprehensive climate model to a broad range of external forcings: Relevance for deep ocean ventilation and the development of late Cenozoic ice ages <https://doi.org/10.1007/s00382-018-4157-8>. Climate Dynamics, 52(1–2), 653–679.

Galbraith, E. D., & Jaccard, S. L. (2015, February). Deglacial weakening of the oceanic soft tissue pump: Global constraints from sedimentary nitrogen isotopes and oxygenation proxies <https://doi.org/10.1016/j.quascirev.2014.11.012>. Quaternary Science Reviews, 109, 38–48.

Galbraith, E. D., Jaccard, S. L., Pedersen, T. F., Sigman, D. M., Haug, G. H., Cook, M., Southon, J. R., & Francois, R. (2007, October). Carbon dioxide release from the North Pacific abyss during the last deglaciation <https://doi.org/10.1038/nature06227>. Nature, 449(7164), 890–893.

Galbraith, E. D., & Skinner, L. C. (2020, January 3). The biological pump during the last glacial maximum <https://doi.org/10.1146/annurev-marine-010419-010906>. Annual Review of Marine Science, 12(1), 559–586.

Ganopolski, A., & Rahmstorf, S. (2001, January 11). Rapid changes of glacial climate simulated in a coupled climate model <https://doi.org/10.1038/35051500>. Nature, 409(6817), 153–158.

Gebbie, G., & Huybers, P. (2010, August 1). Total matrix intercomparison: A method for determining the geometry of water-mass pathways <https://doi.org/10.1175/2010JPO4272.1>. Journal of Physical Oceanography, 40(8), 1710–1728.

Geike, J. (1874). The great ice age: And its relation to the antiquity of man. W. Isbister.

Geike, J. (1896). The great ice age: And its relation to the antiquity of man. D. Appleton.

Genthon, G., Barnola, J. M., Raynaud, D., Lorius, C., Jouzel, J., Barkov, N. I., Korotkevich, Y. S., & Kotlyakov, V. M. (1987, October). Vostok ice core: Climatic response to CO2 and orbital forcing changes over the last climatic cycle <https://doi.org/10.1038/329414a0>. Nature, 329(6138), 414–418.

Gloor, M., Sarmiento, J. L., & Gruber, N. (2010, August 20). What can be learned about carbon cycle climate feedbacks from the CO2 airborne fraction? <https://doi.org/10.5194/acp-10-7739-2010> Atmospheric Chemistry and Physics, 10(16), 7739–7751.

Gosse, J. C., & Phillips, F. M. (2001, August). Terrestrial in situ cosmogenic nuclides: Theory and application <https://doi.org/10.1016/S0277-3791(00)00171-2>. Quaternary Science Reviews, 20(14), 14751560.

Gottschalk, J., Battaglia, G., Fischer, H., Frölicher, T. L., Jaccard, S. L., Jeltsch-Thömmes, A., Joos, F., et al. (2019, September). Mechanisms of millennial-scale atmospheric CO2 change in numerical model simulations <https://doi.org/10.1016/j.quascirev.2019.05.013>. Quaternary Science Reviews, 220, 30–74.

Gowan, E. J., Zhang, X., Khosravi, S., Rovere, A., Stocchi, P., Hughes, A. L. C., Gyllencreutz, R., Mangerud, J., Svendsen, J.-I., & Lohmann, G. (2021, February 23). A new global ice sheet reconstruction for the past 80 000 years <https://doi.org/10.1038/s41467-021-21469-w>. Nature Communications, 12(1), 1199.

Grant, K. M., Rohling, E. J., Bar-Matthews, M., Ayalon, A., Medina-Elizalde, M., Bronk Ramsey, C., Satow, C., & Roberts, A. P. (2012, November). Rapid coupling between ice volume and polar temperature over the past 150,000 years <https://doi.org/10.1038/nature11593>. Nature, 491(7426), 744–747.

Gupta, A. K. (2004). Origin of agriculture and domestication of plants and animals linked to early holocene climate amelioration <http://www.jstor.org/stable/24107979>. Current Science, 87(1), 54–59.

Haeberli, M., Baggenstos, D., Schmitt, J., Grimmer, M., Michel, A., Kellerhals, T., & Fischer, H. (2021, April 14). Snapshots of mean ocean temperature over the last 700 000 years using Noble gases in the EPICA Dome C ice Core <https://doi.org/10.5194/cp-17-843-2021>. Climate of the Past, 17(2), 843–867.

Hain, M. P., Allen, K. A., & Kirtland Turner, S. (2024, September 1). Earth system carbon cycle dynamics though time <https://shop.elsevier.com/books/treatise-on-geochemistry/anbar/978-0-323-99762-1>. In A. D. Anbar, & D. Weis (Eds.), Treatise on geochemistry (3rd ed.). Hardback.

Hain, M. P., Foster, G. L., & Chalk, T. (2018, October). Robust constraints on past CO 2 climate forcing from the boron isotope proxy <https://doi.org/10.1029/2018PA003362>. Paleoceanography and Paleoclimatology, 33(10), 1099–1115.

Hain, M. P., Sigman, D. M., & Haug, G. H. (2010, December). Carbon dioxide effects of Antarctic stratification, North Atlantic Intermediate Water formation, and subantarctic nutrient drawdown during the last ice age: Diagnosis and synthesis in a geochemical box model <https://doi.org/10.1029/2010GB003790>. Global Biogeochemical Cycles, 24(4).

Hain, M. P., Sigman, D. M., & Haug, G. H. (2011, February). Shortcomings of the isolated abyssal reservoir model for deglacial radiocarbon changes in the mid-depth Indo-Pacific Ocean <https://doi.org/10.1029/2010GL046158>. Geophysical Research Letters, 38(4).

Hain, Mathis P., Sigman, Daniel M., & Haug, G. H. (2014). The biological pump in the past <https://doi.org/10.1016/B978-0-08-095975-7.00618-5>. In H. D. Holland & K. K. Turekian (Eds.), Treatise on geochemistry (pp. 485–517). Elsevier.

Hain, M. P., Sigman, D. M., Higgins, J. A., & Haug, G. H. (2015, May). The effects of secular calcium and magnesium concentration changes on the thermodynamics of seawater acid/base chemistry: Implications for Eocene and Cretaceous ocean carbon chemistry and buffering

<https://doi.org/10.1002/2014GB004986>. Global Biogeochemical Cycles, 29(5), 517–533.

Hales, B. (2003, December). Respiration, dissolution, and the lysocline <https://doi.org/10.1029/2003PA000915>. Paleoceanography, 18(4).

Hales, B., & Emerson, S. (1996, September). Calcite dissolution in sediments of the Ontong-Java Plateau: In situ measurements of pore water O 2 and p H <https://doi.org/10.1029/96GB01522>. Global Biogeochemical Cycles, 10(3), 527–541.

Hales, B., & Emerson, S. (1997a, February). Calcite dissolution in sediments of the Ceara Rise: In situ measurements of porewater O2, pH, and CO2(Aq) <https://doi.org/10.1016/S0016-7037(96)00366-3>. Geochimica et Cosmochimica Acta, 61(3), 501–514.

Hales, B., & Emerson, S. (1997b, April). Evidence in support of first-order dissolution kinetics of calcite in seawater <https://doi.org/10.1016/S0012-821X(97)00017-4>. Earth and Planetary Science Letters, 148(1–2), 317–327.

Hann, J. (1908). Handbuch der Klimalehre <https://www.abebooks.com/9783864445811/HandbuchKlimatologie-German-Edition-Hann-3864445817/plp> (vol. 1). J. Engelhorn.

Hansen, J., Russell, G., Lacis, A., Fung, I., Rind, D., & Stone, P. (1985, August 30). Climate response times: Dependence on climate sensitivity and ocean mixing <https://doi.org/10.1126/science.229.4716.857>. Science, 229(4716), 857–859.

Harrison, P. J., Waters, R. E., & Taylor, F. J. R. (1980, March). A broad spectrum artificial sea water medium for coastal and open ocean phytoplankton <https://doi.org/10.1111/j.0022-3646.1980.00028.x>. Journal of Phycology, 16(1), 28–35.

Harvey, H. W. (1945). Recent advances in the chemistry & biology of sea water. Cambridge University Press. Harvey, H. W. (1955). The chemistry & fertility of sea waters. Cambridge University Press.

Hayes, C. T., Costa, K. M., Anderson, R. F., Calvo, E., Chase, Z., Demina, L. L., et al. (2021). Global ocean sediment composition and burial flux in the deep sea <https://doi.org/10.1029/2020GB006769>. Global Biogeochemical Cycles, 35, e2020GB006769.

Hays, J. D., Imbrie, J., & Shackleton, N. J. (1976, December 10). Variations in the Earth's orbit: Pacemaker of the ice ages; For 500,000 years, major climatic changes have followed Variations in obliquity and precession <https://doi.org/10.1126/science.194.4270.1121>. Science, 194(4270), 1121–1132.

Headly, M. A., & Severinghaus, J. P. (2007, October 10). A method to measure Kr/N 2 ratios in air bubbles trapped in ice cores and its application in reconstructing past mean ocean temperature <https://doi.org/10.1029/2006JD008317>. Journal of Geophysical Research, 112(D19), D19105. Hegerl, G. C., Zwiers, F. W., Braconnot, P., Gillett, N. P., Luo, Y., Marengo Orsini, J. A., Nicholls, N., Penner, J. E., & Stott, P. A. (2007). Understanding and attributing climate change. In S. Solomon, D. Qin, M. Manning, Z. Chen, M. Marquis, K. B. Averyt, M. Tignor, & H. L. Miller (Eds.), Climate change 2007: The physical science basis. Contribution of Working Group I to the Fourth Assessment Report of the Intergovernmental Panel on Climate Change. Cambridge University Press.

Heinrich, H. (1988, March). Origin and consequences of cyclic ice ra"ing in the Northeast Atlantic Ocean during the past 130,000 years <https://doi.org/10.1016/0033-5894(88)90057-9>. Quaternary Research, 29(2), 142–152.

Held, I. M. (1982, May). Climate models and the astronomical theory of the ice ages <https://doi.org/10.1016/0019-1035(82)90135-X>. Icarus, 50(2–3), 449–461.

Held, I. M., & Soden, B. J. (2000, November). Water vapor feedback and global warming <https://doi.org/10.1146/annurev.energy.25.1.441>. Annual Review of Energy and the Environment, 25(1), 441–475.

Hemming, S. R. (2004, March). Heinrich events: Massive late Pleistocene detritus layers of the North Atlantic and their global climate imprint <https://doi.org/10.1029/2003RG000128>. Reviews of Geophysics, 42(1), 143.

Henry, W. (1803, December 31). III: Experiments on the quantity of gases absorbed by water, at different temperatures, and under different pressures <https://doi.org/10.1098/rstl.1803.0004>. Philosophical Transactions of the Royal Society of London, 93, 29–274.

Hernández-Almeida, I., Ausín, B., Saavedra-Pellitero, M., Baumann, K.-H., & Stoll, H. M. (2019, February). Quantitative reconstruction of primary productivity in low latitudes during the last glacial maximum and the mid-to-late Holocene from a global Florisphaera profunda calibration dataset <https://doi.org/10.1016/j.quascirev.2018.12.016>. Quaternary Science Reviews, 205, 166–181.

Hobbie, E. A., & Werner, R. A. (2004, February). Intramolecular, compound-specific, and bulk carbon isotope patterns in C 3 and C 4 plants: A review and synthesis. <https://doi.org/10.1111/j.1469-8137.2004.00970.x> New Phytologist, 161(2), 371–385.

Hodell, D. A., Venz, K. A., Charles, C. D., & Ninnemann, U. S. (2003, January). Pleistocene vertical carbon isotope and carbonate gradients in the South Atlantic sector of the Southern Ocean <https://doi.org/10.1029/2002GC000367>. Geochemistry, Geophysics, Geosystems, 4(1), 1–19.

Högbom, A. G. (1894). Om Sannolikheten for Sekulara Forandringar i Atmosfarens Kolsyrehalt [On the probability of secular Variations of atmospheric carbon dioxide]. Svensk Kemisk Tidskrift, 6, 169–176.

Hönisch, B., Hemming, N. G., Archer, D., Siddall, M., & McManus, J. F. (2009, June 19). Atmospheric carbon dioxide concentration across the mid-Pleistocene transition <https://doi.org/10.1126/science.1171477>. Science, 324(5934), 1551–1554.

Honjo, S., & Erez, J. (1978, July). Dissolution rates of calcium carbonate in the deep ocean: An in-situ experiment in the North Atlantic Ocean <https://doi.org/10.1016/0012-821X(78)90099-7>. Earth and Planetary Science Letters, 40(2), 287–300.

Hoogakker, B. A. A., Lu, Z., Umling, N., Jones, L., Zhou, X., Rickaby, R. E. M., Thunell, R., Cartapanis, O., & Galbraith, E. (2018, October). Glacial expansion of oxygen-depleted seawater in the eastern tropical Pacific <https://doi.org/10.1038/s41586-018-0589-x>. Nature, 562(7727), 410–413.

Hopkins, D. M. (1959, June 5). Cenozoic history of the Bering land bridge: The seaway between the Pacific and Arctic basins has o"en been a land route between Siberia and Alaska. <https://doi.org/10.1126/science.129.3362.1519> Science, 129(3362), 1519–1528.

Hugelius, G., Strauss, J., Zubrzycki, S., Harden, J. W., Schuur, E. A. G., Ping, C.-L., Schirrmeister, L., et al. (2014, December 1). Estimated stocks of circumpolar permafrost carbon with quantified uncertainty ranges and identified data gaps <https://doi.org/10.5194/bg-11-6573-2014>. Biogeosciences, 11(23), 6573–6593.

Humphreys, M. P., Lewis, E. R., Sharp, J. D., & Pierrot, D. (2022, January 4). PyCO2SYS v1.8: Marine carbonate system calculations in python. <https://doi.org/10.5194/gmd-15-15-2022> Geoscientific Model Development, 15(1), 15–43.

Huybers, P. (2011, December). Combined obliquity and precession pacing of late Pleistocene deglaciations <https://doi.org/10.1038/nature10626>. Nature, 480(7376), 229–232.

Huybers, P., & Denton, G. (2008, November). Antarctic temperature at orbital timescales controlled by local summer duration <https://doi.org/10.1038/ngeo311>. Nature Geoscience, 1(11), 787–792.

Huybers, P., & Wunsch, C. (2005, March). Obliquity pacing of the late Pleistocene glacial terminations <https://doi.org/10.1038/nature03401>. Nature, 434(7032), 491–494.

Imbrie, J., Berger, A., Boyle, E. A., Clemens, S. C., Duffy, A., Howard, W. R., Kukla, G., et al. (1993, December). On the structure and origin of major glaciation cycles 2: The 100,000-year cycle <https://doi.org/10.1029/93PA02751>. Paleoceanography, 8(6), 699–735.

Imbrie, J., Boyle, E. A., Clemens, S. C., Duffy, A., Howard, W. R., Kukla, G., Kutzbach, J., et al. (1992). On the structure and origin of major glaciation cycles 1: Linear responses to Milankovitch forcing. <https://doi.org/10.1029/92PA02253> Paleoceanography, 7(6), 701–738.

Imbrie, J., Hays, J. D., Martinson, D. G., McIntyre, A., Mix, A. C., Morley, J. J., Pisias, N. G., Prell, W. L., & Shackleton, N. J. (1984). The orbital theory of Pleistocene climate: Support from a revised chronology of the marine $D^{18}O$ record <https://epic.awi.de/id/eprint/41839/1/Imbrie-etal_1984.pdf>. In A. Berger (Ed.), Milankovitch and climate, 1 (pp. 269–305). D. Reidel.

Intergovernmental Panel on Climate Change (2000). Land use, land-use change and forestry: Summary for policymakers <https://archive.ipcc.ch/ipccreports/sres/land_use> (p. 375). Cambridge University Press.

Ito, T., & Follows, M. J. (2005, July 1). Preformed phosphate, soft tissue pump and atmospheric CO 2 <https://elischolar.library.yale.edu/journal_of_marine_research/102/>. Journal of Marine Research, 63(4), 813–839.

Ito, T., & Follows, M. J. (2013, December). Air-sea disequilibrium of carbon dioxide enhances the biological carbon sequestration in the Southern Ocean <https://doi.org/10.1002/2013GB004682>. Global Biogeochemical Cycles, 27(4), 1129–1138.

Jaccard, S. L., Galbraith, E. D., Martínez-García, A., & Anderson, R. F. (2016, February). Covariation of deep Southern Ocean oxygenation and atmospheric CO2 through the last ice age <https://doi.org/10.1038/nature16514>. Nature, 530(7589), 207–210.

Jaccard, S. L., Galbraith, E. D., Sigman, D. M., Haug, G. H., Francois, R., Pedersen, T. F., Dulski, P., & Thierstein, H. R. (2009, January). Subarctic Pacific evidence for a glacial deepening of the oceanic respired carbon pool <https://doi.org/10.1016/j.epsl.2008.10.017>. Earth and Planetary Science Letters, 277(1–2), 156–165.

Jaccard, S. L., Hayes, C. T., Martinez-Garcia, A., Hodell, D. A., Anderson, R. F., Sigman, D. M., & Haug, G. H. (2013, March 22). Two modes of change in Southern Ocean productivity over the past million years <https://doi.org/10.1126/science.1227545>. Science, 339(6126), 1419–1423.

Jacobel, A. W., Anderson, R. F., Jaccard, S. L., McManus, J. F., Pavia, F. J., & Winckler, G. (2020, February). Deep Pacific storage of respired carbon during the last ice age: Perspectives from bottom water oxygen reconstructions <https://doi.org/10.1016/j.quascirev.2019.106065>. Quaternary Science Reviews, 230, 106065.

Jahnke, R. A., Craven, D. B., & Gaillard, J.-F. (1994, July). The Influence of organic matter diagenesis on CaCO3 dissolution at the deep-sea floor <https://doi.org/10.1016/0016-7037(94)90115-5>. Geochimica et Cosmochimica Acta, 58(13), 2799–2809.

Jansen, M. F. (2017, January 3). Glacial ocean circulation and stratification explained by reduced atmospheric temperature <https://doi.org/10.1073/pnas.1610438113>. Proceedings of the National Academy of Sciences, 114(1), 45–50.

Jansen, M. F., Nadeau, L.-P., & Merlis, T. M. (2018, July). Transient versus equilibrium response of the ocean's overturning circulation to warming <https://doi.org/10.1175/JCLI-D-17-0797.1>. Journal of Climate, 31(13), 5147–5163.

Jeltsch-Thömmes, A., Battaglia, G., Cartapanis, O., Jaccard, S. L., & Joos, F. (2019, April 30). Low terrestrial carbon storage at the last glacial maximum: Constraints from multi-proxy data <https://doi.org/10.5194/cp15-849-2019>. Climate of the Past, 15(2), 849–879.

Jeltsch-Thömmes, A., & Joos, F. (2023, February). Carbon cycle responses to changes in weathering and the long-term fate of stable carbon isotopes <https://doi.org/10.1029/2022PA004577>. Paleoceanography and Paleoclimatology, 38(2), e2022PA004577.

Jochum, M., Jahn, A., Peacock, S., Bailey, D. A., Fasullo, J. T., Kay, J., Levis, S., & Otto-Bliesner, B. (2012, April 1). True to Milankovitch: Glacial inception in the new community climate system model <https://doi.org/10.1175/JCLI-D-11-00044.1>. Journal of Climate, 25(7), 2226–2239.

Joos, F., Roth, R., Fuglestvedt, J. S., Peters, G. P., Enting, I. G., Von Bloh, W., Brovkin, V., et al. (2013, March 8). Carbon dioxide and climate impulse response functions for the computation of greenhouse gas metrics: A multi-model analysis <https://doi.org/10.5194/acp-13-2793-2013>. Atmospheric Chemistry and Physics, 13(5), 2793–2825.

Joos, F., Sarmiento, J. L., & Siegenthaler, U. (1991, February). Estimates of the effect of Southern Ocean iron fertilization on atmospheric CO2 concentrations <https://doi.org/10.1038/349772a0>. Nature, 349(6312), 772–775.

Jouzel, J., Masson-Delmotte, V., Cattani, O., Dreyfus, G., Falourd, S., Hoffmann, G., Minster, B., et al. (2007, August 10). Orbital and millennial Antarctic climate variability over the past 800,000 years <https://doi.org/10.1126/science.1141038>. Science, 317(5839), 793–796.

Jouzel, J., Vaikmae, R., Petit, J. R., Martin, M., Duclos, Y., Stievenard, M., Lorius, C., et al. (1995, April). The two-step shape and timing of the last deglaciation in Antarctica <https://doi.org/10.1007/BF00223498>. Climate Dynamics, 11(3), 151–161.

Karl, D. M., Knauer, G. A., & Martin, J. H. (1988, March). Downward flux of particulate organic matter in the ocean: A particle decomposition paradox <https://doi.org/10.1038/332438a0>. Nature, 332(6163), 438–441.

Kawamura, K., Parrenin, F., Lisiecki, L., Uemura, R., Vimeux, F., Severinghaus, J. P., Hutterli, M. A., et al. (2007, August). Northern hemisphere forcing of climatic cycles in Antarctica over the past 360,000 years <https://doi.org/10.1038/nature06015>. Nature, 448(7156), 912–916.

Keeling, C. D. (1960, January). The concentration and isotopic abundances of carbon dioxide in the atmosphere <https://doi.org/10.3402/tellusa.v12i2.9366>. Tellus, 12(2), 200–203.

Keeling, C. D. (1973). The carbon dioxide cycle: Reservoir models to depict the exchange of atmospheric carbon dioxide with the Oceans and land plants <https://doi.org/10.1007/978-1-4684-1986-3_6>. In S. I. Rasool (Ed.), Chemistry of the lower atmosphere (pp. 251–329). Springer US.

Keeling, C. D., & Bolin, B. (1968, January 1). The simultaneous use of chemical tracers in Oceanic studies: II, A three-Reservoir model of the north and South Pacific Ocean <https://doi.org/10.3402/tellusa.v20i1.9917>. Tellus A: Dynamic Meteorology and Oceanography, 20(1), 17.

Keigwin, L. D., & Schlegel, M. A. (2002, June). Ocean ventilation and sedimentation since the glacial maximum at 3 km in the Western North Atlantic <https://doi.org/10.1029/2001GC000283>. Geochemistry, Geophysics, Geosystems, 3(6), 1–14.

Keir, R. S. (1988, August). On the Late Pleistocene ocean geochemistry and circulation <https://doi.org/10.1029/PA003i004p00413>. Paleoceanography, 3(4), 413–445.

Kemeny, P. C., Kast, E. R., Hain, M. P., Fawcett, S. E., Fripiat, F., Studer, A. S., Martínez-García, A., Haug, G. H., & Sigman, D. M. (2018, December). A seasonal model of nitrogen isotopes in the ice age Antarctic Zone: Support for weakening of the Southern Ocean upper overturning cell <https://doi.org/10.1029/2018PA003478>. Paleoceanography and Paleoclimatology, 33(12), 1453–1471.

Kerr, J., Rickaby, R., Yu, J., Elderfield, H., & Sadekov, A. Y. (2017, August). The effect of ocean alkalinity and carbon transfer on deep-sea carbonate ion concentration during the past five glacial cycles <https://doi.org/10.1016/j.epsl.2017.04.042>. Earth and Planetary Science Letters, 471, 42–53.

Khatiwala, S., Schmittner, A., & Muglia, J. (2019, June 7). Air-sea disequilibrium enhances ocean carbon storage during glacial periods <https://doi.org/10.1126/sciadv.aaw4981>. Science Advances, 5(6), eaaw4981.

Klaas, C., & Archer, D. E. (2002, December). Association of sinking organic matter with various types of mineral ballast in the deep sea: Implications for the rain ratio <https://doi.org/10.1029/2001GB001765>. Global Biogeochemical Cycles, 16(4), 63-1–63-14.

Knox, F., & McElroy, M. B. (1984). Changes in atmospheric CO 2: Influence of the marine biota at high latitude <https://doi.org/10.1029/JD089iD03p04629>. Journal of Geophysical Research, 89(D3), 4629.

Kohfeld, K. E., & Harrison, S. P. (2001, June). DIRTMAP: The geological record of dust <https://doi.org/10.1016/S0012-8252(01)00042-3>. Earth-Science Reviews, 54(1–3), 81–114.

Kohfeld, K. E., Le Quéré, C., Harrison, S. P., & Anderson, R. F. (2005, April). Role of marine biology in glacialinterglacial CO 2 cycles <https://doi.org/10.1126/science.1105375>. Science, 308(5718), 74–78.

Kohfeld, K. E., & Ridgwell, A. (2009). Glacial-interglacial variability in atmospheric CO2 <https://doi.org/10.1029/2008GM000845>. In C. Le Quéré & E. S. Saltzman (Eds.), Geophysical Monograph Series (pp. 251–286). American Geophysical Union.

Köhler, P., Bintanja, R., Fischer, H., Joos, F., Knutti, R., Lohmann, G., & Masson-Delmotte, V. (2010, January). What caused Earth's temperature variations during the last 800,000 years? Data-based evidence on radiative forcing and constraints on climate sensitivity <https://doi.org/10.1016/j.quascirev.2009.09.026>. Quaternary Science Reviews, 29(1–2), 129–145.

Köhler, P., Knorr, G., & Bard, E. (2014, December). Permafrost thawing as a possible source of abrupt carbon release at the onset of the Bølling/Allerød <https://doi.org/10.1038/ncomms6520>. Nature Communications, 5(1), 5520.

Kopp, R. E., Simons, F. J., Mitrovica, J. X., Maloof, A. C., & Oppenheimer, M. (2013, May 1). A probabilistic assessment of sea level variations within the last interglacial stage <https://doi.org/10.1093/gji/ggt029>. Geophysical Journal International, 193(2), 711–716.

Köppen, W., & Wegener, A. (1924). Die Klimate der geologischen Vorzeit. Gebrüder Borntraeger.

Krüger, T. (2013). Discovering the ice ages: International reception and consequences for a historical understanding of climate (Vol. 37). History of Science and Medicine Library. Brill.

Kukla, G., Berger, A., Lotti, R., & Brown, J. (1981, March). Orbital signature of Interglacials <https://doi.org/10.1038/290295a0>. Nature, 290(5804), 295–300.

Kumar, N., Anderson, R. F., Mortlock, R. A., Froelich, P. N., Kubik, P., Dittrich-Hannen, B., & Suter, M. (1995,December). Increased biological productivity and export production in the glacial Southern Ocean <https://doi.org/10.1038/378675a0>. Nature, 378(6558), 675–680.

Kwon, E. Y., Hain, M. P., Sigman, D. M., Galbraith, E. D., Sarmiento, J. L., & Toggweiler, J. R. (2012, June). North Atlantic ventilation of "southern-sourced" deep water in the glacial ocean <https://doi.org/10.1029/2011PA002211>. Paleoceanography, 27(2).

Kwon, E. Y., Primeau, F., & Sarmiento, J. L. (2009, September). The impact of remineralization depth on the air–sea carbon balance. <https://doi.org/10.1038/ngeo612> Nature Geoscience, 2(9), 630–635.

Kwon, E. Y., Sarmiento, J. L., Toggweiler, J. R., & DeVries, T. (2011, September). The control of atmospheric p CO 2 by ocean ventilation change: The effect of the oceanic storage of biogenic carbon <https://doi.org/10.1029/2011GB004059>. Global Biogeochemical Cycles, 25(3).

Labeyrie, L. D., Duplessy, J. C., & Blanc, P. L. (1987, June). Variations in mode of formation and temperature of oceanic deep waters over the past 125,000 years <https://doi.org/10.1038/327477a0>. Nature, 327(6122), 477–482.

Lambeck, K., Rouby, H., Purcell, A., Sun, Y., & Sambridge, M. (2014, October 28). Sea level and global ice volumes from the last glacial maximum to the Holocene <https://doi.org/10.1073/pnas.1411762111>. Proceedings of the National Academy of Sciences, 111(43), 15296–15303.

Lambert, F., Delmonte, B., Petit, J. R., Bigler, M., Kaufmann, P. R., Hutterli, M. A., Stocker, T. F., Ruth, U., Steffensen, J. P., & Maggi, V. (2008, April). Dust-climate couplings over the past 800,000 years from the EPICA Dome C ice core <https://doi.org/10.1038/nature06763>. Nature, 452(7187), 616–619.

Lambert, F., Opazo, N., Ridgwell, A., Winckler, G., Lamy, F., Shaffer, G., Kohfeld, K., Ohgaito, R., Albani, S., & Abe-Ouchi, A. (2021, January). Regional patterns and temporal evolution of ocean iron fertilization and CO2 drawdown during the last glacial termination <https://doi.org/10.1016/j.epsl.2020.116675>. Earth and Planetary Science Letters, 554, 116675.

Landing, W. M., & Bruland, K. W. (1987, January). The contrasting biogeochemistry of iron and manganese in the Pacific Ocean <https://doi.org/10.1016/0016-7037(87)90004-4>. Geochimica et Cosmochimica Acta, 51(1), 29–43.

Laskar, J. (1988). Secular evolution of the solar system over 10 million years <https://ui.adsabs.harvard.edu/abs/1988A&A...198..341L>. Astronomy and Astrophysics, 198(1–2), 341362.

Laskar, J., Fienga, A., Gastineau, M., & Manche, H. (2011, August). La2010: A new orbital solution for the longterm motion of the Earth <https://doi.org/10.1051/0004-6361/201116836>. Astronomy & Astrophysics, 532, A89.

Laskar, J., Robutel, P., Joutel, F., Gastineau, M., Correia, A. C. M., & Levrard, B. (2004, December). A long-term numerical solution for the insolation quantities of the Earth <https://doi.org/10.1051/0004-6361:20041335>. Astronomy & Astrophysics, 428(1), 261–285.

Lauderdale, J. M., Braakman, R., Forget, G., Dutkiewicz, S., & Follows, M. J. (2020, March 3). Microbial feedbacks optimize ocean iron availability <https://doi.org/10.1073/pnas.1917277117>. Proceedings of the National Academy of Sciences, 117(9), 4842–4849.

Lefèvre, N., & Watson, A. J. (1999, September). Modeling the geochemical cycle of iron in the oceans and its impact on atmospheric CO 2 concentrations <https://doi.org/10.1029/1999GB900034>. Global Biogeochemical Cycles, 13(3), 727–736.

Lhardy, F., Bouttes, N., Roche, D. M., Abe-Ouchi, A., Chase, Z., Crichton, K. A., Ilyina, T., et al. (2021a, October). A first intercomparison of the simulated LGM carbon results within PMIP-carbon: Role of the ocean boundary conditions <https://doi.org/10.1029/2021PA004302>. Paleoceanography and Paleoclimatology, 36(10).

Lhardy, F., Bouttes, N., Roche, D. M., Crosta, X., Waelbroeck, C., & Paillard, D. (2021b, June 7). Impact of Southern Ocean surface conditions on deep ocean circulation during the LGM: A model analysis <https://doi.org/10.5194/cp-17-1139-2021>. Climate of the Past, 17(3), 1139–1159.

Li, Y.-H., & Peng, T.-H. (2002, December). Latitudinal change of remineralization ratios in the oceans and its implication for nutrient cycles <https://doi.org/10.1029/2001GB001828>. Global Biogeochemical Cycles, 16(4), 77-1–77-16.

Li, Y.-H., Takahashi, T., & Broecker, W. S. (1969, October 20). Degree of saturation of CaCO 3 in the oceans <https://doi.org/10.1029/JC074i023p05507>. Journal of Geophysical Research, 74(23), 5507–5525.

Lindgren, A., Hugelius, G., & Kuhry, P. (2018, August). Extensive loss of past permafrost carbon but a net accumulation into present-day soils <https://doi.org/10.1038/s41586-018-0371-0>. Nature, 560(7717), 219222.

Lisiecki, L. E., & Raymo, M. E. (2005, March). A Pliocene-Pleistocene stack of 57 globally distributed benthic δ 18 O records <https://doi.org/10.1029/2004PA001071>. Paleoceanography, 20(1).

Lisiecki, L. E., & Raymo, M. E. (2007, January). Plio–Pleistocene climate evolution: Trends and transitions in glacial cycle dynamics <https://doi.org/10.1016/j.quascirev.2006.09.005>. Quaternary Science Reviews, 26(12), 56–69.

López-Urrutia, Á., Martin, E. S., Harris, R. P., & Irigoien, X. (2006, June 6). Scaling the metabolic balance of the oceans <https://doi.org/10.1073/pnas.0601137103>. Proceedings of the National Academy of Sciences, 103(23), 8739–8744.

Loulergue, L., Schilt, A., Spahni, R., Masson-Delmotte, V., Blunier, T., Lemieux, B., Barnola, J.-M., Raynaud, D., Stocker, T. F., & Chappellaz, J. (2008, May). Orbital and millennial-scale features of atmospheric CH4 over the past 800,000 years <https://doi.org/10.1038/nature06950>. Nature, 453(7193), 383–386.

Lourens, L. J., Becker, J., Bintanja, R., Hilgen, F. J., Tuenter, E., van de Wal, R. S. W., & Ziegler, M. (2010, January). Linear and non-linear response of late Neogene glacial cycles to obliquity forcing and implications for the Milankovitch theory <https://doi.org/10.1016/j.quascirev.2009.10.018.>. Quaternary Science Reviews, 29(1–2), 352–365.

Loutre, M. F. (2003). Ice ages (Milankovitch theory). In J. R. Holton (Ed.), Encyclopedia of atmospheric sciences (pp. 995–1003). Academic Press.

Lu, W., Wang, Y., Oppo, D. W., Nielsen, S. G., & Costa, K. M. (2022, August). Comparing paleo-oxygenation proxies (benthic foraminiferal surface porosity, I/Ca, Authigenic uranium) on modern sediments and the glacial Arabian Sea <https://doi.org/10.1016/j.gca.2022.06.001>. Geochimica et Cosmochimica Acta, 331, 6985.

Lund, D. C., Adkins, J. F., & Ferrari, R. (2011, March 19). Abyssal Atlantic circulation during the last glacial maximum: Constraining the ratio between transport and vertical mixing <https://doi.org/10.1029/2010PA001938>. Paleoceanography, 26(1), PA1213.

Lüthi, D., Le Floch, M., Bereiter, B., Blunier, T., Barnola, J.-M., Siegenthaler, U., Raynaud, D., et al. (2008, May). High-resolution carbon dioxide concentration record 650,000–800,000 years before present <https://doi.org/10.1038/nature06949>. Nature, 453(7193), 379–382.

Lynch-Stieglitz, J., Adkins, J. F., Curry, W. B., Dokken, T., Hall, I. R., Herguera, J. C., Hirschi, J. J.-M., et al. (2007, April 6). Atlantic meridional overturning circulation during the last glacial maximum <https://doi.org/10.1126/science.1137127>. Science, 316(5821), 66–69.

Maher, B. A., Prospero, J. M., Mackie, D., Gaiero, D., Hesse, P. P., & Balkanski, Y. (2010, April). Global connections between Aeolian dust, climate and ocean biogeochemistry at the present day and at the last glacial maximum <https://doi.org/10.1016/j.earscirev.2009.12.001>. Earth-Science Reviews, 99(1–2), 61–97.

Mahowald, N., Kohfeld, K., Hansson, M., Balkanski, Y., Harrison, S. P., Prentice, I. C., Schulz, M., & Rodhe, H. (1999, July 20). Dust sources and deposition during the last glacial maximum and current climate: A comparison of model results with Paleodata from ice cores and marine sediments <https://doi.org/10.1029/1999JD900084>. Journal of Geophysical Research: Atmospheres, 104(D13), 15895–15916.

Maier-Reimer, E., & Hasselmann, K. (1987, August). Transport and storage of CO2 in the ocean—An Inorganic Ocean-circulation carbon cycle model <https://doi.org/10.1007/BF01054491>. Climate Dynamics, 2(2), 6390.

Manabe, S., & Broccoli, A. J. (2020). Beyond global warming: How numerical models revealed the secrets of climate change. Princeton University Press.

Manabe, S., & Stouffer, R. J. (1988). Two stable equilibria of a coupled ocean-atmosphere model. Journal of Climate, 1(9), 841–866.

Marchitto, T. M., Lehman, S. J., Ortiz, J. D., Flückiger, J., & van Geen, A. (2007). Marine radiocarbon evidence for the mechanism of deglacial atmospheric CO2 rise <https://doi.org/10.1126/science.1138679>. Science, 316(5830), 1456–1459.

Marchitto, T. M., Lynch-Stieglitz, J., & Hemming, S. R. (2005, March). Deep Pacific CaCO3 compensation and glacial–interglacial atmospheric CO2 <https://doi.org/10.1016/j.epsl.2004.12.024>. Earth and Planetary Science Letters, 231(3–4), 317–336.

Marconi, D., Sigman, D. M., Casciotti, K. L., Campbell, E. C., Weigand, M. A., Fawcett, S. E., Knapp, A. N., Rafter, P. A., Ward, B. B., & Haug, G. H. (2017, October). Tropical dominance of N 2 fixation in the North Atlantic Ocean <https://doi.org/10.1002/2016GB005613>. Global Biogeochemical Cycles, 31(10), 1608–1623.

Marcott, S. A., Bauska, T. K., Buizert, C., Steig, E. J., Rosen, J. L., Cuffey, K. M., Fudge, T. J., et al. (2014, October 30). Centennial-scale changes in the global carbon cycle during the last deglaciation <https://doi.org/10.1038/nature13799>. Nature, 514(7524), 616–619.

Marinov, I., Follows, M., Gnanadesikan, A., Sarmiento, J. L., & Slater, R. D. (2008, July 22). How does ocean biology affect atmospheric p CO 2 ? Theory and models <https://doi.org/10.1029/2007JC004598>. Journal of Geophysical Research, 113(C7), C07032.

Marinov, I., Gnanadesikan, A., Sarmiento, J. L., Toggweiler, J. R., Follows, M., & Mignone, B. K. (2008, September). Impact of oceanic circulation on biological carbon storage in the ocean and atmospheric p CO 2 <https://doi.org/10.1029/2007GB002958>. Global Biogeochemical Cycles, 22(3).

Marinov, I., Gnanadesikan, A., Toggweiler, J. R., & Sarmiento, J. L. (2006, June). The Southern Ocean biogeochemical divide <https://doi.org/10.1038/nature04883>. Nature, 441(7096), 964–967.

Marsay, C. M., Sanders, R. J., Henson, S. A., Pabortsava, K., Achterberg, E. P., & Lampitt, R. S. (2015, January 27). Attenuation of sinking particulate organic carbon flux through the mesopelagic ocean <https://doi.org/10.1073/pnas.1415311112>. Proceedings of the National Academy of Sciences, 112(4), 1089–1094.

Martin, J. H. (1990, February). Glacial-interglacial CO 2 change: The iron hypothesis <https://doi.org/10.1029/PA005i001p00001>. Paleoceanography, 5(1), 1–13.

Martin, J. H., & Fitzwater, S. E. (1988, January). Iron deficiency limits phytoplankton growth in the NorthEast Pacific subarctic <https://doi.org/10.1038/331341a0>. Nature, 331(6154), 341–343.

Martin, J. H., & Gordon, R. M. (1988, February). Northeast Pacific iron distributions in relation to phytoplankton productivity <https://doi.org/10.1016/0198-0149(88)90035-0>. Deep Sea Research Part A: Oceanographic Research Papers, 35(2), 177–196.

Martin, J. H., Knauer, G. A., Karl, D. M., & Broenkow, W. W. (1987, February). VERTEX: Carbon cycling in the northeast Pacific <https://doi.org/10.1016/0198-0149(87)90086-0>. Deep Sea Research Part A: Oceanographic Research Papers, 34(2), 267–285.

Martin, P. A., Lea, D. W., Rosenthal, Y., Shackleton, N. J., Sarnthein, M., & Papenfuss, T. (2002, April 30). Quaternary deep sea temperature histories derived from benthic foraminiferal Mg/Ca <https://doi.org/10.1016/S0012-821X(02)00472-7>. Earth and Planetary Science Letters, 198(1–2), 193209.

Martínez-Botí, M. A., Foster, G. L., Chalk, T. B., Rohling, E. J., Sexton, P. F., Lunt, D. J., Pancost, R. D., Badger, M. P. S., & Schmidt, D. N. (2015, February 5). Plio-Pleistocene climate sensitivity evaluated using high-resolution CO2 records <https://doi.org/10.1038/nature14145>. Nature, 518(7537), 49–54.

Martínez-Botí, M. A., Marino, G., Foster, G. L., Ziveri, P., Henehan, M. J., Rae, J. W. B., Mortyn, P. G., & Vance, D. (2015, February 12). Boron isotope evidence for oceanic carbon dioxide leakage during the last deglaciation

<https://doi.org/10.1038/nature14155>. Nature, 518(7538), 219–222.

Martínez-Garcia, A., Rosell-Melé, A., Geibert, W., Gersonde, R., Masqué, P., Gaspari, V., & Barbante, C. (2009, March). Links between iron supply, marine productivity, sea surface temperature, and CO 2 over the last 1.1 Ma <https://doi.org/10.1029/2008PA001657>. Paleoceanography, 24(1).

Martínez-García, A., Sigman, D. M., Ren, H., Anderson, R. F., Straub, M., Hodell, D. A., Jaccard, S. L., Eglinton, T. I., & Haug, G. H. (2014, March 21). Iron fertilization of the Subantarctic ocean during the last ice age <https://doi.org/10.1126/science.1246848>. Science, 343(6177), 1347–1350.

Martiny, A. C., Pham, C. T. A., Primeau, F. W., Vrugt, J. A., Moore, J. K., Levin, S. A., & Lomas, M. W. (2013, April). Strong latitudinal patterns in the elemental ratios of marine plankton and organic matter <https://doi.org/10.1038/ngeo1757>. Nature Geoscience, 6(4), 279–283.

Marzocchi, A., & Jansen, M. F. (2019, December). Global cooling linked to increased glacial carbon storage via changes in Antarctic Sea ice <https://doi.org/10.1038/s41561-019-0466-8>. Nature Geoscience, 12(12), 1001–1005.

Matsumoto, K. (2007, October 26). Biology-mediated temperature control on atmospheric p CO 2 and ocean biogeochemistry <https://doi.org/10.1029/2007GL031301>. Geophysical Research Letters, 34(20), L20605.

Matsumoto, K., & Sarmiento, J. L. (2008, June). A corollary to the silicic acid leakage hypothesis <https://doi.org/10.1029/2007PA001515>. Paleoceanography, 23(2).

Matsumoto, K., Sarmiento, J. L., & Brzezinski, M. A. (2002, September). Silicic acid leakage from the Southern Ocean: A possible explanation for glacial atmospheric p CO 2 <https://doi.org/10.1029/2001GB001442>. Global Biogeochemical Cycles, 16(3), 5-1–5-23.

McElroy, M. B. (1983, March). Marine biological controls on atmospheric CO2 and climate <https://doi.org/10.1038/302328a0>. Nature, 302(5906), 328–329.

McManus, J. F., Francois, R., Gherardi, J.-M., Keigwin, L. D., & Brown-Leger, S. (2004, April). Collapse and rapid resumption of Atlantic meridional circulation linked to deglacial climate changes <https://doi.org/10.1038/nature02494>. Nature, 428(6985), 834–837.

Menking, J. A., Shackleton, S. A., Bauska, T. K., Buffen, A. M., Brook, E. J., Barker, S., Severinghaus, J. P., Dyonisius, M. N., & Petrenko, V. V. (2022, September 16). Multiple carbon cycle mechanisms associated with the glaciation of Marine Isotope Stage 4 <https://doi.org/10.1038/s41467-022-33166-3>. Nature Communications, 13(1), 5443.

Menviel, L., Joos, F., & Ritz, S. P. (2012, November). Simulating atmospheric CO2, ^{13}C and the marine carbon cycle during the last glacial–interglacial cycle: Possible role for a deepening of the mean remineralization depth and an increase in the oceanic nutrient inventory <https://doi.org/10.1016/j.quascirev.2012.09.012>. Quaternary Science Reviews, 56, 46–68.

Menviel, L., Spence, P., Yu, J., Chamberlain, M. A., Matear, R. J., Meissner, K. J., & England, M. H. (2018, June 27). Southern Hemisphere westerlies as a driver of the early deglacial atmospheric CO2 rise <https://doi.org/10.1038/s41467-018-04876-4>. Nature Communications, 9(1), 2503.

Menviel, L., Timmermann, A., Elison Timm, O., & Mouchet, A. (2011, May). Deconstructing the Last Glacial termination: The role of millennial and orbital-scale forcings <https://doi.org/10.1016/j.quascirev.2011.02.005>. Quaternary Science Reviews, 30(9–10), 11551172.

Menviel, L., Yu, J., Joos, F., Mouchet, A., Meissner, K. J., & England, M. H. (2017, January). Poorly ventilated deep ocean at the last glacial maximum inferred from carbon isotopes: A data-model comparison study <https://doi.org/10.1002/2016PA003024>. Paleoceanography, 32(1), 2–17.

Mesolella, K. J., Matthews, R. K., Broecker, W. S., & Thurber, D. L. (1969, May). The astronomical theory of climatic change: Barbados data <https://doi.org/10.1086/627434>. The Journal of Geology, 77(3), 250–274.

Milankovitch, M. (1920). Théorie Mathématique Des Phénomènes Thermiques Produits Par La Radiation Solaire. Gauthiers-Villars.

Milankovitch, M. (1930). Mathematische Klimalehre Und Astronomische Theorie Der Klimaschwankungen. In W. Köppen & R. Geiger (Eds.), Allgemeine Klimalehre (Vol. 1, pp. 1–176). Handbuch Der Klimatologie. Borntraeger.

Milankovitch, M. (1941). Kanon Der Erdbestrahlung Und Seine Anwendung Auf Das Eiszeitenproblem (Vol. 132). Royal Serbian Academy Special Publications..

Milliman, J. D., Troy, P. J., Balch, W. M., Adams, A. K., Li, Y.-H., & Mackenzie, F. T. (October 1999). Biologically mediated dissolution of calcium carbonate above the chemical lysocline? <https://doi.org/10.1016/S09670637(99)00034-5> Deep Sea Research Part I: Oceanographic Research Papers, 46(10), 1653–1669.

Monnin, E., Indermühle, A., Dällenbach, A., Flückiger, J., Stauffer, B., Stocker, T. F., Raynaud, D., & Barnola, J.-M. (2001, January 5). Atmospheric CO 2 concentrations over the last glacial termination <https://doi.org/10.1126/science.291.5501.112>. Science, 291(5501), 112–114.

Moore, C. M. (2016, November 28). Diagnosing oceanic nutrient deficiency <https://doi.org/10.1098/rsta.2015.0290>. Philosophical Transactions of the Royal Society A: Mathematical, Physical and Engineering Sciences, 374(2081), 20150290.

Moore, C. M., Mills, M. M., Arrigo, K. R., Berman-Frank, I., Bopp, L., Boyd, P. W., Galbraith, E. D., et al. (2013, September). Processes and patterns of oceanic nutrient limitation <https://doi.org/10.1038/ngeo1765>. Nature Geoscience, 6(9), 701–710.

Moore, J. K., Abbott, M. R., Richman, J. G., & Nelson, D. M. (2000, March). The Southern Ocean at the last glacial maximum: A strong sink for atmospheric carbon dioxide <https://doi.org/10.1029/1999GB900051>. Global Biogeochemical Cycles, 14(1), 455–475.

Morel, F., & Hering, J. G. (1993). Principles and applications of aquatic chemistry. Wiley.

Mortlock, R. A., Charles, C. D., Froelich, P. N., Zibello, M. A., Saltzman, J., Hays, J. D., & Burckle, L. H. (1991, May). Evidence for lower productivity in the Antarctic Ocean during the last glaciation <https://doi.org/10.1038/351220a0>. Nature, 351(6323), 220–223.

Ne"el, A., Oeschger, H., Schwander, J., Stauffer, B., & Zumbrunn, R. (1982, January). Ice core sample measurements give atmospheric CO2 content during the past 40,000 Yr <https://doi.org/10.1038/295220a0>. Nature, 295(5846), 220–223.

Oliver, K. I. C., Hoogakker, B. A. A., Crowhurst, S., Henderson, G. M., Rickaby, R. E. M., Edwards, N. R., & Elderfield, H. (2010, October 8). A synthesis of marine sediment core $\delta^{13}C$ data over the last 150 000 years <https://doi.org/10.5194/cp-6-645-2010>. Climate of the Past, 6(5), 645–673.

Opdyke, B. N., & Walker, C. G. (1992). Return of the coral reef hypothesis: Basin to shelf partitioning of CaCO3 and its effect on atmospheric CO_2 <https://doi.org/10.1130/00917613(1992)020%3C0733:ROTCRH%3E2.3.CO;2>. Geology, 20(8), 733–736.

Osman, M. B., Tierney, J. E., Zhu, J., Tardif, R., Hakim, G. J., King, J., & Poulsen, C. J. (2021, November 11). Globally resolved surface temperatures since the last glacial maximum <https://doi.org/10.1038/s41586021-03984-4>. Nature, 599(7884), 239–244.

Otto-Bliesner, B. L., Hewitt, C. D., Marchitto, T. M., Brady, E., Abe-Ouchi, A., Crucifix, M., Murakami, S., & Weber, S. L. (2007, June 20). Last glacial maximum ocean thermohaline circulation: PMIP2 model intercomparisons and data constraints <https://doi.org/10.1029/2007GL029475>. Geophysical Research Letters, 34(12), L12706.

Pales, J. C., & Keeling, C. D. (1965, December 15). The concentration of atmospheric carbon dioxide in Hawaii <https://doi.org/10.1029/JZ070i024p06053>. Journal of Geophysical Research, 70(24), 6053–6076.

Palter, J. B., Sarmiento, J. L., Gnanadesikan, A., Simeon, J., & Slater, D. (2010, June 1). Fueling primary productivity: Nutrient return pathways from the deep ocean and their dependence on the meridional overturning circulation <https://doi.org/10.5194/bgd-7-4045-2010>. Preprint. Biogeochemistry: Open Ocean.

Parekh, P., Joos, F., & Müller, S. A. (2008, December). A modeling assessment of the interplay between aeolian iron fluxes and iron-binding ligands in controlling carbon dioxide fluctuations during Antarctic warm events <https://doi.org/10.1029/2007PA001531>. Paleoceanography, 23(4).

Parrenin, F., Masson-Delmotte, V., Köhler, P., Raynaud, D., Paillard, D., Schwander, J., Barbante, C., Landais, A., Wegner, A., & Jouzel, J. (2013, March). Synchronous change of atmospheric CO 2 and Antarctic temperature during the last deglacial warming <https://doi.org/10.1126/science.1226368>. Science, 339(6123), 1060–1063.

Passow, U., & Carlson, C. A. (2012). The biological pump in a high CO2 world. Marine Ecology Progress Series, 470, 249–271.

Paulmier, A., Kriest, I., & Oschlies, A. (2009, May 28). Stoichiometries of remineralisation and denitrification in global biogeochemical ocean models <https://doi.org/10.5194/bg-6-923-2009>. Biogeosciences, 6(5), 923935.

Pavia, F. J., Anderson, R. F., Lam, P. J., Cael, B. B., Vivancos, S. M., Fleisher, M. Q., Lu, Y., Zhang, P., Cheng, H., & Edwards, R. L. (2019, May 14). Shallow particulate organic carbon regeneration in the South Pacific Ocean <https://doi.org/10.1073/pnas.1901863116>. Proceedings of the National Academy of Sciences, 116(20), 9753–9758.

Peltier, W. R. (2004, May 19). Global glacial isostasy and the surface of the ice-age Earth: The ICE-5G (VM2) model and GRACE <https://doi.org/10.1146/annurev.earth.32.082503.144359>. Annual Review of Earth and Planetary Sciences, 32(1), 111–149.

Penck, A., & Brückner, E. (1901). Die Alpen Im Eiszeitalter (3 vols.). Tauchnitz.

Peterson, C. D., Lisiecki, L. E., & Stern, J. V. (2014, June). Deglacial whole-ocean δ 13 C change estimated from 480 benthic foraminiferal records <https://doi.org/10.1002/2013PA002552>. Paleoceanography, 29(6), 549–563.

Petit, J. R., Jouzel, J., Raynaud, D., Barkov, N. I., Barnola, J.-M., Basile, I., Bender, M., et al. (1999, June). Climate and atmospheric history of the past 420,000 years from the Vostok ice core, Antarctica <https://doi.org/10.1038/20859>. Nature, 399(6735), 429–436.

Phillips, F. M., Zreda, M. G., Gosse, J. C., Klein, J., Evenson, E. B., Hall, R. D., Chadwick, O. A., & Sharma, P. (1997, November). Cosmogenic 36Cl and 10Be ages of Quaternary glacial and fluvial deposits of the Wind River Range, Wyoming <https://doi.org/10.1130/0016-7606(1997)109%3c1453:CCABAO%3e2.3.CO;2>. Geological Society of America Bulletin, 109(11), 1453–1463.

Phillips, F. M., Zreda, M. G., Smith, S. S., Elmore, D., Kubik, P. W., & Sharma, P. (1990, June 22). Cosmogenic chlorine-36 chronology for glacial deposits at bloody canyon, Eastern Sierra Nevada <https://doi.org/10.1126/science.248.4962.1529>. Science, 248(4962), 1529–1532.

Piccione, G., Blackburn, T., Tulaczyk, S., Rasbury, E. T., Hain, M. P., Ibarra, D. E., Methner, K., et al. (2022)

September 15). Subglacial precipitates record Antarctic ice sheet response to late Pleistocene millennial climate cycles <https://doi.org/10.1038/s41467-022-33009-1>. Nature Communications, 13(1), 5428.

Plass, G. N. (1956a, May). The carbon dioxide theory of climatic change <https://doi.org/10.1111/j.21533490.1956.tb01206.x>. Tellus, 8(2), 140–154.

Plass, G. N. (1956b, January). The influence of the 9.6 micron ozone band on the atmospheric infra-red cooling rate <https://doi.org/10.1002/qj.49708235104>. Quarterly Journal of the Royal Meteorological Society, 82(351), 30–44.

Plass, G. N. (1956c, July). The influence of the 15μ carbon-dioxide band on the atmospheric infra-red cooling rate <https://doi.org/10.1002/qj.49708235307>. Quarterly Journal of the Royal Meteorological Society, 82(353), 310–324.

Pöppelmeier, F., Baggenstos, D., Grimmer, M., Liu, Z., Schmitt, J., Fischer, H., & Stocker, T. F. (2023, March 28). The effect of past saturation changes on noble gas reconstructions of mean ocean temperature <https://doi.org/10.1029/2022GL102055>. Geophysical Research Letters, 50(6), e2022GL102055.

Porter, S. C. (2005, September). Pleistocene snowlines and glaciation of the Hawaiian Islands <https://doi.org/10.1016/j.quaint.2005.02.009>. Quaternary International, 138–139, 118–128.

Prentice, I. C., Sykes, M. T., Lautenschlager, M., Harrison, S. P., Denissenko, O., & Bartlein, P. J. (1993, May). Modelling global vegetation patterns and terrestrial carbon storage at the last glacial maximum <https://doi.org/10.2307/2997548>. Global Ecology and Biogeography Letters, 3(3), 67.

Primeau, F. W., Holzer, M., & DeVries, T. (2013, May). Southern Ocean nutrient trapping and the efficiency of the biological pump <https://doi.org/10.1002/jgrc.20181>. Journal of Geophysical Research: Oceans, 118(5), 2547–2564.

Putnam, A. E., Schaefer, J. M., Denton, G. H., Barrell, D. J. A., Birkel, S. D., Andersen, B. G., Kaplan, M. R., Finkel, R. C., Schwartz, R., & Doughty, A. M. (2013, February). The last glacial maximum at 44°S documented by a 10Be moraine chronology at Lake Ohau, Southern Alps of New Zealand <https://doi.org/10.1016/j.quascirev.2012.10.034>. Quaternary Science Reviews, 62, 114–141.

Rae, J. W. B., & Broecker, W. (2018, June 21). What fraction of the Pacific and Indian Oceans' deep water is formed in the Southern Ocean? <https://doi.org/10.5194/bg-15-3779-2018> Biogeosciences, 15(12), 37793794.

Rae, J. W. B., Burke, A., Robinson, L. F., Adkins, J. F., Chen, T., Cole, C., Greenop, R., et al. (2018, October). CO2 storage and release in the deep Southern Ocean on millennial to centennial timescales <https://doi.org/10.1038/s41586-018-0614-0>. Nature, 562(7728), 569–573.

Rafter, P. A., Gray, W. R., Hines, S. K. V., Burke, A., Costa, K. M., Gottschalk, J., Hain, M. P., Rae, J. W. B., Southon, J. R., Walczak, M. H., Yu, J., Adkins, J. F., & DeVries, T. (2022). Global reorganization of deep-sea circulation and carbon storage a"er the last ice age <https://doi.org/10.1126/sciadv.abq5434>. Science Advances, 8(46), eabq5434.

Rafter, P. A., Sigman, D. M., & Mackey, K. R. M. (2017, October 24). Recycled iron fuels new production in the eastern equatorial Pacific Ocean <https://doi.org/10.1038/s41467-017-01219-7>. Nature Communications, 8(1), 1100.

Raymo, M. E., & Huybers, P. (2008, January). Unlocking the mysteries of the ice ages <https://doi.org/10.1038/nature06589>. Nature, 451(7176), 284–285.

Raymo, M. E., Lisiecki, L. E., & Nisancioglu, K. H. (2006, July 28). Plio-Pleistocene ice volume, Antarctic climate, and the global δ 18 O record <https://doi.org/10.1126/science.1123296>. Science, 313(5786), 492495.

Raynaud, D., & Barnola, J. (1985). An Antarctic ice core reveals atmospheric CO2 variations over the past few centuries <https://doi.org/10.1038/315309a0>. Nature, 315, 309–311.

Raynaud, D., Delmas, R., Ascencio, J. M., & Legrand, M. (1982). Gas extraction from polar ice cores: A critical issue for studying the evolution of atmospheric CO 2 and ice-sheet surface elevation <https://doi.org/10.3189/S0260305500002895>. Annals of Glaciology, 3, 265–268.

Redfield, A. C. (1934). On the proportions of organic derivatives in sea water and their relation to the composition of plankton. In R.

J. Daniel (Ed.), James Johnstone memorial volume (pp. 176–192). University Press of Liverpool.

Redfield, A. C., Ketchum, B. H., & Richards, F. A. (1963). The Influence of organisms on the composition of sea-water. In M. N. Hill (Ed.), The sea (Vol. 2, pp. 26–77). Wiley Interscience.

Reimer, P. J., Austin, W. E. N., Bard, E., Bayliss, A., Blackwell, P. G., Ramsey, C. B., Butzin, M., et al. (2020, August). The IntCal20 Northern Hemisphere radiocarbon age calibration curve (0–55 Cal kBP) <https://doi.org/10.1017/RDC.2020.41>. Radiocarbon, 62(4), 725–757.

Ren, H., Sigman, D. M., Martínez-García, A., Anderson, R. F., Chen, M.-T., Ravelo, A. C., Straub, M., Wong, G. T. F., & Haug, G. H. (2017, August 15). Impact of glacial/interglacial sea level change on the ocean nitrogen cycle <https://doi.org/10.1073/pnas.1701315114>. Proceedings of the National Academy of Sciences, 114(33), E6759–E6766.

Ren, H., Sigman, D. M., Meckler, A. N., Plessen, B., Robinson, R. S., Rosenthal, Y., & Haug, G. H. (2009, January 9). Foraminiferal isotope evidence of reduced nitrogen fixation in the ice age Atlantic Ocean <https://doi.org/10.1126/science.1165787>. Science, 323(5911), 244–248.

Ren, H., Sigman, D. M., Thunell, R. C., & Prokopenko, M. G. (2012). Nitrogen isotopic composition of planktonic foraminifera from the modern ocean and recent sediments <https://doi.org/10.4319/lo.2012.57.4.1011>. Limnology and Oceanography, 57.

Revelle, R., & Suess, H. E. (1957, January). Carbon dioxide exchange between atmosphere and ocean and the question of an increase of atmospheric CO2 during the past decades <https://doi.org/10.3402/tellusa.v9i1.9075>. Tellus, 9(1), 18–27.

Rickaby, R. E. M., Elderfield, H., Roberts, N., Hillenbrand, C.-D., & Mackensen, A. (2010, March). Evidence for elevated alkalinity in the glacial Southern Ocean <https://doi.org/10.1029/2009PA001762>. Paleoceanography, 25(1), 1–15.

Ridgwell, A. J. (2003a, June). An end to the “rain ratio” reign? <https://doi.org/10.1029/2003GC000512> Geochemistry, Geophysics, Geosystems, 4(6).

Ridgwell, A. J. (2003b, September). Implications of the glacial CO 2 “iron hypothesis” for Quaternary climate change. <https://doi.org/10.1029/2003GC000563> Geochemistry, Geophysics, Geosystems, 4(9).

Ridgwell, A. J., Watson, A. J., & Archer, D. E. (2002, December). Modeling the response of the oceanic Si inventory to perturbation, and consequences for atmospheric CO 2 <https://doi.org/10.1029/2002GB001877>. Global Biogeochemical Cycles, 16(4), 19-1–19-25.

Ritz, S. P., Stocker, T. F., & Joos, F. (2011, January 15). A coupled dynamical ocean–energy balance atmosphere model for Paleoclimate studies <https://doi.org/10.1175/2010JCLI3351.1>. Journal of Climate, 24(2), 349–375.

Robinson, L. F., Adkins, J. F., Keigwin, L. D., Southon, J., Fernandez, D. P., Wang, S.-L., & Scheirer, D. S. (2005, December 2). Radiocarbon variability in the Western North Atlantic during the last deglaciation <https://doi.org/10.1126/science.1114832>. Science, 310(5753), 1469–1473.

Robinson, R. S., & Sigman, D. M. (2008). Nitrogen isotopic evidence for a poleward decrease in surface nitrate within the ice age Antarctic <https://doi.org/10.1016/j.quascirev.2008.02.005>. Quaternary Science Reviews, 27(9–10), 1076–1090.

Robinson, R. S., Sigman, D. M., DiFiore, P. J., Rohde, M. M., Mashiotta, T. A., & Lea, D. W. (2005, September). Diatom-bound 15 N/ 14 N: New support for enhanced nutrient consumption in the ice age subantarctic <https://doi.org/10.1029/2004PA001114>. Paleoceanography, 20(3).

Rohling, E. J., Foster, G. L., Grant, K. M., Marino, G., Roberts, A. P., Tamisiea, M. E., & Williams, F. (2014, April 24). Sea-level and deep-sea-temperature variability over the past 5.3 million years <https://doi.org/10.1038/nature13230>. Nature, 508(7497), 477–482.

Rose, K. A., Sikes, E. L., Guilderson, T. P., Shane, P., Hill, T. M., Zahn, R., & Spero, H. J. (2010, August). Upperocean-to-atmosphere radiocarbon offsets imply fast deglacial carbon dioxide release <https://doi.org/10.1038/nature09288>. Nature, 466(7310), 1093–1097.

Roth, R., Ritz, S. P., & Joos, F. (2014, October 16). Burial-nutrient feedbacks amplify the sensitivity of atmospheric carbon dioxide to changes in organic matter remineralisation <https://doi.org/10.5194/esd-5321-2014>. Earth System Dynamics, 5(2), 321–343.

Röthlisberger, R. (2004). Ice core evidence for the extent of past atmospheric CO 2 change due to iron fertilisation <https://doi.org/10.1029/2004GL020338>. Geophysical Research Letters, 31(16), L16207.

Röthlisberger, R., Crosta, X., Abram, N. J., Armand, L., & Wolff, E. W. (2010). Potential and limitations of marine and ice core sea ice proxies: An example from the Indian Ocean sector <https://doi.org/10.1016/j.quascirev.2009.10.005>. Quaternary Science Reviews, 29(1–2), 296–302.

Ruttenberg, K. C. (2003). The global phosphorus cycle <https://doi.org/10.1016/B0-08-043751-6/08153-6>. In Heinrich D. Holland & Karl K. Turekian (Eds.), Treatise on geochemistry (pp. 585–643). Elsevier.

Sabine, C. L., Key, R. M., Feely, R. A., & Greeley, D. (2002, December). Inorganic carbon in the Indian Ocean: Distribution and dissolution processes <https://doi.org/10.1029/2002GB001869>. Global Biogeochemical Cycles, 16(4), 15-1–15-18.

Sarmento, H., Montoya, J. M., Vázquez-Domínguez, E., Vaqué, D., & Gasol, J. M. (2010, July 12). Warming effects on marine microbial food web processes: How far can we go when it comes to predictions? <https://doi.org/10.1098/rstb.2010.0045> Philosophical Transactions of the Royal Society B: Biological Sciences, 365(1549), 2137–2149.

Sarmiento, J. L., & Gruber, N. (2006). Ocean biogeochemical dynamics. Princeton University Press.

Sarmiento, J. L., Gruber, N., Brzezinski, M. A., & Dunne, J. P. (2004, January 1). High-latitude controls of thermocline nutrients and low latitude biological productivity <https://doi.org/10.1038/nature02127>. Nature, 427(6969), 56–60.

Sarmiento, J. L., & Toggweiler, J. R. (1984, April). A new model for the role of the oceans in determining atmospheric P CO2 <https://doi.org/10.1038/308621a0>. Nature, 308(5960), 621–624.

Schaefer, J. M., Denton, G. H., Barrell, D. J. A., Ivy-Ochs, S., Kubik, P. W., Andersen, B. G., Phillips, F. M., Lowell, T. V., & Schlüchter, C. (2006, June 9). Near-synchronous interhemispheric termination of the last glacial maximum in mid-latitudes <https://doi.org/10.1126/science.1122872>. Science, 312(5779), 15101513.

Schilt, A., Baumgartner, M., Blunier, T., Schwander, J., Spahni, R., Fischer, H., & Stocker, T. F. (2010, January). Glacial–interglacial and millennial-scale variations in the atmospheric nitrous oxide concentration during the last 800,000 years <https://doi.org/10.1016/j.quascirev.2009.03.011>. Quaternary Science Reviews, 29(12), 182–192.

Schimper, K. F. (1837). Auszug Aus Dem Briefe Des H. Dr Schimper: Über Die Eiszeit <https://www.eperiodica.ch/digbib/view?pid=sng-004:1837:22::96#5>. In Actes de la Societe Helvetique des Sciences Naturelles, Session 22, Imprimerie de Petitpierre, Neuchatel (pp. 38–52).

Schimper, K. F. (1885). Die Eiszeit. In Fünfzigster Und Einundfünfzigster Jahresbericht Des Mannheimer Vereins Für Naturkunde Für Die Jahre 1883 Und 1884 (pp. 55–59). Mannheimer Vereins Für Naturkunde.

Schindler, D. W. (1977). Evolution of phosphorus limitation in lakes. Science, 195(4275), 260–262.

Schmitt, J., Schneider, R., Elsig, J., Leuenberger, D., Lourantou, A., Chappellaz, J., Köhler, P., et al. (2012, May 11). Carbon isotope constraints on the deglacial CO 2 rise from ice cores <https://doi.org/10.1126/science.1217161>. Science, 336(6082), 711–714.

Schmittner, A., & Galbraith, E. D. (2008, November). Glacial greenhouse-gas fluctuations controlled by ocean circulation changes <https://doi.org/10.1038/nature07531>. Nature, 456(7220), 373–376.

Schneider, R., Schmitt, J., Köhler, P., Joos, F., & Fischer, H. (2013, November 6). A reconstruction of atmospheric carbon dioxide and its stable carbon isotopic composition from the penultimate glacial maximum to the last glacial inception <https://doi.org/10.5194/cp-9-2507-2013>. Climate of the Past, 9(6), 2507–2523.

Schrag, D. P., et al. (1996). Pore fluid constraints on the temperature and oxygen isotopic composition of the Glacial ocean <https://doi.org/10.1126/science.272.5270.1930>. Science, 272, 1930–1932.

Schuur, E. A. G., McGuire, A. D., Schädel, C., Grosse, G., Harden, J. W., Hayes, D. J., Hugelius, G., et al. (2015, April). Climate change and the permafrost carbon feedback <https://doi.org/10.1038/nature14338>. Nature, 520(7546), 171–179.

Seltzer, A. M., Ng, J., Aeschbach, W., Kipfer, R., Kulongoski, J. T., Severinghaus, J. P., & Stute, M. (2021, May 13). Widespread six degrees Celsius cooling on land during the last glacial maximum <https://doi.org/10.1038/s41586-021-03467-6>. Nature, 593(7858), 228–232.

Shackleton, N. J. (1977). Carbon-13 in Uvigerina: Tropical rain forest history and the equatorial Pacific carbonate dissolution cycle. In N. R. Andersen & A. Malahoff (Eds.), The fate of fossil fuel in the oceans (pp. 401–427). Plenum.

Shackleton, N. J., & Opdyke, N. D. (1973, June). Oxygen isotope and palaeomagnetic stratigraphy of equatorial Pacific Core V28-238: Oxygen isotope temperatures and ice volumes on a 10 5 year and 10 6 year scale <https://doi.org/10.1016/0033-5894(73)90052-5>. Quaternary Research, 3(1), 39–55.

Shakun, J. D., Clark, P. U., He, F., Marcott, S. A., Mix, A. C., Liu, Z., Otto-Bliesner, B., Schmittner, A., & Bard, E. (2012, April). Global warming preceded by increasing carbon dioxide concentrations during the last deglaciation <https://doi.org/10.1038/nature10915>. Nature, 484(7392), 49–54.

Shemesh, A., Macko, S. A., Charles, C. D., & Rau, G. H. (1993, October 15). Isotopic evidence for reduced productivity in the glacial Southern Ocean <https://doi.org/10.1126/science.262.5132.407>. Science, 262(5132), 407–410.

Sherwood, S. C., Webb, M. J., Annan, J. D., Armour, K. C., Forster, P. M., Hargreaves, J. C., Hegerl, G., et al. (2020, December). An assessment of Earth’s climate sensitivity using multiple lines of evidence <https://doi.org/10.1029/2019RG000678>. Reviews of Geophysics, 58(4), 1–92.

Siegenthaler, U., Stocker, T. F., Monnin, E., Lüthi, D., Schwander, J., Stauffer, B., Raynaud, D., Barnola, J. M., Fischer, H., Masson-Delmotte, V., & Jouzel, J. (2005). Stable carbon cycle-climate relationship during the Late Pleistocene <https://doi.org/10.1126/science.1120130>. Science, 310(5752), 1313–1317.

Siegenthaler, U., & Wenk, T. (1984, April). Rapid atmospheric CO2 variations and ocean circulation <https://doi.org/10.1038/308624a0>. Nature, 308(5960), 624–626.

Sigman, D. M., Altabet, M. A., Francois, R., McCorkle, D. C., & Gaillard, J.-F. (1999, April). The isotopic composition of diatom-bound nitrogen in Southern Ocean sediments <https://doi.org/10.1029/1998PA900018>. Paleoceanography, 14(2), 118–134.

Sigman, D. M., & Boyle, E. A. (2000, October). Glacial/interglacial variations in atmospheric carbon dioxide <https://doi.org/10.1038/35038000>. Nature, 407(6806), 859–869.

Sigman, D. M., de Boer, A. M., & Haug, G. H. (2007). Antarctic stratification, atmospheric water vapor, and Heinrich Events: A hypothesis for Late Pleistocene deglaciations <https://doi.org/10.1029/GM173>. In A. Schmittner, J. C. H. Chiang, & S. R. Hemming (Eds.), Ocean circulation: Mechanisms and impacts—Past and future changes of meridional overturning (Vol. 173, pp. 335–349). Geophysical Monograph Series. American Geophysical Union.

Sigman, D. M., Fripiat, F., Studer, A. S., Kemeny, P. C., Martínez-García, A., Hain, M. P., Ai, X., Wang, X., Ren, H., & Haug, G. H. (2021, February). The Southern Ocean during the ice ages: A review of the Antarctic surface isolation hypothesis, with comparison to the North Pacific <https://doi.org/10.1016/j.quascirev.2020.106732>. Quaternary Science Reviews, 254, 106732.

Sigman, D. M., & Hain, M. P. (2012). The Biological Productivity of the Ocean <https://doi.org/10.5281/zenodo.13370237>. In Nature Education Knowledge, 3(6), 1–16.

Sigman, D. M., & Hain, M. P. (2024). Ocean oxygen, preformed nutrients, and the cause of the lower carbon dioxide concentration in the atmosphere of the last glacial maximum <https://doi.org/10.1029/2023PA004775>. Paleoceanography and Paleoclimatology, 39, e2023PA004775.

Sigman, D. M., Hain, M. P., & Haug, G. H. (2010, July). The Polar Ocean and glacial cycles in atmospheric CO2 concentration <https://doi.org/10.1038/nature09149>. Nature, 466(7302), 47–55.

Sigman, D. M., & Haug, G. H. (2003). The biological pump in the past <https://doi.org/10.1016/B0-08-0437516/06118-1>. In H. D. Holland & K. K. Turekian (Eds.), Treatise on geochemistry (pp. 491–528). Elsevier.

Sigman, D. M., Jaccard, S. L., & Haug, G. H. (2004, March). Polar Ocean stratification in a cold climate <https://doi.org/10.1038/nature02357>. Nature, 428(6978), 59–63.

Sigman, D. M., Lehman, S. J., & Oppo, D. W. (2003, September). Evaluating mechanisms of nutrient depletion and 13 C enrichment in the Intermediate-depth Atlantic during the last ice age <https://doi.org/10.1029/2002PA000818>. Paleoceanography, 18(3).

Sigman, D. M., McCorkle, D. C., & Martin, W. R. (1998, September). The calcite lysocline as a constraint on glacial/interglacial low-latitude production changes <https://doi.org/10.1029/98GB01184>. Global Biogeochemical Cycles, 12(3), 409–427.

Sikes, E. L., Samson, C. R., Guilderson, T. P., & Howard, W. R. (2000, June). Old radiocarbon ages in the Southwest Pacific Ocean during the last glacial period and deglaciation <https://doi.org/10.1038/35014581>. Nature, 405(6786), 555–559.

Sikes, E. L., Umling, N. E., Allen, K. A., Ninnemann, U. S., Robinson, R. S., Russell, J. L., & Williams, T. J. (2023, June 9). Southern Ocean glacial conditions and their Influence on deglacial events <https://doi.org/10.1038/s43017-023-00436-7>. Nature Reviews Earth & Environment, (4), 454–470.

Sillén, L. G. (1967). Master variables and activity scales <https://pubs.acs.org/doi/10.1021/ba-19670067.ch003>. In W. Stumm (Ed.), Equilibrium concepts in natural water systems (Vol. 67, pp. 45–56). Advances in Chemistry. American Chemical Society.

Singer, B. S., Brown, L. L., Rabassa, J. O., & Guillou, H. (2013). 40 Ar/ 39 Ar chronology of Late Pliocene and Early Pleistocene geomagnetic and glacial events in Southern Argentina <https://doi.org/10.1029/145GM13>. In J. E. T. Channell, D. V. Kent, W. Lowrie, & J. G. Meert (Eds.) , Geophysical Monograph Series (pp. 175–190). American Geophysical Union.

Skinner, L. C., & Bard, E. (2022, March). Radiocarbon as a dating tool and tracer in Paleoceanography <https://doi.org/10.1029/2020RG000720>. Reviews of Geophysics, 60(1), 64.

Skinner, L. C., Fallon, S., Waelbroeck, C., Michel, E., & Barker, S. (2010, May 28). Ventilation of the deep Southern Ocean and deglacial CO 2 rise <https://doi.org/10.1126/science.1183627>. Science, 328(5982), 1147–1151.

Skinner, L. C., Primeau, F., Freeman, E., De La Fuente, M., Goodwin, P. A., Gottschalk, J., Huang, E., McCave, I. N., Noble, T. L., & Scrivner, A. E. (2017, July 13). Radiocarbon constraints on the glacial ocean circulation and its Impact on atmospheric CO2 <https://doi.org/10.1038/ncomms16010>. Nature Communications, 8(1), 16010.

Smith, J. A., Seltzer, G. O., Farber, D. L., Rodbell, D. T., & Finkel, R. C. (2005, April 29). Early local last glacial maximum in the tropical Andes <https://doi.org/10.1126/science.1107075>. Science, 308(5722), 678–681.

Snyder, C. W. (2016, October 13). Evolution of global temperature over the past two million years. <https://doi.org/10.1038/nature19798> Nature, 538(7624), 226–228.

Sosdian, S. M., Rosenthal, Y., & Toggweiler, J. R. (2018, June). Deep Atlantic carbonate ion and CaCO 3 compensation during the ice ages <https://doi.org/10.1029/2017PA003312>. Paleoceanography and Paleoclimatology, 33(6), 546–562.

Sowers, T., & Bender, M. (1995, July 14). Climate records covering the last deglaciation <https://doi.org/10.1126/science.269.5221.210>. Science, 269(5221), 210–214.

Sowers, T., Bender, M., & Raynaud, D. (1989). Elemental and isotopic composition of occluded O 2 and N 2 in polar ice <https://doi.org/10.1029/JD094iD04p05137>. Journal of Geophysical Research, 94(D4), 5137.

Stauffer, B., Hofer, H., Oeschger, H., Schwander, J., & Siegenthaler, U. (1984). Atmospheric CO 2 concentration during the last glaciation <https://doi.org/10.3189/1984AoG5-1-160-164>. Annals of Glaciology, 5, 160–164.

Stephens, B. B., & Keeling, R. F. (2000, March). The influence of Antarctic Sea ice on glacial–interglacial CO2 Variations <https://doi.org/10.1038/35004556>. Nature, 404(6774), 171–174.

Stocker, T. F. (1998, October 2). The seesaw effect <https://doi.org/10.1126/science.282.5386.61>. Science, 282(5386), 61–62.

Stommel, H., & Arons, A. B. (1959, January). On the abyssal circulation of the world ocean—II: An idealized model of the circulation pattern and amplitude in oceanic basins <https://doi.org/10.1016/01466313(59)90075-9>. Deep Sea Research, 6, 217–233.

Stott, L., & Timmermann, A. (2011). Hypothesized link between glacial/interglacial atmospheric CO2 cycles and storage/release CO2- rich fluids from the deep sea <https://doi.org/10.1029/2010GM001052>. In Understanding the causes, mechanisms and extent of the abrupt climate change, geophysical monograph series (pp. 123–128). American Geophysical Union.

Stott, L., Timmermann, A., & Thunell, R. (2007, October 19). Southern Hemisphere and deep-sea warming led deglacial atmospheric CO 2 rise and tropical warming <https://doi.org/10.1126/science.1143791>. Science, 318(5849), 435–438.

Stouffer, R. J., & Manabe, S. (2003, May 1). Equilibrium response of thermohaline circulation to large changes in atmospheric CO2 concentration <https://doi.org/10.1007/s00382-002-0302-4>. Climate Dynamics, 20(7–8), 759–773.

Straub, M., Sigman, D. M., Ren, H., Martínez-García, A., Meckler, A. N., Hain, M. P., & Haug, G. H. (2013, September). Changes in North Atlantic nitrogen fixation controlled by ocean circulation <https://doi.org/10.1038/nature12397>. Nature, 501(7466), 200–203.

Studer, A. S., Sigman, D. M., Martínez-García, A., Benz, V., Winckler, G., Kuhn, G., Esper, O., et al. (2015, July). Antarctic Zone nutrient conditions during the last two glacial cycles <https://doi.org/10.1002/2014PA002745>. Paleoceanography, 30(7), 845–862.

Summerhayes, C. P. (2019). Archibald Geikie and the ice age controversy <https://doi.org/10.1144/SP480.1>. Geological Society, London, Special Publications, 480(1), 183–190.

Suwa, M., & Bender, M. L. (2008, June). Chronology of the Vostok ice core constrained by O2/N2 ratios of occluded air, and its implication for the Vostok climate records <https://doi.org/10.1016/j.quascirev.2008.02.017>. Quaternary Science Reviews, 27(11–12), 10931106.

Szarka, L., Soon, W. W.-H., & Cionco, R. G. (2021, January). How the astronomical aspects of climate science were settled? On the Milankovitch and Bacsák anniversaries, with lessons for today <https://doi.org/10.1016/j.asr.2020.09.020>. Advances in Space Research, 67(1), 700–707.

Takahashi, T. (1975). Carbonate chemistry of sea water and the calcite compensation depth in the oceans. In W. V. Sliter, A. W. H. Bé, & W. H. Berger (Eds.), Dissolution of deep-sea carbonates 13:0 (pp. 11–27). Cushman Foundation for Foraminiferal Research.

Takahashi, T., Broecker, W. S., & Langer, S. (1985). Redfield ratio based on chemical data from isopycnal surfaces <https://doi.org/10.1029/JC090iC04p06907>. Journal of Geophysical Research, 90(C4), 6907.

Taucher, J., Bach, L. T., Riebesell, U., & Oschlies, A. (2014, April). The viscosity effect on marine particle flux: A climate relevant feedback mechanism <https://doi.org/10.1002/2013GB004728>. Global Biogeochemical Cycles, 28(4), 415–422.

Teng, Y.-C., Primeau, F. W., Moore, J. K., Lomas, M. W., & Martiny, A. C. (2014, December). Global-scale variations of the ratios of carbon to phosphorus in exported marine organic matter <https://doi.org/10.1038/ngeo2303>. Nature Geoscience, 7(12), 895–898.

Thurber, D. L., Broecker, W. S., Blanchard, R. L., & Potratz, H. A. (1965, July 2). Uranium-series ages of Pacific atoll coral <https://doi.org/10.1126/science.149.3679.55>. Science, 149(3679), 55–58.

Tierney, J. E., Zhu, J., King, J., Malevich, S. B., Hakim, G. J., & Poulsen, C. J. (2020, August 27). Glacial cooling and climate sensitivity revisited <https://doi.org/10.1038/s41586-020-2617-x>. Nature, 584(7822), 569–573.

Timmermann, A., Friedrich, T., Timm, O. E., Chikamoto, M. O., Abe-Ouchi, A., & Ganopolski, A. (2014, March 1). Modeling obliquity and CO2 effects on Southern Hemisphere climate during the past 408 Ka <https://doi.org/10.1175/JCLI-D-13-00311.1>. Journal of Climate, 27(5), 1863–1875.

Timmermann, A., Timm, O., Stott, L., & Menviel, L. (2009, April 1). The roles of CO2 and orbital forcing in driving Southern Hemispheric temperature variations during the last 21 000 Yr <https://doi.org/10.1175/2008JCLI2161.1>. Journal of Climate, 22(7), 1626–1640.

Toggweiler, J. R. (1999, October). Variation of atmospheric CO 2 by ventilation of the ocean's deepest water <https://doi.org/10.1029/1999PA900033>. Paleoceanography, 14(5), 571–588.

Toggweiler, J. R., Joellen, L. R., & Carson, S. R. (2006, June). Midlatitude westerlies, atmospheric CO2, and climate change during the ice ages <https://doi.org/10.1029/2005PA001154>. Paleoceanography, 21(2), 1–13.

Toggweiler, J. R., Murnane, R., Carson, S., Gnanadesikan, A., & Sarmiento, J. L. (2003, March). Representation of the carbon cycle in box models and GCMs, 2, organic pump <https://doi.org/10.1029/2001GB001841>. Global Biogeochemical Cycles, 17(1), 1–13.

Toggweiler, J. R., & Sarmiento, J. L. (1985). Glacial to interglacial changes in atmospheric carbon dioxide: The critical role of ocean surface water in high latitudes <https://doi.org/10.1029/GM032p0163>. In E. T.

Sundquist & W. S. Broecker (Eds.), Geophysical Monograph Series (pp. 163–184). American Geophysical Union.

Tsandev, I., Slomp, C. P., & Van Cappellen, P. (2008, December). Glacial-interglacial variations in marine phosphorus cycling: Implications for ocean productivity <https://doi.org/10.1029/2007GB003054>. Global Biogeochemical Cycles, 22(4).

Tschumi, T., Joos, F., Gehlen, M., & Heinze, C. (2011, July 22). Deep ocean ventilation, carbon isotopes, marine sedimentation and the deglacial CO2 rise <https://doi.org/10.5194/cp-7-771-2011>. Climate of the Past, 7(3), 771–800.

Tyndall, J. (1861). I. The Bakerian Lecture.—On the absorption and radiation of heat by gases and vapours, and on the physical connexion of radiation, absorption, and conduction. Philosophical Transactions of the Royal Society of London, 151, 1–36.

Tyrrell, T. (1999, August). The relative influences of nitrogen and phosphorus on oceanic primary production <https://doi.org/10.1038/22941>. Nature, 400(6744), 525–531.

Vallelonga, P., Barbante, C., Cozzi, G., Gabrieli, J., Schüpbach, S., Spolaor, A., & Turetta, C. (2013, March 8). Iron fluxes to Talos Dome, Antarctica, over the past 200 Kyr <https://doi.org/10.5194/cp-9-597-2013>. Climate of the Past, 9(2), 597–604.

Valletta, R. D., Willenbring, J. K., & Lewis, A. R. (2017, August). "Difference dating": A novel approach towards dating alpine glacial moraines <https://doi.org/10.1016/j.quageo.2017.05.001>. Quaternary Geochronology, 41, 1–10.

Vernekar, A. D. (1972). Long-period global Variations of incoming solar radiation <https://doi.org/10.1007/978-1-935704-34-8_1>. In A. D. Vernekar (Ed.), Long-period global Variations of incoming solar radiation (pp. 1–128). American Meteorological Society.

Volk, T., & Hoffert, M. I. (1985). Ocean carbon pumps: Analysis of relative strengths and efficiencies in oceandriven atmospheric CO 2 changes <https://doi.org/10.1029/GM032p0099>. In E. T. Sundquist & W. S. Broecker (Eds.), Geophysical Monograph Series (pp. 99–110). American Geophysical Union.

Vollmer, T. D., Ito, T., & Lynch-Stieglitz, J. (2022, November). Proxy-based preformed phosphate estimates point to increased biological pump efficiency as primary cause of last glacial maximum CO 2 drawdown <https://doi.org/10.1029/2021PA004339>. Paleoceanography and Paleoclimatology, 37(11), 1–19.

Wadham, J. L., Hawkings, J. R., Tarasov, L., Gregoire, L. J., Spencer, R. G. M., Gutjahr, M., Ridgwell, A., & Kohfeld, K. E. (2019, August 15). Ice sheets matter for the global carbon cycle <https://doi.org/10.1038/s41467-019-11394-4>. Nature Communications, 10(1), 3567.

Waelbroeck, C., Labeyrie, L., Michel, E., Duplessy, J. C., McManus, J. F., Lambeck, K., Balbon, E., & Labracherie, M. (2002, January). Sea-level and deep water temperature changes derived from benthic foraminifera isotopic records <https://doi.org/10.1016/S0277-3791(01)00101-9>. Quaternary Science Reviews,21(1–3), 295–305.

WAIS Divide Project Members. (2013, August). Onset of deglacial warming in West Antarctica driven by local orbital forcing <https://doi.org/10.1038/nature12376>. Nature, 500(7463), 440–444.

WAIS Divide Project Members. (2015, April). Precise interpolar phasing of abrupt climate change during the last ice age <https://doi.org/10.1038/nature14401>. Nature, 520(7549), 661–665.

Wallmann, K. (2003, September). Feedbacks between oceanic redox states and marine productivity: A model perspective focused on benthic phosphorus cycling <https://doi.org/10.1029/2002GB001968>. Global Biogeochemical Cycles, 17(3).

Wallmann, K. (2010, December). Phosphorus imbalance in the global ocean? <https://doi.org/10.1029/2009GB003643> Global Biogeochemical Cycles, 24(4).

Wallmann, K., Schneider, B., & Sarnthein, M. (2016, February 18). Effects of Eustatic Sea-level change, ocean dynamics, and nutrient utilization on atmospheric pCo2 and seawater composition over the last 130 000 years: A model study <https://doi.org/10.5194/cp-12-339-2016>. Climate of the Past, 12(2), 339–375.

Wang, X. T., Sigman, D. M., Prokopenko, M. G., Adkins, J. F., Robinson, L. F., Hines, S. K., Chai, J., Studer, A. S., Martínez-García, A., Chen, T., Haug, G. H. (2017). Deep-sea coral evidence for lower Southern Ocean surface nitrate concentrations during the last ice age <https://doi.org/10.1073/pnas.1615718114>. Proceedings of the National Academy of Sciences of the United States of America, 114(13), 3352–3357.

Watson, A. J., Bakker, D. C. E., Ridgwell, A. J., Boyd, P. W., & Law, C. S. (2000, October). Effect of iron supply on Southern Ocean CO2 uptake and implications for glacial atmospheric CO2 <https://doi.org/10.1038/35037561>. Nature, 407(6805), 730–733.

Watson, A. J., & Naveira Garabato, A. C. (2006, January 1). The role of Southern Ocean mixing and upwelling in glacial-interglacial atmospheric CO2 change <https://doi.org/10.1111/j.1600-0889.2005.00167.x>. Tellus B: Chemical and Physical Meteorology, 58(1), 73.

Watson, A. J., Vallis, G. K., & Nikurashin, M. (2015, November). Southern Ocean buoyancy forcing of ocean ventilation and glacial atmospheric CO2 <https://doi.org/10.1038/ngeo2538>. Nature Geoscience, 8(11), 861–864.

Weart, S. R. (2008). The discovery of global warming (Rev. and Expanded ed.). New Histories of Science, Technology, and Medicine. Harvard University Press.

Weber, M. E., Bailey, I., Hemming, S. R., Martos, Y. M., Reilly, B. T., Ronge, T. A., Brachfeld, S., et al. (2022, April 19). Antiphased dust deposition and productivity in the Antarctic Zone over 1.5 million years <https://doi.org/10.1038/s41467-022-29642-5>. Nature Communications, 13(1), 2044.

Weiss, R. F. (1974, November). Carbon dioxide in water and seawater: The solubility of a non-ideal gas <https://doi.org/10.1016/0304-4203(74)90015-2>. Marine Chemistry, 2(3), 203–215.

Williams, R. G., & Follows, M. J. (2011). Ocean dynamics and the carbon cycle: Principles and mechanisms <https://doi.org/10.1017/CBO9780511977817> (1st ed.). Cambridge University Press.

Winterfeld, M., Mollenhauer, G., Dummann, W., Köhler, P., Lembke-Jene, L., Meyer, V. D., He"er, J., et al. (2018, December). Deglacial mobilization of pre-aged terrestrial carbon from degrading permafrost <https://doi.org/10.1038/s41467-018-06080-w>. Nature Communications, 9(1), 3666.

Wohlers, J., Engel, A., Zöllner, E., Breithaupt, P., Jürgens, K., Hoppe, H.-G., Sommer, U., & Riebesell, U. (2009, April 28). Changes in biogenic carbon flow in response to sea surface warming <https://doi.org/10.1073/pnas.0812743106>. Proceedings of the National Academy of Sciences, 106(17), 7067–7072.

Wolff, E. W., Fischer, H., Fundel, F., Ruth, U., Twarloh, B., Littot, G. C., Mulvaney, R., et al. (2006, March 23). Southern Ocean sea-ice extent, productivity and iron flux over the past eight glacial cycles <https://doi.org/10.1038/nature04614>. Nature, 440(7083), 491–496.

Wolf-Gladrow, D. A., Zeebe, R. E., Klaas, C., Körtzinger, A., & Dickson, A. G. (2007, July). Total alkalinity: The explicit conservative expression and its application to biogeochemical processes <https://doi.org/10.1016/j.marchem.2007.01.006>. Marine Chemistry, 106(1–2), 287–300.

Wood, M., Hayes, C. T., & Paytan, A. (2023, January 3). Global quaternary carbonate burial: Proxy- and model-based reconstructions and persisting uncertainties <https://doi.org/10.1146/annurev-marine031122-031137>. Annual Review of Marine Science, 15(1), annurev-marine-031122–031137.

Wu, Y., Hain, M. P., Humphreys, M. P., Hartman, S., & Tyrrell, T. (2019, July 11). What drives the latitudinal gradient in open-ocean surface dissolved inorganic carbon concentration?

<https://doi.org/10.5194/bg-162661-2019> Biogeosciences, 16(13), 2661–2681.
Yamamoto, M., Clemens, S. C., Seki, O., Tsuchiya, Y., Huang, Y., O'ishi, R., & Abe-Ouchi, A. (2022, April). Increased interglacial atmospheric CO2 levels followed the mid-Pleistocene transition <https://doi.org/10.1038/s41561-022-00918-1>. Nature Geoscience, 15(4), 307–313.
Yu, J., Anderson, R. F., Jin, Z., Menviel, L., Zhang, F., Ryerson, F. J., & Rohling, E. J. (2014, April). Deep South Atlantic carbonate chemistry and increased interocean deep water exchange during last deglaciation <https://doi.org/10.1016/j.quascirev.2014.02.018>. Quaternary Science Reviews, 90, 80–89.
Yu, J., Broecker, W. S., Elderfield, H., Jin, Z., McManus, J., & Zhang, F. (2010, November 19). Loss of carbon from the deep sea since the last glacial maximum <https://doi.org/10.1126/science.1193221>. Science, 330(6007), 1084–1087.
Yu, Z., Joos, F., Bauska, T. K., Stocker, B. D., Fischer, H., Loisel, J., Brovkin, V., et al. (2021, July). No support for carbon storage of >1,000 GtC in northern peatlands <https://doi.org/10.1038/s41561-021-00769-2>. Nature Geoscience, 14(7), 465–467.
Zeng, N. (2003, September). Glacial-interglacial atmospheric CO2 change—The glacial burial hypothesis <https://doi.org/10.1007/BF02915395>. Advances in Atmospheric Sciences, 20(5), 677–693.
Zhao, N., Marchal, O., Keigwin, L., Amrhein, D., & Gebbie, G. (2018, February). A synthesis of deglacial deep-sea radiocarbon records and their (in)consistency with modern ocean ventilation <https://doi.org/10.1002/2017PA003174>. Paleoceanography and Paleoclimatology, 33(2), 128151.
Zhu, C., Zhang, J., Liu, Z., Otto-Bliesner, B. L., He, C., Brady, E. C., Tomas, R., et al. (2022, November 15). Antarctic warming during Heinrich Stadial 1 in a transient isotope-enabled deglacial simulation <https://doi.org/10.1175/JCLI-D-22-0094.1>. Journal of Climate, 35(22), 7353–7365.

[i] *Henry's Law (1803) states that, for ideal gases, the equilibrium concentration of a dissolved gas is proportional to the partial pressure (Dalton, 1802) of that gas in the atmosphere, commonly expressed as a fraction of standard surface air pressure in units of µatm. The partial pressure of CO_2 corresponds to the product of the total surface air pressure and the mole fraction of CO_2, commonly expressed in µatm. Correcting for moisture yields the "dry mixing ratio" of CO_2 (xCO_2), commonly expressed in units of parts per million (ppm, ppmv), which is 0%–2% higher than the "wet" pCO_2 in their respective units. The effective partial pressure of CO_2 in a solution ("fugacity," fCO_2 , in µatm) differs from ideal partial pressure (pCO_2) by less than 0.5% (e.g., Weiss, 1974). For example, seawater with a temperature of 5 °C, salinity of 34.7, DIC of 2150 µmol/kg and ALK of 2360 µmol/kg has fCO_2, pCO_2 and xCO_2 of 286.5 µatm, 287.7 µatm and 290.1 ppm, respectively. Throughout this article, these minor distinctions are avoided, and CO_2 concentration is simply referred to in terms of atmospheric mixing ratio xCO_2 in units of ppm, the Earth system property most pertinent to the greenhouse effect and the global carbon cycle mass balance. A constant atmospheric total of $1.773 * 10^{20}$ mole N_2-O_2-Ar is used (see Table A.1 in Sarmiento & Gruber, 2006).*

[ii] *Throughout the text, a distinction is made between the Subantarctic Zone (SAZ) and Polar Antarctic Zone (PAZ) of the Southern Ocean, a simplification that is meant to highlight the biogeochemical divide (Marinov et al., 2006) between Southern Ocean deep upwelling that is either bound to head north into the upper cell via the SAZ or south into the lower cell via the PAZ (Box 1; Figures 4c, 7, 8). However, most existing paleoceanographic data relevant to the PAZ are from the open Antarctic Zone (the AZ) where the upwelling occurs, as opposed to the PAZ proper. This explains the usage of AZ in this figure but of PAZ elsewhere.*